Flexoelectric Fluid Membranes in External Electric Fields

Sayedeh Niloufar Abtahi

Submitted to the
Institute of Graduate Studies and Research
in partial fulfillment of the requirements for the degree of

Doctor of Philosophy
in
Physics

Eastern Mediterranean University
September 2020
Gazimağusa, North Cyprus

Approval of the Institute of Graduate Studies and Research

Prof. Dr. Ali Hakan Ulusoy
Director

I certify that this thesis satisfies all the requirements as a thesis for the degree of Doctor of Philosophy in Physics.

Prof. Dr. İzzet Sakallı
Chair, Department of Physics

We certify that we have read this thesis and that in our opinion it is fully adequate in scope and quality as a thesis for the degree of Doctor of Philosophy in Physics.

Assoc. Prof. Dr. Martin Michael Müller
Co-Supervisor

Prof. Dr. S. Habib Mazharimousavi
Supervisor

Examining Committee

1. Prof. Dr. Özay Gürtuğ
2. Prof. Dr. S. Habib Mazharimousavi
3. Prof. Dr. Omar Mustafa
4. Prof. Dr. Özlem Yeşiltaş
5. Asst. Prof. Dr. Mustafa Riza

ABSTRACT

This manuscript presents a geometrical framework for flexoelectric membranes based on stress tensors which mimic the response of a flexoelectric fluid membrane to an external electric field. This framework is used to study numerically the morphology of spherically confined flexoelectric fluid membrane vesicles in an external uniform electric field. The confinement induces membrane deformations, which lead to its polarization and interactions with the external field. Without such electric fields, the equilibrium shapes of the vesicle were categorized in a geometrical phase diagram as a function of reduced volume and the scaled area in the past [1, 2].

When the area of the flexoelectric fluid membrane is a bit larger than the area of the confining sphere, an axisymmetric invagination can be found with a simple numerical integration scheme. A non-vanishing electric field induces an additional elongation of the confined vesicle, which is either perpendicular or parallel depending on the sign of the electric field parameter. Higher values of surface area or the electric field parameter reduce the symmetry of the system resulting in more complex folding. To find equilibrium configurations as a function of volume, area and coupling with the electric field, two numerical methods were employed. Despite some rather crude approximations such as assuming a constant electric field, interesting shape transformations and symmetry breaking are found. Moreover, the resulting shapes indicate that transition lines are shifted in the presence of an electric field, which leads to the transition shapes reminiscent of the main protagonist in the video game "Pac-Man". In these shapes, the invagination of the membrane is not axisymmetric but deforms into a large elongated slit reminiscent of shapes that can be found with the area-difference-elasticity (ADE) model for confined membranes without an

electric field [3].

Self-contacts, as observed in this work, can potentially lead to a shape transition, from a spherical to a toroidal vesicle topology *via* membrane fusion. It turns out that the spherical topology is preferred for typical values of the material parameters when the electric field vanishes. Flexoelectricity could potentially facilitate topology changes. The obtained folding patterns could be of interest to biophysical and technological applications alike.

Keywords: Membranes, bilayers, vesicles, flexoelectricity, elasticity theory and dielectric thin films.

ÖZ

Bu taslak, bir fleksoelektrik akışkan membranının bir dış elektrik alanına tepkisini taklit eden ve stres tensörlerine dayanan fleksoelektrik membranlar için geometrik bir çerçeve kurmayı amaçlamaktadır. Bu çerçeve, bir dış üniform elektrik alanı içerisinde bulunan küresel olarak sınırlanmış fleksoelektrik sıvı membran veziküllerinin morfolojisini sayısal olarak incelemek için kullanılır. Sınırlandırma, membran deformasyonlarını tetikler böylece dış alanla polarizasyonuna ve etkileşimlere yol açar. Bu tür elektrik alanları olmadan, vezikülün denge şekilleri, ölçeklendirilmiş alanın bir fonksiyonu ve ötesinde azaltılmış hacim olarak bir geometrik faz diyagramında sınıflandırılmıştır [1, 2].

Membranın alanı sınırlandırma küresinin alanından sadece biraz daha büyük olduğunda, basit bir sayısal entegrasyon şeması ile tek bir eksenel simetrik invajinasyon bulunabilir. Kaybolmayan bir elektrik alanı, sınırlandırılan vezikülde ek bir uzamaya neden olur ve bu elektrik alan parametresinin işaretine bağlı olarak dik veya paraleldir. Daha yüksek yüzey alanı veya elektrik alanı parametresi, sistemin simetrisini azaltarak daha karmaşık katlanmaya neden olur. Alan, hacim ve elektrik alanı ile eşleşmenin bir fonksiyonu olarak denge konfigürasyonlarını bulmak için iki sayısal çözüm yönteminden faydalanılmıştır. Sabit bir elektrik alanı varsaymak gibi oldukça kaba yaklaşımlara rağmen, ilginç şekil dönüşümleri ve simetri kırılması bulunur. Ayrıca, ortaya çıkan şekiller geçiş hatlarının bir elektrik alanının varlığında değiştiğini gösterir, bu da video oyunundaki “Pac-Man” ana kahramanını andıran geçiş şekillerine yol açar. Bu şekillerde, membranın invajinasyonu eksenel simetrik değildir, ancak elektrik alanı olmayan kapalı membranlar için alan farkı esnekliği (ADE) modeliyle bulunabilen şekilleri anımsatan büyük bir uzun yarık şeklinde

deforme olur [3].

Bu çalışmada gözlemlendiği gibi kendiliğinden temaslar potansiyel olarak membran füzyonu yoluyla küreselden toroidal vezikül topolojisine geçişe yol açabilir. Elektrik alanı kaybolduğunda, küresel topolojinin maddesel parametrelerinin tipik değerleri için tercih edildiği ortaya çıkmaktadır. Fleksoelektrik, potansiyel olarak topoloji değişikliklerine olanak tanıyabilir. Elde edilen katlama paternleri, biyofiziksel ve teknolojik uygulamaların her ikisini de ilgilendirebilir.

Anahtar Kelimeler: Membranlar, iki katmanlı yapılar, veziküüller, fleksoelektriklik, elastikiyet teorisi ve dielektrik ince filmler.

To my family

ACKNOWLEDGMENT

The last five and a half years were spent on this PhD, and it was a fantastic journey. At this point, I feel like there are many people whom I need to thank. I like to thank my supervisor, Prof. Sayed Habib Mazharimousavi, for his knowledge, support, and guidance.

This manuscript is prepared with the excellent mentorship of my co-supervisor, Dr Martin Michael Müller. I am remarkably thankful to him for taking me on as his PhD student. I appreciate his constant support, encouragement, patience, motivation, and kindness during my PhD studies. It is a wish for me to mentor my student as he mentored me.

During my PhD research, I have collaborated with Dr. Lila Bouzar, who is a supportive and motivated person. I am grateful for her to be always available for discussions and advice in the way that I always felt motivated after our discussion. Prof. Jemal Guven is acknowledged for introducing this field right after I have started my PhD.

Part of my research done at the Université de Lorraine where I received financial and technological support under the direction of Dr Martin Michael Müller. I am grateful for their hospitality during my PhD training visits and for their warm support.

I am grateful for the support and kindness of the head of the physics department of Eastern Mediterranean University Prof. Izzet Sakallli during my PhD study. I want to thank Fabien Pascale for his help on some programming issues.

TABLE OF CONTENTS

LIST OF FIGURES

Chapter 1

INTRODUCTION

By the early 1980s, the electromechanical behavior of biological membranes, vesicles, and cells had already received a lot of attention leading to applications and the interpretation of the mechanical properties of cells, organs, and tissues in the following years [4, 5]. Significant applications that have been developed in biomedicine and biotechnology include wound healing, cancer treatment, cell control and manipulation [6, 7]. For example, applying strong electric fields on lipid membranes substantially increases the electric conductivity and permeability of the membranes, which led to the development of electroporation[1] as an established treatment method for gene therapy and delivering drugs into the cells [9]. This method allows small molecules to pass into different cell types through temporary membrane pores [8–13].

On the theoretical side, continuum mechanical models of lipid membranes, vesicles, and cells have been developed mostly without considering the microstructure of cells [14–23]. Recent research has also studied the dynamical behavior of cell membranes using discrete cytoskeleton models [24, 25], in which actin microtubules and filaments are modeled as rods, cords, and junction network with specific topological structures [24, 25]. These microstructure models help to understand the

[1] Electroporation is a phenomenon in which cell membranes become temporarily destabilized in specific regions due to electric field pulses. During a DC pulse, the membrane is immensely permeable to exogenous adjacent molecules [8].

nonlinear mechanics of cell membranes (e.g., adhesion). However, some of the properties of lipid membranes like flexoelectricity, or dielectric anisotropy, with their associated phase transformations are not yet fully understood theoretically. For instance, in the context of flexoelectric fluid membranes Petrov and coworkers have shown its relevance for biological membranes in experiments [26–28], which motivated several subsequent theoretical studies [29–32]. Only recently it has been shown with extensive molecular dynamics simulations that uniform electric fields can induce biologically relevant membrane deformations [33].

In the context of the formation of cells, vesicles, and organelles, some important open questions are: "What sort of mechanisms will generate a peculiar structure?", "What are the possible electromechanical shape deformations of biological membranes subjected to certain boundary conditions?", and "What are the forces and stresses transmitted in fluid membranes in an external electric field?". The answer to these questions has a geometric origin. To be able to understand and control the cell's electrophysiological[2] properties, morphological phase diagrams of vesicles responding to electric fields can be helpful. Even though biological membranes have a very complex structure, it is possible to find answers to such questions by taking advantage of differential geometry with and without specific parameterizations.

In this thesis, the interplay of electromechanical constraints and the geometry of flexoelectric fluid membranes is studied in detail. We will see that the correlation between geometry and stresses exerted on the system leads to an explanation for the nonlinear electromechanical behavior of flexoelectric membranes. This non-linearity

[2] Electrophysiology is to study the effect of electric phenomena in the body (e.g., nerves, cells and tissues).

demands a combination of different approaches, such as analytical theory and several numerical solution methods. While one approach has its limitations, the other gives a better view of the problem. In the following, the presented model will be based on the general theory of electromechanics of polarized lipid bilayers introduced by David J. Steigmann and Ashutosh Agrawal in 2016 [32].

- Chapter. 2 introduces a general review of the mechanical behaviour of biological membranes characterized as two-dimensional fluid surfaces. The generalized Monge parametrization framework is developed to capture the Gaussian and total curvature of curved surfaces. This approach is applied to spherical and cylindrical surfaces. Moreover, an overview of the different elastic energies associated with the varying shapes of the fluid membranes in terms of metric and extrinsic curvatures is provided by using continuum mechanics.
- Chapter. 3 illustrates how fluid membranes interact with an electric field. A theoretical framework to capture the behaviour of polarized membranes, flexoelectric membranes, based on the flexoelectric stress tensor, is illustrated. To describe their equilibrium behaviour, the shape equation of flexoelectric membranes in an electric field is derived.
- Chapter. 4 considers the folding patterns of flexoelectric fluid membrane vesicles in a uniform electric field due to spherical confinement as a non-trivial example of such systems. The electric field inside the confining cavity is calculated. By making use of the angle-arc-length parametrization, the behaviour of the confined flexoelectric fluid membrane vesicles in response to the uniform electric field is scrutinized. Moreover, the transition of the morphological phase diagram of the system is exhibited.

- Chapter. 5 wraps up this manuscript with some concluding remarks and future directions.
- Appendix. A provides some basic mathematical concepts of the differential geometry of fluid membranes.
- Appendix. B applies the Monge gauge parametrization approach to particular cases.
- Appendix. C addresses the numerical approaches used in this manuscript.
- Appendix. D discusses a dielectric sphere model within an electrolyte in an applied uniform electric field.

Chapter 2

MECHANICS OF FLUID MEMBRANES

In this chapter, an introduction to the basic phenomenological concepts of biological membranes is provided.

2.1 Structure and Functions of Biological Membranes

In biology, lipid membranes are a fundamental part of all cell types. They are involved in different tasks, such as sending nutrients into cells and waste products out. They can be considered similar to our largest organ, the skin, which separates our body from the external environment and supports a variety of processes occurring in our body. Biological membranes also furnish the surface of cells and separate the extracellular environment from the cell's interior and its organelles. The cells of unicellular organisms, such as bacteria, possess only a single main membrane whereas the cells of multicellular organisms, plants and animals, contain additional internal membrane-limited subcompartments called organelles. Due to all of the different tasks that involve membranes, a cell's molecular membrane is highly inhomogeneous [34].

Despite this complexity, the biological membrane can be interpreted in a simple way by looking at its structure. In the last three decades, theoretical biophysicists have realized that the geometrical diversity of cells needs further explanation, which is why they have started to look closely at the morphology of cells [1, 2, 22, 23, 35, 36]. Cells are multi-scale entities with a size of $10\mu m$ to $100\mu m$, containing organelles ranging from $100nm$ to $10\mu m$ in diameter, and with even smaller objects such as

membrane-embedded proteins varying from 1*nm* to 5*nm* [37]. By zooming out from the membranes' molecular structure and shifting to the mesoscopic scale, it is possible to model lipid membranes abstractly. From this point of view, the lipid bilayer membrane is what all living cells have in common.

2.2 Lipid Bilayer Membranes

The structure of lipids: Lipids are made of amphiphilic molecules with two different segments: the **hydrophilic** head segment (*i.e.*, "in love with water") and **hydrophobic** segment (*i.e.*, "afraid of water"). This dual characteristics is governed by the chemical properties of each part of the lipid. Although lipids are in many different sorts in nature, a few plausible classes of them are used by nature to build the cell membranes of animal [38]. In terms of the structure of lipids, the tail typically consists of two hydrocarbon chains created from a varied number of fatty acids (usually 16 to 24 C-atoms) and some double bonds, such as palmitic acid [34]. The hydrocarbon chain attaches via amide covalent bonds, ester bonds, to linker groups to bind with a hydrophilic head group. Physicists will not concentrate on the chemical details of the lipids, but pay attention to the following characteristics: i. **the length of the fatty acids**: the longer they are, the thicker the lipid membrane, ii. **double bonds**: the tails tend to be tilted, and iii. **charged head groups** [39].

The morphology of lipids: The lipids' hydrophobic tails hate to dissolve in water. When inserted in an aqueous environment, they try to avoid the water and aggregate with a cooperative strategic move in which the tails protect each other from surrounding water by using the hydrophilic head groups. Therefore, lipid molecules self-assemble in different morphologies to please the dual characteristic of both segments. Such aggregations can be micelles, spheres, with all tails inside and all heads on the surface. In wormlike cylindrical shapes again tails aggregate in the

inside and the heads on the surface and the opposite as well. Lipids can also form double-layer surfaces in which two planes of hydrophilic heads will sandwich the tails. This configuration, called *lipid bilayer* is the object of interest in this manuscript (see Figure. 2.1).

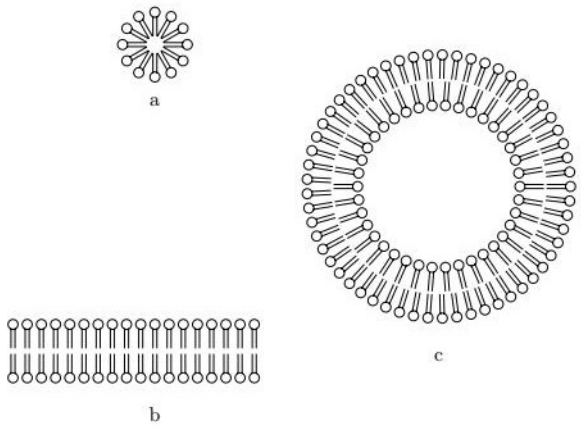

Figure 2.1: Lipid molecules' morphologies: (a) micelle, (b) bilayer surface, (c) vesicle.

Phase behavior of lipid bilayer membranes: Lipid bilayer membranes are quasi-two-dimensional arrangements which form in an aqueous environment due to the hydrophobic effect. The fact that most of the cells' containers- the boundary which separates the two different phases of water and plasma solutions- are built by lipid bilayers was discovered in 1925 [40]. Depending on the water concentration and the temperature, lipid membranes exhibit interesting phase behavior: the two-dimensional gel phase with a crystal system at low temperature, and a liquid-crystalline phase at biological temperatures. In the liquid-crystal phase, the lipid molecules move freely in their tangential plane and form a two-dimensional fluid membrane [41, 42].

2.3 Generalized Monge Parametrization

As mentioned earlier, it is possible to consider bilayer lipid membranes as two-dimensional surfaces. Differential geometry, which has been considered a

sophisticated tool to study lipid membranes, makes the parametrization of biological membranes possible. In this respect, there exist some parametrization framework to describe the curvature of surfaces embedded in three-dimensional space. Among all Monge parametrization, which mostly applied on the horizontal plane, is the interest of this section (for more details see appendix. B).

By shifting to the terminology of the Einstein theory of gravity, biological membranes are quite similar to timelike thin-shells, which are membranes in spacetime. Although the spacetime has been assigned to be $3+1-$dimensional, the lower dimensional spacetime *i.e.*, $2+1$ is also a well-known model. The analogy between the $1+1-$dimensional thin-shells in $2+1-$dimensional spacetime and the $2-$dimensional surfaces in $3-$dimensional space is the point that we shall get into the formalism in this section. To this end, by making use of mathematical rules of general relativity for thin-shells, it is possible to develop a new terminology for the basic tools used in the study of biological membranes. One of the most used concepts in the early development of the biological membranes is the so-called Monge Gauge (MG). The MG [43] is a parametrization / mapping of a $2-$dimensional surface which is defined by a height function $h(x,y)$ over a flat plane as a function of orthonormal coordinate on the plane x and y into a $3-$dimensional flat space of coordinates x,y and z. This parametrization describes the surface by a height function above an arbitrary reference flat surface as following:

$$h:\begin{cases} \mathbb{R}^2 \supset U \longrightarrow \mathbb{R}^3 \\ (x,y) \longrightarrow h(x,y) \end{cases}. \tag{2.1}$$

By making use of the standard definition [43], the total curvature is as follows:

$$\kappa = \frac{h_{,xx}\left(1+h_{,y}^2\right)+h_{,yy}\left(1+h_{,x}^2\right)-2h_{,xy}h_{,x}h_y}{2\left(1+h_{,x}^2+h_{,y}^2\right)^2} \tag{2.2}$$

and the Gaussian curvature is:

$$\kappa_G = \frac{h_{,xx}h_{,yy}-h_{,xy}^2}{\left(1+h_{,x}^2+h_{,y}^2\right)^2} \tag{2.3}$$

By introducing $\nabla = \begin{pmatrix} \frac{\partial}{\partial x} \\ \\ \frac{\partial}{\partial y} \end{pmatrix}$ the above usually are compacted as

$$2\kappa = \nabla.\left(\frac{\nabla h}{\sqrt{1+(\nabla h)^2}}\right) \tag{2.4}$$

and

$$\kappa_G = \frac{\det\left(\partial^2 h\right)}{\left(1+(\nabla h)^2\right)^2} \tag{2.5}$$

in which the Hessian $\partial^2 h$ is given by

$$\partial^2 h = \begin{pmatrix} h_{,xx} & h_{,xy} \\ \\ h_{,yx} & h_{,yy} \end{pmatrix}. \tag{2.6}$$

For instance, in the research has done by Seifert and Langer [44], the height function was set to $h(x,y) = h\exp[iqx] + c.c.$ in which h and q are two constants. For more recent research one may look at the work done by Bingham, Smye, and Olmsted [45]. As of [44] and [45], the other studies where the Monge Gauge used, the original unperturbed surface is locally flat. However, in the case of a blood cell, it is not possible to consider its membrane flat. Therefore and fluctuation from its original rest shape needs to be analyzed exactly without using Monge Gauge. Here one may use a proper Monge gauge which of course is not the one introduced above. Spherically and cylindrically symmetries are the most common symmetries which occur in nature.

Hence in the following, this parametrization used for curved coordinate systems.

2.3.1 The Spherical Monge Gauge

Let's start with a spherical shell of radius R with some fluctuation on its surface given by the spherical height function $h(\theta,\varphi)$ in which θ and φ are the polar and azimuthal angle. Unlike the Cartesian height function, the non fluctuated sphere is given by $h(\theta,\varphi)=R$. Here, the aim is to find the first and second fundamental forms as well as the extrinsic curvature tensor and the scalar curvature of the hypersurface Σ in terms of $h(\theta,\varphi)$ only. The outward normal vector on the surface Σ is defined as [46]:

$$n_\gamma = \frac{1}{\sqrt{\Delta}}\frac{dF}{dx^\gamma}\bigg|_\Sigma \tag{2.7}$$

in which $F := r - h(\theta,\varphi) = 0$ is the definition of the surface Σ in three dimensional flat spherical symmetric bulk space M with line element:

$$ds_M^2 = g_{\alpha\beta}dx^\alpha dx^\beta = dr^2 + r^2\left(d\theta^2 + \sin^2\theta d\varphi^2\right). \tag{2.8}$$

Herein Δ is defined as:

$$\Delta = g^{\alpha\beta}\frac{dF}{dx^\alpha}\frac{dF}{dx^\beta}\bigg|_\Sigma \tag{2.9}$$

in which $g^{\alpha\beta}$ is the metric tensor of the bulk and $n_\gamma n^\gamma = 1$. Let's note that the Greek letters $\alpha,\beta,\ldots = 1,2,3$ are used for the bulk space while the Latin letters $i,j,\ldots = 2,3$ shall be used for the hypersurface. Using the definition (2.1) we find:

$$n_r = \tfrac{1}{\sqrt{\Delta}}\,, \tag{2.10a}$$

$$n_\theta = \tfrac{-1}{\sqrt{\Delta}}h_{,\theta}\,, \tag{2.10b}$$

$$n_\varphi = \tfrac{-1}{\sqrt{\Delta}}h_{,\varphi}\,. \tag{2.10c}$$

in which:

$$\Delta = 1 + \frac{h_{,\theta}^2}{h^2} + \frac{h_{,\varphi}^2}{h^2 \sin^2\theta} \,. \tag{2.11}$$

The induced metric on the hypersurface Σ is given by:

$$g_{ij} = \frac{\partial x^\alpha}{\partial \xi^i} \frac{\partial x^\beta}{\partial \xi^j} g_{\alpha\beta} \tag{2.12}$$

in which the line element on the hypersurface is written as:

$$ds_\Sigma^2 = g_{ij} d\xi^i d\xi^j. \tag{2.13}$$

Explicitly one finds:

$$ds_\Sigma^2 = \left(h^2 + h_{,\theta}^2\right) d\theta^2 + \left(h^2 \sin^2\theta + h_{,\varphi}^2\right) d\varphi^2 + 2 h_{,\theta} h_{,\varphi} d\theta d\varphi \tag{2.14}$$

or simply:

$$g_{ij} = \begin{bmatrix} h^2 + h_{,\theta}^2 & h_{,\theta} h_{,\varphi} \\ h_{,\theta} h_{,\varphi} & h^2 \sin^2\theta + h_{,\varphi}^2 \end{bmatrix} \tag{2.15}$$

with its inverse:

$$g^{ij} = \frac{1}{h^4 \sin^2\theta \Delta} \begin{bmatrix} h^2 \sin^2\theta + h_{,\varphi}^2 & -h_{,\theta} h_{,\varphi} \\ -h_{,\theta} h_{,\varphi} & h^2 + h_{,\theta}^2 \end{bmatrix} . \tag{2.16}$$

Having the induced metric and the normal vector on the hypersurface Σ, one can use the definition of extrinsic curvature tensor of the surface Σ:

$$K_{ij} = -n_\gamma \left(\frac{\partial^2 x^\gamma}{\partial \xi^i \partial \xi^j} + \Gamma^\gamma_{\alpha\beta} \frac{\partial x^\alpha}{\partial \xi^i} \frac{\partial x^\beta}{\partial \xi^j} \right) \Bigg|_\Sigma \tag{2.17}$$

to find the nonzero components of the extrinsic curvature or second fundamental form. We note that $\Gamma^{\gamma}_{\alpha\beta}$ are the Christoffel symbols of the second kind of the bulk space with the only nonzero components given by:

$$\Gamma^{\theta}_{r\theta} = \Gamma^{\theta}_{\theta r} = \Gamma^{\varphi}_{r\varphi} = \Gamma^{\varphi}_{\varphi r} = \frac{1}{r}\,, \tag{2.18}$$

$$\Gamma^{r}_{\theta\theta} = -r\,,\ \Gamma^{r}_{\varphi\varphi} = -r\sin^2\theta\,, \tag{2.19}$$

and

$$\Gamma^{\varphi}_{\varphi\theta} = \Gamma^{\varphi}_{\theta\varphi} = \frac{\cos\theta}{\sin\theta},\ \Gamma^{\theta}_{\varphi\varphi} = -\sin\theta\cos\theta\,. \tag{2.20}$$

The components of the extrinsic curvature tensor are:

$$K_{\theta\theta} = \frac{h^2 + 2h^2_{,\theta} - hh_{,\theta\theta}}{h\sqrt{\Delta}}\,, \tag{2.21a}$$

$$K_{\varphi\varphi} = \frac{h^2\sin^2\theta - hh_{,\theta}\sin\theta\cos\theta + 2h^2_{,\varphi} - hh_{,\varphi\varphi}}{h\sqrt{\Delta}}\,, \tag{2.21b}$$

$$K_{\varphi\theta} = K_{\theta\varphi} = \frac{2h_{,\theta}h_{,\varphi} + hh_{,\varphi}\frac{\cos\theta}{\sin\theta} - hh_{,\theta\varphi}}{h\sqrt{\Delta}}\,. \tag{2.21c}$$

In order to find the total and the Gaussian curvature, K^j_i is obtained:

$$K^{\theta}_{\theta} = \left[\frac{\left(h^2 - hh_{,\theta\theta} + 2h^2_{,\theta}\right)h\sin^3\theta + \left(hh^2_{,\varphi} + h_{,\theta}h_{,\varphi}h_{,\theta\varphi} - h^2_{,\varphi}h_{,\theta\theta}\right)\sin\theta - h_{,\theta}h^2_{,\varphi}\cos\theta}{h^4\sin^3\theta\Delta^{3/2}}\right], \tag{2.22a}$$

$$K^{\varphi}_{\varphi} = \left[\frac{\left(h^2 + h^2_{,\theta}\right)\left(h\sin^2\theta - h_{,\theta}\sin\theta\cos\theta - h_{,\varphi\varphi}\right)\sin\theta + \left(2hh^2_{,\varphi} + h_{,\theta}h_{,\varphi}h_{,\theta\varphi}\right)\sin\theta - h_{,\theta}h^2_{,\varphi}\cos\theta}{h^4\sin^3\theta\Delta^{3/2}}\right], \tag{2.22b}$$

$$K^{\theta}_{\varphi} = \left[\frac{\left(h_{,\theta}h_{,\varphi} - hh_{,\theta\varphi}\right)h\sin^3\theta + h_{,\varphi}\left(h^2_{,\theta} + h^2\right)\sin^2\theta\cos\theta + \left(h_{,\theta}h_{,\varphi\varphi} - h_{,\varphi}h_{,\theta\varphi}\right)h_{,\varphi}\sin\theta + h^3_{,\varphi}\cos\theta}{h^4\sin^3\theta\Delta^{3/2}}\right], \tag{2.22c}$$

$$K_{\theta}^{\varphi}=\left[\frac{\left(h_{,\theta}^{2}+h^{2}\right)\left(-h_{,\theta\varphi}\sin\theta+h_{,\varphi}\cos\theta\right)+\sin\theta\left(h_{,\theta}h_{,\varphi}\left(h+h_{,\varphi\varphi}\right)\right)}{h^{4}\sin^{3}\theta\Delta^{3/2}}\right]. \tag{2.22d}$$

The mean curvature $\kappa=\frac{1}{2}tr\left(K_{i}^{j}\right)$:

$$\kappa=\frac{\alpha_{1}\sin^{3}\theta+\alpha_{2}\sin^{2}\theta\cos\theta+\alpha_{3}\sin\theta+\alpha_{4}\cos\theta}{2h^{4}\Delta^{\frac{3}{2}}\sin^{3}\theta} \tag{2.23}$$

in which

$$\begin{pmatrix}\alpha_{1}\\ \alpha_{2}\\ \alpha_{3}\\ \alpha_{4}\end{pmatrix}=\begin{pmatrix}3hh_{,\theta}^{2}+2h^{3}-h^{2}h_{,\theta\theta}\\ -h_{,\theta}\left(h^{2}+h_{,\theta}^{2}\right)\\ h_{,\varphi}^{2}\left(3h-h_{,\theta\theta}\right)+2h_{,\theta}h_{,\varphi}h_{,\theta\varphi}-h_{,\varphi\varphi}\left(h^{2}+h_{,\theta}^{2}\right)\\ -2h_{,\theta}h_{,\varphi}^{2}\end{pmatrix}, \tag{2.24}$$

The Gaussian curvature $\kappa_{G}=\det\left(K_{i}^{j}\right)$ obtains as:

$$\begin{aligned}\kappa_{G}=\Bigg(&\frac{\left(h_{,\varphi}^{2}+\left(h^{2}+h_{,\theta}^{2}\right)\sin^{2}\theta\right)}{h^{7}\Delta^{3}\sin^{6}\theta}\\ &\frac{\left(\beta_{1}\sin^{4}\theta+\beta_{2}\sin^{3}\theta\cos\theta+\beta_{3}\sin^{2}\theta+\beta_{4}\sin\theta\cos\theta+\beta_{5}\cos^{2}\theta\right)}{h^{7}\Delta^{3}\sin^{6}\theta}\Bigg),\end{aligned} \tag{2.25}$$

in which:

$$\begin{pmatrix}\beta_{1}\\ \beta_{2}\\ \beta_{3}\\ \beta_{4}\\ \beta_{5}\end{pmatrix}=\begin{pmatrix}h\left(h^{2}+2h_{,\theta}^{2}-hh_{,\theta\theta}\right)\\ -h_{\theta}\left(h^{2}+2h_{,\theta}^{2}-hh_{,\theta\theta}\right)\\ -h_{,\varphi\varphi}h^{2}+\left(h_{,\theta\theta}h_{,\varphi\varphi}-h_{,\theta\varphi}^{2}+2h_{,\varphi}^{2}\right)h+4h_{,\theta}h_{,\varphi}h_{,\theta\varphi}-2h_{,\theta}^{2}h_{,\varphi\varphi}-2h_{,\varphi}^{2}h_{,\theta\theta}\\ 2h_{,\varphi}\left(-2h_{,\theta}h_{,\varphi}+h_{,\theta\varphi}h\right)\\ -hh_{,\varphi}^{2}\end{pmatrix}. \tag{2.26}$$

respectively.

2.3.2 The Cylindrical Monge Gauge

By making use of the Generalized Monge parametrization, it is possible to parametrize a cylindrical shell of radius ρ with some fluctuation on the cylindrical height function $h(\varphi, z)$ where φ is azimuthal angle and z is height distance. Using the standard method of differential geometry leads us to obtain the first and second fundamental forms of the general surface. This first fundamental form is the metric tensor of the surface, and the second fundamental form is the extrinsic curvature tensor of the surface. To this end, the outward normal vector on the membrane Σ defines as [46]:

$$n_\gamma = \frac{1}{\sqrt{\Delta}} \frac{dF}{dx^\gamma}\bigg|_\Sigma \tag{2.27}$$

Where $F := \rho - h(\varphi, z) = 0$ is the definition of the surface Σ in three dimensional flat cylindrical symmetric bulk space M with the line element:

$$ds_M^2 = g_{\alpha\beta} dx^\alpha dx^\beta = d\rho^2 + \rho^2 d\varphi^2 + dz^2. \tag{2.28}$$

Also, Δ is the normalization factor given by:

$$\Delta = g^{\alpha\beta} \frac{dF}{dx^\alpha} \frac{dF}{dx^\beta}\bigg|_\Sigma \tag{2.29}$$

In which $g^{\alpha\beta}$ is the metric tensor of the bulk and n_γ satisfies $n_\gamma n^\gamma = 1$. As an extra explanation the Greek letters $\alpha, \beta, ... = 1, 2, 3$ and the Latin letters $i, j, ... = 2, 3$ are used for the bulk space and the hypersurface Σ respectively. Using the definition of the normal vector one finds:

$$n_\rho = \frac{1}{\sqrt{\Delta}}\,, \tag{2.30}$$

$$n_\varphi = \frac{-1}{\sqrt{\Delta}} h_{,\varphi}\,, \tag{2.31}$$

and

$$n_z = \frac{-1}{\sqrt{\Delta}} h_{,z} \,, \tag{2.32}$$

with

$$\Delta = 1 + \frac{h_{,\varphi}^2}{h^2} + h_{,z}^2 \,. \tag{2.33}$$

In which a subindex implies the partial derivative concerning the subletter. The induced line element of the membrane Σ found to be [46]:

$$ds_\Sigma^2 = \left(h^2 + h_{,\varphi}^2\right) d\varphi^2 + \left(1 + h_{,z}^2\right) dz^2 + 2h_{,\varphi} h_{,z} d\varphi dz \tag{2.34}$$

or equivalently the metric tensor is written as:

$$g_{ij} = \begin{bmatrix} h^2 + h_{,\varphi}^2 & h_{,\varphi} h_{,z} \\ h_{,\varphi} h_{,z} & 1 + h_{,z}^2 \end{bmatrix} , \tag{2.35}$$

with its inverse:

$$g^{ij} = \frac{1}{h^2 \Delta} \begin{bmatrix} 1 + h_{,z}^2 & -h_{,\varphi} h_{,z} \\ -h_{,\varphi} h_{,z} & h^2 + h_{,\varphi}^2 \end{bmatrix} . \tag{2.36}$$

The extrinsic curvature tensor of the surface Σ is defined by:

$$K_{ij} = -n_\gamma \left(\frac{\partial^2 x^\gamma}{\partial \xi^i \partial \xi^j} + \Gamma_{\alpha\beta}^\gamma \frac{\partial x^\alpha}{\partial \xi^i} \frac{\partial x^\beta}{\partial \xi^j} \right) \Bigg|_\Sigma \tag{2.37}$$

In which $\Gamma_{\alpha\beta}^\gamma$ is the Christoffel symbol of the second kind defined by:

$$\Gamma_{kl}^i = \frac{g^{im} \left(g_{mk,l} + g_{ml,k} - g_{kl,m} \right)}{2} \,. \tag{2.38}$$

To find the Christoffel symbols of the bulk metric tensor the only nonzero components given by:

$$\Gamma^{\varphi}_{\varphi\rho} = \Gamma^{\varphi}_{\rho\varphi} = \frac{1}{\rho}\,, \tag{2.39}$$

$$\Gamma^{\rho}_{\varphi\varphi} = -\rho\,. \tag{2.40}$$

and, using the definition of the extrinsic curvature tensor are find:

$$K_{\varphi\varphi} = \frac{-hh_{,\varphi\varphi} + h^2 + 2h^2_{,\varphi}}{h\sqrt{\Delta}}\,, \tag{2.41}$$

$$K_{zz} = \frac{hh_{,zz}}{h\sqrt{\Delta}}\,, \tag{2.42}$$

$$K_{\varphi z} = \frac{h_{,\varphi}h_{,z} - hh_{,\varphi z}}{h\sqrt{\Delta}}\,, \tag{2.43}$$

$$K_{z\varphi} = \frac{h_{,\varphi}h_{,z} - hh_{,z\varphi}}{h\sqrt{\Delta}}\,. \tag{2.44}$$

Furthermore, using the inverse induced metric and $K^j_i = g^{jk}K_{ik}$ one can obtain:

$$K^{\varphi}_{\varphi} = \frac{\left(1+h^2_{,z}\right)\left(-hh_{,\varphi\varphi}+h^2\right) + 2h^2_{,\varphi} + h_{,\varphi}h_z\left(hh_{,z\varphi}\right) + (h_\varphi h_z)^2}{h^3\Delta^{3/2}}\,, \tag{2.45}$$

$$K^{\varphi}_{z} = \frac{\left(1+h^2_{,z}\right)\left(h_{,\varphi}h_z - hh_{,z\varphi}\right) + h_\varphi h_{,z} hh_{,zz}}{h^3\Delta^{3/2}}\,, \tag{2.46}$$

$$K^{z}_{\varphi} = \frac{(h^2+h^2_{,\varphi})(h_{,\varphi}h_z - hh_{,z\varphi}) - h_{,\varphi}h_z(hh_{,\varphi\varphi} - h^2 + 2h^2_{,\varphi})}{h^3\Delta^{3/2}}, \tag{2.47}$$

and

$$K^{z}_{z} = \frac{(h^2+h^2_{,\varphi})(-hh_{zz}) - h_{,\varphi}h_z(h_{,\varphi}h_z - hh_{,z\varphi})}{h^3\Delta^{3/2}}\,. \tag{2.48}$$

We can finally find the mean curvature which is defined as $\kappa = \frac{1}{2}tr\left(K^j_i\right)$ and the

Gaussian curvature which the definition $\kappa_G = \det\left(K_i^j\right)$, as:

$$\kappa = \frac{(1+h_{,z}^2)(h^2 - hh_{,\varphi\varphi}) + 2h_{,\varphi} - h^3 h_{zz} + hh_{,\varphi}(2h_{,z\varphi}h_z - h_{zz}h_{,\varphi}))}{2h^3\Delta^{3/2}} \tag{2.49}$$

and

$$\kappa_G = \left(\frac{(-h^3 h_{,zz} + h^2 h_{,zz}h_{,\varphi\varphi} - h^2 h_{,z\varphi}^2 - 2hh_{,zz}h_{,\varphi}^2 + 2hh_{,z\varphi}h_{,\varphi}h_{,z} - h_{,z}{}^2 h_{,\varphi})}{h^6\Delta^3} \right.$$
$$\left. \frac{((h_{,z}^2+1)h^2 + h_\varphi{}^2)}{h^6\Delta^3} \right) \tag{2.50}$$

2.4 Membrane Deformations

Thus far lipid molecules morphologies have introduced which induces different spontaneous curvature to membranes. Besides, Monge parametrization of the curved surfaces was developed to capture the curvature of membranes embedded in three-dimensional space. To give the feeling of the connection between different membranes' geometry and their curvature, Physicists become interested in capturing the minimal energy of organelles' forms or membranes deformations. These deformations are common phenomena in nature and life science. From geometry's angle, the thickness of biological membranes ($\sim 5nm$), is small compared to their lateral extension, such that they can be considered as two-dimensional surfaces embedded in three-dimensional space. The following chapter will aim to model the specific biological membranes' configuration. In this respect, it is helpful to address the four main classes of mechanical and membrane deformations.

2.4.1 Stretching Energy

By stretching the membrane, a force per unit of area on the planar membrane is exerted, which identified as a tension, σ. The reaction force appears as internal stresses, which is energy costing deformation. The probability of finding free lipids is low because of

the repulsion of the hydrocarbon tails in an aqueous environment. So in the stationary states, lipids have a small exchange rate possibility between the membrane and the aqueous surrounding [34]. This means that the surface area, A, is a constant which implies a constraint on the area. Besides, it can translate into the mechanical energy via a Lagrange multiplier σ. Subsequently, change in the area of the patch of membrane illustrates its stretch energy due to the non-elasticity of the biological membrane. This leads us to examine the stretch mechanical deformation by an area energy function [2, 34]. Thus, the area energy associated with a closed biological membrane without holes is given by:

$$E_{area} = \int \sigma dA \tag{2.51}$$

where σ is surface tension and $dA = \sqrt{g}dx^i dx^j$ is the surface area element (see more detailes in Appendix. A).

2.4.2 Bending Energy

Among all classes of energies associated with fluid membrane surfaces, the energy due to bending deformations is the dominant one [34]. Consequently, considering the contribution of the bending energy can help us to identify the energy of two-dimensional surfaces, plasma membranes. This energy is captured by the geometry of surfaces, known as **the curvature** concept of surfaces (see Appendix. A).

Bending energy is scale-invariant since the dimension of curvature is an length. The unique characteristic of three-dimensional bending energy is not only scale-invariance but, additionally, invariance with respect first-order conformal transformations of the two-dimensional induced metric [34]. Here the proper terminology is differential geometry. To understand what is behind the morphology of the cells' membrane, one

can use the Canham-Helfrich-Evans Hamiltonian [46–48] of isotropic and homogeneous membranes as following:

$$E_{bending} = \int_{\Omega} \left(\frac{\kappa}{2}(K - C_0)^2 + \overline{\kappa} K_G \right) dA \tag{2.52}$$

where Ω is the surface domain, $K = \frac{c_1+c_2}{2}$ is the mean curvature, and $K_G = c_1 c_2$ is the Gaussian curvature in which c_1 and c_2 are the principal curvatures [3] . C_0 is the spontaneous curvature, which represents an asymmetry of the bilayer membrane in its ground state. κ and $\overline{\kappa}$ denote the bending rigidity, and the saddle-splay modulus respectively. The well-known Gauss-Bonnet theorem, $\overline{\kappa} \int_{\Omega} K_G dA = 4\pi(1-g)$, implies that for a specific topology of genus g, the Gaussian curvature is a topological invariant. Therefore, for spherical topology, the second term in Eq. (2.52) is constant, which leads to a vanishing variation. In the stationary state, this term is negligible and the bending energy reads:

$$E_{bending} = \int_{\Omega} \frac{\kappa}{2}(K - C_0)^2 dA \tag{2.53}$$

2.4.3 Energy Due to the Changes in the Thickness

Membrane proteins can deform biological membranesdue to their hydrophobic segments. In such a situation, their hydrophobic segment can align with the surrounding membrane to deform the membrane. This deformation will appear as a change in the thickness of the biological membrane (For details see section 11.6.2 of [34]). It turns out that the thickness deformation has the lowest energy contribution. It can be obtained similar to Hooke's law as:

$$E_{width} = \frac{K_w}{2} \int \left(\frac{w - w_0}{w_0} \right) dA \tag{2.54}$$

[3] Principal curvatures are the eigenvalues of $K_a^b = g_{ab} K_{cb}$

where w_0 is the half-thickness equilibrium, and w is the half-thickness deformation of the membrane. Besides, the units of $K_w \approx 60 k_B T / nm^2$ is an energy over unit of area.

2.4.4 Shearing Energy

Lipids form bilayer membranes, and they can move around without costing energy while remaining in the tangential plane. Therefore, they do not assist any shear energy. According to their similar behavior with fluid in their tangent plane, they are known as fluid membranes even though they are not fluid in their normal direction [34].

Chapter 3

HOW TO MODEL A FLEXOELECTRIC FLUID MEMBRANE IN AN ELECTRIC FIELD

The current chapter aims to model a flexoelectric fluid membrane, by making use of the basic phenomenological concepts of biological membranes which were introduced in Chap. 2. The overarching concepts give answers to the questions: "How do fluid membranes interact with an electric field?". Finding the answer to this question is the focus of this chapter. Biological membranes are dielectric materials that display a variety of electromechanical coupling mechanisms [49]. A classic example is piezoelectricity, which was discovered by the Jacques and Pierre Curie in 1880 [50]. Piezoelectricity results from a linear coupling allowing a crystalline material with no inversion symmetry to convert a uniformly applied electric field into a mechanical contraction or dilatation and vice-versa. For instance, barium titanate, lead zirconate titanate, and quartz are piezoelectric with a non-centrosymmetric crystalline structure [49]. Piezoelectricity has been exploited for industrial and biomedical applications such as sensorics [51], artificial muscles [52], or implantology [53].

In 1969 Robert B. Meyer suggested a similar linear coupling mechanism between the electric polarization and the curvature strain of liquid crystals [54]. In contrast to piezoelectricity, flexoelectricity is a ubiquitous phenomenon displayed by all dielectrics. In particular, bendable two-dimensional structures like fluid lipid

membranes and graphene sheets exhibit the flexoelectric effect [49]. In the context of flexoelectric fluid membranes Petrov and coworkers have shown its relevance for biological membranes in experiments [26–28], which motivated several subsequent theoretical studies [29–32]. Only recently it has been shown with extensive molecular dynamics simulations that uniform electric fields can induce biologically relevant membrane deformations [33].

This chapter focuses on introducing a generic geometrical framework to investigate the response of a flexoelectric fluid membrane to electric field stresses exerted on the system. To include the flexoelectric effect, we base our model on a recent theory by Steigmann and Agrawal, which was obtained as the thin-film limit of the continuum electrodynamics of nematic liquid crystals [32]. In this model, the authors assume free charges to be absent. Moreover, it is supposed that the polarisation vector is tangential to the membrane surface, a simplification which is supported to a certain extent by molecular dynamics simulations and quantum mechanical considerations [55–57]. The electric self-field of the membrane can be neglected in this case, which yields a justification for its suppression [32]. Here, lipid bilayers consider as thin-film nematic liquid crystals, as it was introduced in Chap. 2, in an analogous method with what was suggested for the first time in 1973 by Helfrich and resulted in the growing literature on this subject (see for example Ou-Yang et al. 1999 and David Steigmann et al. 2016).

To understand the effect of electromechanical stresses, one has to determine the shapes that flexoelectric fluid membranes adopt in equilibrium under given boundary conditions in a first step. By minimizing the energy, one can mathematically determine the shapes of such membranes. This minimization is, for instance, possible

with the help of the Lagrange multiplier framework (see [58]), which allows identifying the electromechanical stresses and the stresses due to the elasticity of the membrane.

To this end, the starting point is to introduce the analytical model for the case of a general electric field. In the next step, the electric field stress tensor governed by the membrane and its geometry will be derived. The shape equation of the system by introducing a generic electric field Hamiltonian will then be obtained. Finally, the general boundary conditions at the flexoelectric fluid membranes' interface located in an inhomogeneous electric field $\mathbf{E_{ext}}$ will be discussed.

3.1 Equilibrium Theoretical Model

As discussed in chap. 2, fluid membranes are composed of two layers of polar lipids held together by their amphiphilic properties. The thickness of such a bilayer is typically much smaller than its lateral extension, which implies that it can be modelled as a two-dimensional surface Ω. Moreover, since the lipids can move freely within each layer, one can consider the bilayer as fluid in the tangential plane. Including flexoelectricity, it is possible to describe the mechanical characteristics of the fluid membranes by taking into account four main contributions [2, 32] (see also discussion in chap. 2): the bending energy, which penalizes the curvature of the surface, and, the surface energy of the membrane which originates from changes of the membrane's area, the pressure difference between the inner and the outer part of the membrane, and finally, the electromechanical energy which arises from the response of the electrically polarized surface to an external electric field.

Accordance to the classical spontaneous curvature model, the Canham-Helfrich-Evans Hamiltonian description, the bending energy E_b of a vesicle described by a surface

integral involving a second-order expansion in curvatures [22, 46–48, 59] is given by:

$$E_b = \int_\Omega \left[\frac{\kappa}{2}(K - C_0)^2 + \overline{\kappa} K_G \right] dA, \tag{3.1}$$

where K, K_G, and C_0 are the mean, the Gaussian, and the spontaneous curvature, respectively. The constant κ is the bending rigidity, and $\overline{\kappa}$ denotes the saddle-splay modulus. In the following, only vesicles of spherical topology and zero spontaneous curvature will be considered. This allows discarding all terms but the first one involving the square of the mean curvature. Based on the Gauss-Bonnet theorem for a surface of genus g , $\int \overline{\kappa} K dA = 4\pi(1-g)$, where g refers to the number of "handles" of flexoelectric fluid membrane vesicles this term can be neglected in Eq. (3.1) leading to:

$$E_b = \int_\Omega \frac{\kappa}{2}(K - C_0)^2 dA \, . \tag{3.2}$$

In this section, the total energy of a thin flexoelectric membrane in an external electric field $\mathbf{E}_{\text{ext}}$ will be studied. Molecular dynamics simulation and experimental studies by Warshavic et al. in 2011 [57] have estimated that the dipole potential arises from (i) the dipole moments of the lipid's polar headgroups (phosphatidylcholine (PC) lipids have dipole moment of 18-25 Debye), (ii) the carbonyl group of the acyl chains (the dipole moment is nearly 2.5 Debye), and (iii) the aligned water molecules (dipole moment of a water molecule$\approx$ 1.8 Debye). Besides, they illustrated that the PC head group's dipole moment is placed more parallel to the surface of the bilayer rather than its normal component of 6 ± 3 Debye pointing towards the aqueous phase. As a result the polarization vector is mainly tangential to the membrane surface (see also [55, 56]). As discussed earlier, the effect of the electric self-field for fluid membranes is neglected. Flexoelectricity adds another contribution to the total energy when an external electric

field $\mathbf{E}_{\text{ext}}$ is present. Following Steigmann and Agrawal the corresponding energy of the flexoelectric membrane is given by [32]:

$$E_{\text{f}} = \int_{\Omega} \left[\frac{1}{2D} [(\mathbf{E}_{\text{ext}} \cdot \mathbf{n})^2 - |\mathbf{E}_{\text{ext}}|^2] \right] \mathrm{d}A, \tag{3.3}$$

where $\mathbf{n}$ is the normal vector of the membrane surface. The flexodielectric constant $D = \chi_{\perp} - \frac{c_2^2}{k_3}$ indicates the strength of the flexoelectric effect. It is a combination of the inverse of the electric polarisability, $\chi_{\perp}$, exhibited by the membrane when the electric field $\mathbf{E}_{\text{ext}}$ acts in the tangential plane, the bending modulus k_3 of the Frank energy of nematic liquid crystals, and the flexoelectric constant c_2 in the coupling term between the polarization vector and the tangent vectors of the membrane [32]. The strength of the flexoelectric effect will determine the sign of D. This finally allows writing the total energy functional of a flexoelectric fluid membrane in the presences of pressure and an electric field as:

$$E_{\text{tot}} = \int_{\Omega} dA \left(\frac{\kappa}{2} (2K - C_0)^2 + \overline{\kappa} K_G + \sigma + \frac{1}{2D} [(\mathbf{E}_{\text{ext}} \cdot \mathbf{n})^2 - |\mathbf{E}_{\text{ext}}|^2] \right) + \int dV P \tag{3.4}$$

where $\mathbf{E}_{\text{ext}}$ is the applied electric field, $\mathbf{n}$ is the normal vector, and P is the pressure difference.

3.2 Flexoelectric Field Stress Tensor

This section aims to identify the electric field stress tensor with the help of auxiliary variables that facilitate the variational problem to mimic the response of the surface to the deformation. To this end, it is possible to characterize the surface by an intrinsic tensor of the metric g_{ab}, and an extrinsic curvature tensor K_{ab}, which is an auxiliary field on the curved space. Auxiliary fields are describing the geometry of the flexoelectric membrane by a Hamiltonian, which only depends on metric tensor and extrinsic curvature induced on the surface [58]. In the following, the stress tensor–

multiplier $\tilde{\mathbf{f}}^a$– which originates from the direct derivation of the shape equation will be exploited.

3.2.1 General Hamiltonian

In this section, the behavior of a flexoelectric fluid membrane is discussed for the general case. According to Eq. (3.4), the curvature terms are quadratic. In the case of strong bending deformations, higher-order terms which originate from the nonlinearity of the curvature [60] cannot be neglected, and a generic description of the Hamiltonian is given by [61]:

$$H_\Sigma[\mathbf{X}] = \int_\Sigma dA\mathcal{H}\left(g_{ab}, K_{ab}\right), \qquad a,b,\in\{1,2\}\ , \tag{3.5}$$

where $\mathcal{H}$ depends on the metric g_{ab}, and the extrinsic curvature tensor K_{ab} (see Sec. The Geometry of Fluid Membranes: Variational Principles, Symmetries and Conservation Laws in [62]).

Geometry

It is straightforward if one examine the minimum energy with respect to the surface deformation function $\mathbf{X} = \mathbf{X} + \partial\mathbf{X}$. In this respect, it is possible to track this deformation through g_{ab}, K_{ab}, $\sqrt{g}$, and all covariant derivatives.

$$g_{ab} = e_a \cdot e_b\ , \tag{3.6a}$$

$$K_{ab} = e_a \cdot \partial_b \mathbf{n} = e_a \cdot \nabla_b \mathbf{n}\ . \tag{3.6b}$$

with

$$e_a = \partial\mathbf{X}/\partial\xi^a = \partial_a\mathbf{X} = \nabla_a\mathbf{X}\ , \tag{3.7a}$$

$$e_a \cdot \mathbf{n} = 0\ , \tag{3.7b}$$

$$\mathbf{n}^2 = 1\ . \tag{3.7c}$$

Now by using Lagrange multiplier functions, which was pointed out by Guven [58] for the first time, it is possible to consider g_{ab}, K_{ab}, $\mathbf{e}_a$, and $\mathbf{n}$ as independent variables to reformulate the generic Hamiltonian function as below:

$$\begin{aligned}\widetilde{H}_c = \widetilde{H}[g_{ab}, K_{ab}] + \int_\Sigma dA[\tilde{\lambda}^{ab}(g_{ab} - \mathbf{e}_a \cdot \mathbf{e}_b) + \tilde{\Lambda}^{ab}(K_{ab} - \mathbf{e}_a \cdot \nabla_b \mathbf{n})] \\ + \int_\Sigma dA[\tilde{\mathbf{f}}^a \cdot (\mathbf{e}_a - \nabla_a \mathbf{X}) + \tilde{\lambda}^a_\perp (\mathbf{e}_a \cdot \mathbf{n}) + \tilde{\lambda}_n(\mathbf{n}^2 - 1)] \, .\end{aligned} \tag{3.8}$$

in which Lagrange multipliers fix the constraints Eqs. (3.6) and (3.7).

Flexoelectric Hamiltonian

Using the auxiliary variables approach [61] which simplifies the variational problem, and Eq. (3.8) enables us to derive the new Hamiltonian of the system in the presence of osmotic pressure and electric field as follows:

$$\widetilde{H}_{c,P,\mathbf{E}} = \widetilde{H}_c - \frac{P}{3}\int dA \mathbf{n} \cdot \mathbf{X} - \frac{1}{2D}\int dA \left({\mathbf{E}_{\text{ext}}}^2 - (\mathbf{E}_{\text{ext}} \cdot \mathbf{n})^2 \right) \, . \tag{3.9}$$

Deformations of all these variables lead us to find the response of the Hamiltonian, which will equilibrate in the presence of pressure and electric field. In the following, a straightforward approach to identify the flexoelectric surface stress tensor will be provided.

3.2.2 Euler-Lagrange Equations

The Euler-Lagrange derivatives with respect to $\mathbf{X}$, $\mathbf{e}_a$, $\mathbf{n}$, g_{ab}, and K_{ab}, respectively, are written as:

$$\nabla_a \tilde{\mathbf{f}}^a = \frac{1}{3} P\mathbf{n} + \pi \cdot \frac{\partial \mathbf{E}_{\text{ext}}}{\partial \mathbf{X}} , \tag{3.10a}$$

$$\tilde{\mathbf{f}}^a = (\tilde{\Lambda}^{ac} K_c^b + 2\tilde{\lambda}^{ab})\mathbf{e}_b - \tilde{\lambda}_\perp^a \mathbf{n} , \tag{3.10b}$$

$$\begin{aligned} 0 &= \left[\nabla_b \tilde{\Lambda}^{ab} + \tilde{\lambda}_\perp^a - \frac{1}{3} P\mathbf{X} \cdot \mathbf{e}^a + \frac{1}{D} (\mathbf{E}_{\text{ext}} \cdot \mathbf{n})(\mathbf{E}_{\text{ext}} \cdot \mathbf{e}_b^a) \right] \mathbf{e}_a \\ &+ \left[2\tilde{\lambda}_n - \tilde{\Lambda}^{ab} K_{ab} - \frac{1}{3} P\mathbf{X} \cdot \mathbf{n} + \frac{1}{D} (\mathbf{E}_{\text{ext}} \cdot \mathbf{n})^2 \right] \mathbf{n} , \end{aligned} \tag{3.10c}$$

$$\tilde{\lambda}^{ab} = \frac{1}{2} \tilde{T}^{ab} + \frac{1}{6} P\mathbf{X} \cdot \mathbf{n} g^{ab} + \frac{1}{4D} \left(\mathbf{E}_{\text{ext}}^2 - (\mathbf{E}_{\text{ext}} \cdot \mathbf{n})^2 \right) g^{ab} , \tag{3.10d}$$

$$\tilde{\Lambda}^{ab} = -\tilde{H}^{ab} . \tag{3.10e}$$

To obtain Eq. (3.10), the Weingarten equations $\nabla_a \mathbf{n} = K_a^b \mathbf{e}_b$, and the Gauss equations $\nabla_a \mathbf{e}_b = -K_{ab}\mathbf{n}$ are used. One also uses:

$$\widetilde{\mathcal{H}}^{ab} := \frac{\delta \mathcal{H}}{\delta K_{ab}} \quad \text{and} , \tag{3.11a}$$

$$\widetilde{\mathcal{T}}^{ab} := -\frac{2\delta(\sqrt{g}\mathcal{H})}{\sqrt{g}\delta g_{ab}} . \tag{3.11b}$$

where $\widetilde{\mathcal{T}}^{ab}$ is known as the intrinsic stress tensor associated to the metric tensor g_{ab} [63]. Equation (3.10a) reveals the existence of a non-equilibrium expression for the multiplier $\tilde{\mathbf{f}}^a$ (*i.e.*, equilibrium situation: $\nabla_a \tilde{\mathbf{f}}^a = 0$).

In Eq. (3.10d) it is possible to implement the derivatives of $\sqrt{g}$ with respect to the metric (*i.e.*, $\frac{\partial \sqrt{g}}{\partial g_{ab}} = \frac{1}{2}\sqrt{g} g^{ab}$); in Eq. (3.10c) completeness $\mathbf{X} = (\mathbf{X} \cdot \mathbf{e}^a)\mathbf{e}_a + (\mathbf{X} \cdot \mathbf{n})\mathbf{n}$ is used. Using the equations (3.10c), (3.10d), and (3.10e), it is feasible to easily eliminate the Lagrange multipliers on the right hand side of Eq. (3.10b) to provide an explicit expression for $\tilde{\mathbf{f}}^a$ in terms of geometrical and electoromechanical variables. From Eq. (3.10c) $\tilde{\lambda}_\perp^a = -\nabla_b \tilde{\Lambda}^{ab} + \frac{1}{3} P\mathbf{X} \cdot \mathbf{e}^a - \frac{1}{D}(\mathbf{E}_{\text{ext}} \cdot \mathbf{n})(\mathbf{E}_{\text{ext}} \cdot \mathbf{e}_b^a)$ due to the linear independence of $\mathbf{e}_a$ and $\mathbf{n}$ is found; Eqs. (3.10d) and (3.10e) reveal $\tilde{\lambda}^{ab}$ and $\tilde{\Lambda}^{ab}$. Therefore, with simplifications of Eq. (3.10b) an expression for the multiplier $\tilde{\mathbf{f}}^a$, which pins the tangent vector to the flexoelectric membrane surface is obtained:

$$\begin{aligned}\tilde{\mathbf{f}}^a &= \mathbf{f}^a - \frac{2}{3}P\mathbf{J}^a - \frac{1}{D}\left(\frac{1}{2}\left[\left((\mathbf{E}_{\text{ext}}\cdot\mathbf{n})^2 - \mathbf{E}_{\text{ext}}^2\right)g^{ab}\right]\mathbf{e}_b - \left[(\mathbf{E}_{\text{ext}}\cdot\mathbf{n})(\mathbf{E}_{\text{ext}}\cdot\mathbf{e}^{\mathbf{a}})\right]\mathbf{n}\right) \\ &= \mathbf{f}^a - \frac{2}{3}P\mathbf{J}^a + \mathbf{E}^a\end{aligned} \tag{3.12}$$

where $\mathbf{f}^a = \left(\mathcal{T}^{ab} - \mathcal{H}^{ac}K_c^b\right)\mathbf{e}_b - \left(\nabla_b\mathcal{H}^{ab}\right)\mathbf{n}$, is the original stress tensor without flexoelectricity [62] and osmotic pressure. Moreover,

$$\mathbf{J}^a = \frac{1}{2}\left[(\mathbf{X}\cdot\mathbf{e}^a)\mathbf{n} - (\mathbf{X}\cdot\mathbf{n})\mathbf{e}^a\right] = \frac{1}{2}\mathbf{X}\times(\mathbf{n}\times\mathbf{e}^a)\ . \tag{3.13}$$

is the *Jemal* tensor. The divergence of the *Jemal* tensor equals the normal vector as:

$$\mathbf{n} = \nabla_a\mathbf{J}^{\,a}\ . \tag{3.14}$$

with this in mind, one can reformulate Eq. (3.10a) as:

$$\nabla_a\tilde{\mathbf{f}}^a = P\mathbf{n} + \boldsymbol{\pi}\cdot\frac{\partial\mathbf{E}_{\text{ext}}}{\partial\mathbf{X}}\ . \tag{3.15}$$

which indicates pressure as a source of normal stress [64].

It, then, can be simplified further by defining the new effective flexoelectric stress tensor of the membrane $\mathbf{f}_e^a$, which is normalized by κ as below:

$$\mathbf{f}_e^a = \mathbf{f}^a - \tilde{P}\mathbf{J}^a + \mathbf{E}^a \tag{3.16}$$

Where the flexoelectric stress tensor term stems from the external electric field:

$$\mathbf{E}^a = \frac{1}{D}\left(\frac{1}{2}\left[\mathbf{E}_{\text{ext}}^2 - (\mathbf{E}_{\text{ext}}\cdot\mathbf{n})^2\right]\mathbf{e}^a + \left[(\mathbf{E}_{\text{ext}}\cdot\mathbf{n})(\mathbf{E}_{\text{ext}}\cdot\mathbf{e}^a)\right]\mathbf{n}\right) \tag{3.17}$$

The divergence of the flexoelectric stress tensor (3.17) calculates as below:

$$
\begin{aligned}
\nabla_a \mathbf{E}^a &= \frac{1}{D}\left\{ \frac{-K}{2}\left[\mathbf{E}_{\text{ext}}^2 - (\mathbf{E}_{\text{ext}}\cdot\mathbf{n})^2\right]\mathbf{n} + \nabla_a\left[(\mathbf{E}_{\text{ext}}\cdot\mathbf{n})(\mathbf{E}_{\text{ext}}\cdot\mathbf{e}^a)\right]\mathbf{n} \right. \\
&\left. + \frac{1}{2}\nabla_a\left[\mathbf{E}_{\text{ext}}^2 - (\mathbf{E}_{\text{ext}}\cdot\mathbf{n})^2\right]\mathbf{e}^a + (\mathbf{E}_{\text{ext}}\cdot\mathbf{n})(\mathbf{E}_{\text{ext}}\cdot\mathbf{e}^a)\nabla_a\mathbf{n} \right\} ;, \\
&= \frac{1}{D}\left\{ \frac{-K}{2}\left[\mathbf{E}_{\text{ext}}^2 - (\mathbf{E}_{\text{ext}}\cdot\mathbf{n})^2\right] + \nabla_a\left[(\mathbf{E}_{\text{ext}}\cdot\mathbf{n})(\mathbf{E}_{\text{ext}}\cdot\mathbf{e}^a)\right] \right\}\mathbf{n} + \left[\pi\cdot\nabla_a\mathbf{E}_{\text{ext}}\right]\mathbf{e}^a \, .
\end{aligned}
\tag{3.18}
$$

Therefore, the electric field acts as a source of normal and tangential stresses which have to be equilibrated by the geometrical stresses.

3.2.3 Shape Equation

In the last section, the stress tensor has been obtained. Here, the shape equation expression provided by conservation of the stress tensor and the projection onto the normal vector [62] as below:

$$
\mathcal{E} := \mathbf{n}\cdot\nabla_a\mathbf{f}_e^a \tag{3.19}
$$

Which is zero in equilibrium.

3.2.4 External Forces Across an Arbitrary Contour of Surface

To identify the external forces, the first step is considering the effective stress tensor, $\mathbf{f}_e^a (a\in\{1,2\})$, of the flexoelectric fluid membrane at every point by knowing the shape of the free flexoelectric membrane [62, 64]:

$$
\begin{aligned}
\mathbf{f}_e^a &= \left\{ K(K^{ab} - \frac{K}{2}g^{ab}) - [\frac{\tilde{P}}{2}(\mathbf{X}\cdot\mathbf{n}) + \tilde{\sigma} - \frac{1}{2D}(\mathbf{E}_{\text{ext}}^2 - (\mathbf{E}_{\text{ext}}\cdot\mathbf{n})^2)]g^{ab} \right\}\mathbf{e}_b \\
&- \left\{ \nabla_a K - \frac{\tilde{P}}{2}(\mathbf{X}\cdot\mathbf{e}^a) - \frac{1}{D}(\mathbf{E}_{\text{ext}}\cdot\mathbf{n})(\mathbf{E}_{\text{ext}}\cdot\mathbf{e}^a) \right\}\mathbf{n} \, .
\end{aligned}
\tag{3.20}
$$

The local force density ($\tilde{f}_\perp := l_a\mathbf{e}^a$), *i.e.,* the force per unit length, transmitted along the contour on the flexoelectric membrane, obtained by the projection onto the unit vector, conormal, $\mathbf{l} = l_a\mathbf{e}^a$ which is perpendicular to the contact line, gives the local force density:

$$
\begin{aligned}
l_a \mathbf{f}_e^a = & \left\{ \frac{1}{2}(K_\perp^2 - K_\parallel^2) - \left[\frac{\tilde{P}}{2}(\mathbf{X}\cdot\mathbf{n}) + \tilde{\sigma} - \frac{1}{2D}(E_a^2 - (\mathbf{E}_{\text{ext}}\cdot\mathbf{n})^2) \right] \right\} \mathbf{l} \\
& - \left\{ \nabla_\perp K - \frac{\tilde{P}}{2}(\mathbf{X}\cdot\mathbf{l}) - \frac{1}{D}(\mathbf{E}_{\text{ext}}\cdot\mathbf{n})(\mathbf{E}_{\text{ext}}\cdot\mathbf{l}) \right\} \mathbf{n}
\end{aligned}
\tag{3.21}
$$

where $\mathbf{l}$ and $\mathbf{n}$ are conormal and normal vectors respectively which are perpendicular to the contour and to one another in every point of the curve. Besides, $\mathbf{l}$ is tangential to the flexoelectric membrane while $\mathbf{n}$ is normal. $K_\perp$ and $K_\parallel$ are curvatures perpendicular (in $\mathbf{l}$ direction) and tangential to the curve. The $\nabla_\perp$ shows the derivation along $\mathbf{l}$. Integration of the flux along an arbitrary enclosed curve,γ, on the flexoelectric fluid membrane will give the external force acting on the membrane:

$$
\mathbf{F_{ext}} = -\mathbf{e}_a \cdot \oint_\gamma ds l_a \mathbf{f}_e^a \, . \tag{3.22}
$$

3.3 Inhomogeneous Electric Field

As already described, the total energy function of the flexoelectric fluid membranes provided in Eq. (3.4) is highly nonlinear. Thus, there exists no magical way to find an exact solution for the shape equation. It is feasible to introduce a practical half-numeric method in this section. In this respect, one can shift to the arc-length parametrization ($\psi(s)$) (see details in an appendix. C), where ψ is the angle along the tangent to the flexoelectric membrane and the horizontal axis. It is possible to consider a general inhomogeneous electric field in the cylindrical coordinate system as:

$$
\mathbf{E}_{\text{ext}}(\rho, \mathbf{z}) = E_{ext}{}^{\rho}\rho + E_{ext}{}^{z}\mathbf{z} \, . \tag{3.23}
$$

Shape equation:

By making use of Eqs. (3.12) and (3.19), and the normal vector projection of the conservation law, one can derive an expression for the shape equation as:

$$\begin{aligned}\mathcal{E} = P + \frac{1}{D}\Bigg[& -\frac{K}{2}(\mathbf{E}_{\text{ext}}{}^{\rho 2} + \mathbf{E}_{\text{ext}}{}^{z2} - \mathbf{E}_{\text{ext}}{}^{\rho 2}\sin^2\psi - \\ & - \mathbf{E}_{\text{ext}}{}^{z2}\cos^2\psi - \mathbf{E}_{\text{ext}}{}^{\rho}\mathbf{E}_{\text{ext}}{}^{z}\sin 2\psi) + \\ & + (\partial_\rho(\mathbf{E}_{\text{ext}}{}^{\rho 2})\hat{\rho} - \partial_z(\mathbf{E}_{\text{ext}}{}^{z2})\hat{z})\frac{sin2\psi}{2} + \\ & + \partial_\rho(\mathbf{E}_{\text{ext}}{}^{\rho})\mathbf{E}_{\text{ext}}{}^{z}\hat{\rho}cos2\psi + \partial_z(\mathbf{E}_{\text{ext}}{}^{z})E_a^{\rho}\hat{z}cos2\psi\Bigg]\end{aligned} \tag{3.24}$$

3.3.1 Hamilton Equations for Inhomogeneous Electric Field

In the following, the equation which illustrates the extension of $\psi(s)$ across the cross-section of the free flexoelectric membrane will be examined. This equation is a fourth-order ordinary differential equation. To facilitate the numerical integration, one can reformulate this by making use of the Hamilton formalism.

The scaled energy of the free part of an axisymmetric flexoelectric fluid membrane with purely tangential polarization and subject to the availability of an inhomogeneous electric field can be written as:

$$\begin{aligned}\widetilde{E} &:= \frac{E}{\pi\kappa} \\ &= \int_{\underline{s}}^{\bar{s}} ds \left[\rho\left(\dot{\psi} + \frac{\sin\psi}{\rho}\right)^2 + 2\tilde{\sigma}\rho + \lambda_\rho(\dot{\rho} - \cos\psi) + \lambda_z(\dot{z} - \sin\psi) + \tilde{P}\rho^2\sin\psi \right. \\ &\left. - \frac{\rho}{2D}\Big((\bar{E}^{\rho}_{ext})^2 + (\bar{E}^{z}_{ext})^2 - (\bar{E}^{\rho}_{ext})^2\sin^2\psi - (\bar{E}^{z}_{ext})^2\cos^2\psi - \bar{E}^{\rho}_{ext}\bar{E}^{z}_{ext}\sin 2\psi\Big)\right],\end{aligned} \tag{3.25}$$

where $\tilde{P} := \frac{P}{\kappa}$ is the scaled pressure and $\tilde{\sigma} := \frac{\sigma}{\kappa}$ is the scaled tension. The parametrized angle-arc-length couple to the Euclidean coordinate system (ρ, z) by Lagrange multipliers λ_ρ and λ_z. The last five terms of Eq. (3.25) are obtained from the flexoelectric energy term:

$$\begin{aligned}&\frac{-1}{2D}\left(\mid \mathbf{E}_{\text{ext}} \mid^2 -(\mathbf{E}_{\text{ext}}\cdot\mathbf{n})^{\mathbf{2}}\right)\\ &:= \frac{-1}{2D}\left((\bar{E}^{\rho}_{ext})^2+(\bar{E}^{z}_{ext})^2-(\bar{E}^{\rho}_{ext})^2\sin^2\psi-(\bar{E}^{z}_{ext})^2\cos^2\psi-\bar{E}^{\rho}_{ext}\bar{E}^{z}_{ext}\sin 2\psi\right)\ .\end{aligned} \tag{3.26}$$

The scaled energy, $\widetilde{E} := \frac{E}{\pi\kappa} = \int_{\underline{s}}^{\bar{s}} ds\widetilde{L}$, allows to peel the scaled Lagrangian off the Euler Lagrange equation:

$$\begin{aligned}\widetilde{L} &= \rho\left(\dot{\psi}+\frac{\sin\psi}{\rho}\right)^2+2\tilde{\sigma}\rho+\lambda_\rho\left(\dot{\rho}-\cos\psi\right)+\lambda_z\left(\dot{z}-\sin\psi\right)+\widetilde{P}\rho^2\sin\psi\\ &-\frac{\rho}{2D}\left((\bar{E}^{\rho}_{ext})^2+(\bar{E}^{z}_{ext})^2-(\bar{E}^{\rho}_{ext})^2\sin^2\psi-(\bar{E}^{z}_{ext})^2\cos^2\psi-\bar{E}^{\rho}_{ext}\bar{E}^{z}_{ext}\sin 2\psi\right)\end{aligned} \tag{3.27}$$

The systems' conjugate momenta , $p_i = \frac{\partial\tilde{L}}{\partial q_i}$, read:

$$p_\psi = \frac{\partial\tilde{L}}{\partial\dot{\psi}} = 2\rho\left(\dot{\psi}+\frac{\sin\psi}{\rho}\right)\ , \tag{3.28a}$$

$$p_\rho = \frac{\partial\tilde{L}}{\partial\dot{\rho}} = \lambda_\rho\ , \tag{3.28b}$$

$$p_z = \frac{\partial\tilde{L}}{\partial\dot{z}} = \lambda_z\ . \tag{3.28c}$$

The scaled Hamiltonian is then given by:

$$\begin{aligned}\widetilde{H} &= \dot{\psi}p_\psi+\dot{\rho}p_\rho+\dot{z}p_z-\tilde{L}\\ &= \frac{p_\psi^2}{4\rho}-p_\psi\frac{\sin\psi}{\rho}-2\tilde{\sigma}\rho+p_\rho\cos\psi+p_z\sin\psi-\tilde{P}\rho^2\sin\psi\\ &+\frac{\rho}{2D}\left((\bar{E}^{\rho}_{ext})^2+(\bar{E}^{z}_{ext})^2-(\bar{E}^{\rho}_{ext})^2\sin^2\psi-(\bar{E}^{z}_{ext})^2\cos^2\psi-\bar{E}^{\rho}_{ext}\bar{E}^{z}_{ext}\sin 2\psi\right)\end{aligned} \tag{3.29}$$

$\widetilde{H}$ is a conserved quantity since it does not explicitly depend on the arc-length s. By making use of the Hamiltonian formalism one can obtain six first-order ordinary differential equations instead of having a fourth-order equation. These Hamilton equations are:

$$\dot{\psi} = \frac{\partial \widetilde{H}}{\partial p_\psi} = \frac{p_\psi}{2\rho} - \frac{\sin\psi}{\rho}\,, \tag{3.30a}$$

$$\dot{\rho} = \frac{\partial \widetilde{H}}{\partial p_\rho} = \cos\psi\,, \tag{3.30b}$$

$$\dot{z} = \frac{\partial \widetilde{H}}{\partial p_z} = \sin\psi\,, \tag{3.30c}$$

$$\begin{aligned}\dot{p}_\psi &= -\frac{\partial \widetilde{H}}{\partial \psi} = \left(\frac{p_\psi}{\rho} + \widetilde{P}\rho^2 - p_z\right)\cos\psi + p_\rho \sin\psi \\ &- \frac{\rho}{2D}\left(({E^z_{ext}}^2 - {E^\rho_{ext}}^2)\sin 2\psi - 2E^\rho_{ext}E^z_{ext}\cos 2\psi\right)\,,\end{aligned} \tag{3.30d}$$

$$\begin{aligned}\dot{p}_\rho &= -\frac{\partial \widetilde{H}}{\partial \rho} = \frac{p_\psi}{\rho}\left(\frac{p_\psi}{4\rho} - \frac{\sin\psi}{\rho}\right) + 2\widetilde{\sigma} + 2\widetilde{P}\rho\sin\psi \\ &- \frac{1}{2D}((\bar{E}^\rho_{ext})^2 + (\bar{E}^z_{ext})^2 - (\bar{E}^\rho_{ext})^2\sin^2\psi \\ &- (\bar{E}^z_{ext})^2\cos^2\psi - \bar{E}^\rho_{ext}\bar{E}^z_{ext}\sin 2\psi) \\ &- \frac{\rho}{2D}\left(\partial_\rho({E^\rho_{ext}}^2) - \partial_\rho({E^\rho_{ext}}^2)\sin^2\psi - \partial_\rho(E^\rho_{ext})E^z_{ext}\sin 2\psi\right)\,,\end{aligned} \tag{3.30e}$$

$$\dot{p}_z = -\frac{\partial \widetilde{H}}{\partial z} = -\frac{\rho}{2D}\left(\partial_z({E^z_{ext}}^2) - \partial_z({E^z_{ext}}^2)\cos^2\psi - E^\rho_{ext}\partial_z(E^z_{ext})\sin 2\psi\right) \tag{3.30f}$$

where $\partial_\rho := \frac{\partial}{\partial\rho}$, and $\partial_z := \frac{\partial}{\partial z}$.

It is possible to solve these six Hamilton equations by a shooting method for a given external electric field [65] (see Chap. 4 as an example).

3.3.2 External Force for the Axisymmetric Flexoelectric Membranes

The generic form of the external force Eq. (3.22) cannot be integrated. However, the arc-angle-length axisymmetric parametrization facilitates its integration. In this parametrization, the principal curvatures are $K_\perp := -\dot{\psi}$, and $K_\parallel := \frac{\sin\psi}{\rho}$ where ρ is the polar radius and ψ is the angle between the polar direction, and the tangent along the meridian. Consequently, in this parametrization with an inhomogeneous axisymmetric electric field as $\mathbf{E}_{\text{ext}} = E^\rho_{ext}\boldsymbol{\rho} + E^z_{ext}\mathbf{z}$, we can identify the local force density along the contact line as follows:

$$
\begin{aligned}
l_a \mathbf{f}_e^a = & \left\{ \frac{1}{2}(\dot{\psi}^2 - \frac{\sin^2\psi}{\rho^2}) - [\frac{\tilde{P}}{2}(\mathbf{X}\cdot\mathbf{n}) + \tilde{\sigma} \right. \\
& \left. - \frac{1}{2D}((E_{ext}^{\rho\ 2} + E_{ext}^{z\ 2}) - (E_{ext}^{\rho}\rho\cdot\mathbf{n} + E_{ext}^{z}\mathbf{z}\cdot\mathbf{n})^2] \right\} \mathbf{l} \\
& - \left\{ \ddot{\psi} + \frac{\dot{\psi}\cos\psi}{\rho} - \frac{\cos\psi\sin\psi}{\rho^2} - \frac{\tilde{P}}{2}(\mathbf{X}\cdot\mathbf{l}) \right. \\
& \left. - \frac{1}{D}\left((E_{ext}^{\rho}\rho\cdot\mathbf{n} + E_{ext}^{z}\mathbf{z}\cdot\mathbf{n})(E_{ext}^{\rho}\rho\cdot\mathbf{l} + E_{ext}^{z}\mathbf{z}\cdot\mathbf{l})\right) + \right\} \mathbf{n} \\
= & \left\{ \frac{1}{2}(\dot{\psi}^2 - \frac{\sin^2\psi}{\rho^2}) - [\frac{\tilde{P}}{2}(\mathbf{X}\cdot\mathbf{n}) + \tilde{\sigma} \right. \\
& \left. - \frac{1}{2D}((E_{ext}^{\rho\ 2} + E_{ext}^{z\ 2}) - (-E_{ext}^{\rho}\sin\psi - E_{ext}^{z}\cos\psi)^2] \right\} \mathbf{l} \\
& - \left\{ \ddot{\psi} + \frac{\dot{\psi}\cos\psi}{\rho} - \frac{\cos\psi\sin\psi}{\rho^2} - \frac{\tilde{P}}{2}(\mathbf{X}\cdot\mathbf{l}) \right. \\
& \left. - \frac{1}{D}\left((E_{ext}^{\rho\ 2} - E_{ext}^{z\ 2})\sin\psi\cos\psi + E_{ext}^{\rho}E_{ext}^{z}(1-2\sin\psi)\right) \right\} \mathbf{n} \,,
\end{aligned}
\tag{3.31}
$$

where one can use the projection of the tangent and normal vectors onto the basis vectors as follows:

$$
\mathbf{z}\cdot\mathbf{l} = -\rho\cdot\mathbf{n} = \sin\psi \,, \tag{3.32}
$$

$$
\mathbf{z}\cdot\mathbf{n} = \rho\cdot\mathbf{l} = -\cos\psi \,, \tag{3.33}
$$

in which the normal vector $\mathbf{n}$ points towards the outside of the vesicle. The integral of its flux through an arbitrary contour γ gives the force as below:

$$
\begin{aligned}
-\mathbf{F_{ext}} = & -\mathbf{z}\cdot\oint_\gamma ds\, l_a \mathbf{f}_e^a \\
= & -\oint_\gamma ds \left(\left\{ \frac{1}{2}(\dot{\psi}^2 - \frac{\sin^2\psi}{\rho^2}) - [\frac{\tilde{P}}{2}(\mathbf{X}\cdot\mathbf{n}) + \tilde{\sigma} \right. \right. \\
& \left. - \frac{1}{2D}((E_{ext}^{2\rho} + E_{ext}^{2z}) - (-E_{ext}^{\rho}\sin\psi - E_{ext}^{z}\cos\psi)^2] \right\} (\mathbf{z}\cdot\mathbf{l}) \\
& - \left\{ \ddot{\psi} + \frac{\dot{\psi}\cos\psi}{\rho} - \frac{\cos\psi\sin\psi}{\rho^2} - \frac{\tilde{P}}{2}(\mathbf{X}\cdot\mathbf{l}) \right. \\
& \left. \left. - \frac{1}{D^2}\left((E_{ext}^{2\rho} - E_{ext}^{2z})\sin\psi\cos\psi + E_{ext}^{\rho}E_{ext}^{z}(1-2\sin\psi)\right) \right\} (\mathbf{z}\cdot\mathbf{n}) \right)
\end{aligned}
\tag{3.34}
$$

3.4 Boundary Condition at Contact Lines

In the previous sections, a Hamiltonian has indicated the energy of the flexoelectric fluid membranes. Besides, one can calculate the external forces that imprint the shape equation of the flexoelectric membranes by the integration of the stresses. The surrounding environment can originate such stresses. For example, if there exists an interface with a solid substrate or another fluid surface, the system may have different domains. Consequently, it is possible to face additional stresses along the contact line.

As soon as the system equilibrates, the contact line will locally adapt to minimize the total energy. Subsequently, one can have boundary conditions that are related to the properties of the surface deformation energy. In the following, we derive a general boundary condition due to the jump occurring in the contact line by making use of the geometric framework, which was introduced earlier in this chapter.

3.4.1 Variation of the Contact Line

There exists a discontinuity across the contact line of the membrane's interface due to the form of the energy density. Thus, one can calculate the related boundary conditions by considering the variation of energy change in the contact line to vanish ($\partial H_{cl} = 0$) [63, 66].

The total energy of adhering membranes concerning the contact line's variation along the substrate should be stationary. Suppose that the contact line is moving locally in a way that part of the membrane detaches from the substrate. This will eliminate the corresponding binding energy and lead to a change in the related energy ∂H_{bound}. Besides, the free part of the flexoelectric membrane at the contact line would want to win this energy such that a change in the energy of the free part also occurs ∂H_{free}. Consequently, it is feasible to have the stationary boundary condition at the contact

line as:

$$\partial H_{cl} = \partial H_{bound} + \partial H_{free} = 0 \tag{3.35}$$

where ∂H_{bound} and ∂H_{free} are the change in the energy associated with the bound part and free part respectively.

3.4.2 Discontinuity at the Contact Line

The total energy of the flexoelectric fluid membrane Eq. (3.4) illustrates the continuous behavior of the membranes. Since it is a quadratic equation, the membrane is differentiable along the contact line that varies locally (see chapter 3 of [63]). Thus, we expect a discontinuity in the slope at the contact point as following:

$$\frac{4w}{\kappa} = \frac{1}{2}\left[\kappa_{\nu}\right]^2 + (w_{\vec{\pi}}^{c} - w_{\vec{\pi}}^{f}) \tag{3.36}$$

where w is the adhesion energy [67,68], and $w_{\vec{\pi}} = \frac{1}{2}\vec{D}\,|\vec{\pi}|^2 - \vec{\pi}\cdot\mathbf{E}_{\text{ext}} = \frac{-1}{2}(\phi^2 - |\,\mathbf{E}_{\text{ext}}\,|^2) = \frac{-\mathbf{E}_{\text{ext}}^2}{2D}\sin^2\psi = -\overline{E}_{ext}\sin^2\psi$ [32,69].

$$\frac{2w}{\kappa} = \left[\kappa_{\nu}\right]^2 + \left(\bar{E}_{ext}^{c} - \bar{E}_{ext}^{f}\right)\sin^2\alpha \tag{3.37}$$

with $[\kappa_{\nu}] = 1 - \psi$ and $w = 0$.

Chapter 4

FLEXOELECTRIC FLUID MEMBRANE VESICLES IN SPHERICAL CONFINEMENT

4.1 Folding Patterns in Nature

Among all of the enigmatic shapes in nature, there exist countless mysterious shapes, just think of the shape of mountains, hills or the cerebellum, mitochondria, and kidney [70–72]. **Folding patterns** are observed in all of these forms. Besides, folding patterns give us insight into the morphology of complex shapes occurring in inanimate nature and living matters [73, 74]. To investigate these phenomena, morphologists or zoologists have a very different scientific approach in comparison to physicists [73, 74]. In contrast, physicists, who are dealing with universal laws and the cause and effect of each phenomenon, consider the mechanical stresses that are exerted on the system to capture the folding patterns [1, 2, 14, 18–23, 36, 73]. Therefore, the main question in this context is: "Why do folding patterns in a specific system occur?". As a physics student, the answer to such a question would be: "It happens either by exerting internal stresses on the system which leads to growth [73] or by applying external stresses or constraints on the system [1, 2, 36, 73].

As an example, the folding patterns of spherically confined fluid membrane vesicles have been studied by Kahraman et al. [2]. In this work, the basic deformation patterns of the membranes were identified resulting from an interplay of geometry and mechanics.

This chapter aims to describe how an additional electric field will change these shapes. In this respect, the main task is to capture the folding patterns of a flexoelectric fluid membrane vesicle inside a spherical cavity in the presence of a uniform electric field, which will exert additional stresses on the system. To this end, one can make use of the general expression introduced in Chap. 2 and the specific framework derived in Chap. 3.

4.2 Theoretical Calculation of Electric Fields in a Spherical Confinement

To be able to determine the shape of the flexoelectric membrane vesicle, one first has to calculate the electric field inside the confining cavity when the whole system is immersed in an external electric field. For the sake of simplicity, an applied uniform electric field, $\mathbf{E}_{\text{ext}}$, which is antiparallel to the z-axis is considered. In the calculations, one has to make sure that the electric field fulfils all boundary conditions.

4.2.1 Dielectric Sphere Model in an Applied Uniform Electric Field $\mathbf{E}_{\text{ext}}$

Consider a simple system consisting of a spherical hard shell [4] with inner radius a and outer radius b, which is inserted in an applied uniform electric field, $\mathbf{E}_{\text{ext}} = -E_{ext}\mathbf{z}$, in an aqueous environment (see Fig. 4.1).

Here, the system is divided into three different spherical domains; an inner spherical environment with water, a hard shell dielectric, and the outer environment filled with water. In this system, ε_w is the dielectric constant of the inner and outer environment and, ε_M is the dielectric constant in the shell membrane. In the following, the three domains are labelled by 1, 2, and 3, corresponding to inside, between, and outside of the shell, respectively (see Fig. 4.1). This shell will serve as the confining sphere

[4] This shell corresponds for example to the outer membrane of a mitochondrion

in which we will insert the flexoelectric membrane vesicle in Sec. 4.3. To determine the electric field inside the shell one has to solve the Laplace equation. The general solution of the Laplace equation in spherical coordinates with azimuthal symmetry is [75]:

$$\Phi_l(\vec{r},\theta) = \sum_{l=0}^{\infty} \left[A_l r^l + C_l r^{-(l+1)} \right] P_l(\cos\theta) \, . \tag{4.1}$$

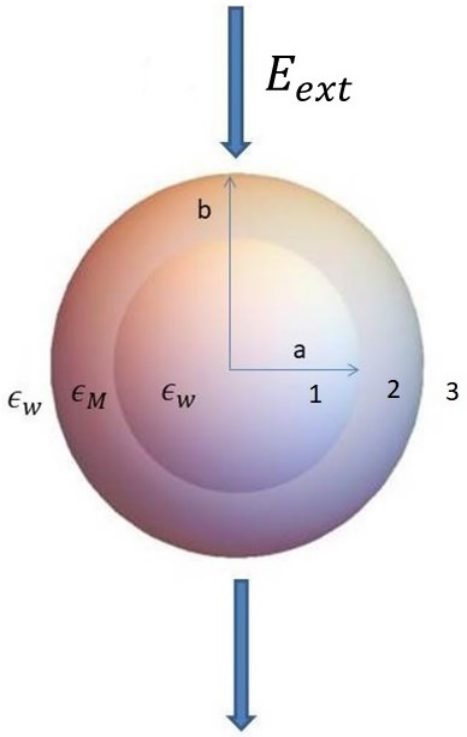

Figure 4.1: Spherical lipid fluid membrane vesicle with inner radius a and outer radius b, which is subjected to an applied uniform electric field in an aqueous environment.

It is possible to obtain the coefficients A_l and C_l with the help of the electrostatic boundary conditions. In this respect, the shell considered being a spherical dielectric which is immersed in a uniform electric field. When the radius of the shell is an infinite, electric potential becomes a constant value of $\phi = -E_{ext} z = E_{ext} r cos(\theta)$, and when the radius is zero, electric potential will be zero. Such that the expressions for the potential at any point in space are given by [75]:

$$\phi_1(\vec{r},\theta) = \left(E_{ext}+\frac{A}{a}\right) r\cos\theta \quad 0<r<a \quad \varepsilon_w\,, \tag{4.2a}$$

$$\phi_2(\vec{r},\theta) = \left(E_{ext}+\frac{B}{a}\right) r\cos\theta + C\frac{b^2}{r^2}\cos\theta \quad a<r<b \quad \varepsilon_M\,, \tag{4.2b}$$

$$\phi_3(\vec{r},\theta) = \left(E_{ext}r + D\frac{b^2}{r^2}\right)\cos\theta \quad r>b \quad \varepsilon_w\,. \tag{4.2c}$$

where ϕ_1, ϕ_2, and ϕ_3 are the electric potentials inside, between, and outside of the shell respectively. Besides, ε_w is the dielectric constant of water and ε_M is the dielectric constant of the spherical confinement. To simplify further, we have scaled our parameters: all lengths are scaled with the inner radius a, and $\widetilde{\varepsilon} = \frac{\varepsilon_M}{\varepsilon_w}$ is the scaled permittivity. All potentials scaled with $E_{\text{ext}}\cdot a$ and $\widetilde{\Phi} = \frac{\Phi}{E_{ext}a}$, $\widetilde{A} = \frac{A}{E_{ext}a}$, $\widetilde{B} = \frac{B}{E_{ext}a}$, $\widetilde{C} = \frac{C}{E_{ext}a}$, $\widetilde{D} = \frac{D}{E_{ext}a}$. Therefore, the scaled electric potentials at any point in space are given by:

$$\widetilde{\Phi}_1(\vec{r},\theta) = \left(1+\widetilde{A}\right)\widetilde{r}\cos\theta \qquad 0<\widetilde{r}<1\,, \tag{4.3a}$$

$$\widetilde{\Phi}_2(\vec{r},\theta) = \left(1+\widetilde{B}\right)\widetilde{r}\cos\theta + \widetilde{C}\left(\frac{\widetilde{b}}{\widetilde{r}}\right)^2\cos\theta \quad 1<\widetilde{r}<\widetilde{b}\,, \tag{4.3b}$$

$$\widetilde{\Phi}_3(\vec{r},\theta) = \left(\widetilde{r}+\widetilde{D}\left(\frac{\widetilde{b}}{\widetilde{r}}\right)^2\right)\cos\theta \qquad \widetilde{r}>\widetilde{b}\,. \tag{4.3c}$$

The scaled boundary conditions due to the continuity of the potential at $r=a$ and $r=b$ can be written as:

$$\widetilde{\Phi}_1(1,\theta) = \widetilde{\Phi}_2(1,\theta)\,, \tag{4.4a}$$

$$\widetilde{\Phi}_3(\widetilde{b},\theta) = \widetilde{\Phi}_2(\widetilde{b},\theta)\,. \tag{4.4b}$$

The boundary conditions of the scaled normal components of the electric displacement field, **D**, are:

$$\frac{\partial\widetilde{\Phi}_1(1)}{\partial\widetilde{r}} = \widetilde{\varepsilon}\frac{\partial\widetilde{\Phi}_2(1)}{\partial\widetilde{r}}\,, \tag{4.5a}$$

$$\widetilde{\varepsilon}\frac{\partial\widetilde{\Phi}_2(\widetilde{b})}{\partial\widetilde{r}} = \frac{\partial\widetilde{\Phi}_3(\widetilde{b})}{\partial\widetilde{r}}\,. \tag{4.5b}$$

Inserting Eq. (4.3) into Eqs. (4.4) and (4.5), results in four linear relations for the scaled coefficients:

$$\widetilde{A} = \widetilde{B} + \widetilde{C}\widetilde{b}^2 \qquad \widetilde{B} = \frac{2\widetilde{C}\widetilde{\varepsilon} - 2\widetilde{D} - \widetilde{\varepsilon} + 1}{\widetilde{\varepsilon}}\,, \tag{4.6a}$$

$$\widetilde{D} = \widetilde{B}\widetilde{b} + \widetilde{C} \qquad \widetilde{C} = \frac{\widetilde{B}\widetilde{\varepsilon} - \widetilde{A} + \widetilde{\varepsilon} - 1}{2\widetilde{\varepsilon}\widetilde{b}}\,. \tag{4.6b}$$

Solving this set of four equations, the general scaled coefficients turn out to be:

$$\widetilde{A} = \frac{2(\widetilde{b}^3\widetilde{\varepsilon} - \widetilde{b}^2\widetilde{\varepsilon}^2 - \widetilde{b}^3 + \widetilde{b}^2\widetilde{\varepsilon} + \widetilde{\varepsilon}^2 - 2\widetilde{\varepsilon} + 1)}{4\widetilde{b}^3\widetilde{\varepsilon} + 2\widetilde{b}^2\widetilde{\varepsilon}^2 + 2\widetilde{b}^3 + \widetilde{b}^2\widetilde{\varepsilon} - 2\widetilde{\varepsilon}^2 + 4\widetilde{\varepsilon} - 2}\,, \tag{4.7a}$$

$$\widetilde{B} = -\frac{2\widetilde{b}^2\widetilde{\varepsilon}^2 - \widetilde{b}^2\widetilde{\varepsilon} - \widetilde{b}^2 - 2\widetilde{\varepsilon}^2 + 4\widetilde{\varepsilon} - 2}{4\widetilde{b}^3\widetilde{\varepsilon} + 2\widetilde{b}^2\widetilde{\varepsilon}^2 + 2\widetilde{b}^3 + \widetilde{b}^2\widetilde{\varepsilon} - 2\widetilde{\varepsilon}^2 + 4\widetilde{\varepsilon} - 2}\,, \tag{4.7b}$$

$$\widetilde{C} = \frac{2\widetilde{b}\widetilde{\varepsilon} - 2\widetilde{b} + \widetilde{\varepsilon} - 1}{4\widetilde{b}^3\widetilde{\varepsilon} + 2\widetilde{b}^2\widetilde{\varepsilon}^2 + 2\widetilde{b}^3 + \widetilde{b}^2\widetilde{\varepsilon} - 2\widetilde{\varepsilon}^2 + 4\widetilde{\varepsilon} - 2}\,, \tag{4.7c}$$

$$\widetilde{D} = -\frac{2\widetilde{b}^3\widetilde{\varepsilon}^2 - \widetilde{b}^3\widetilde{\varepsilon} - \widetilde{b}^3 - 2\widetilde{b}\widetilde{\varepsilon}^2 + 2\widetilde{b}\widetilde{\varepsilon} - \widetilde{\varepsilon} + 1}{4\widetilde{b}^3\widetilde{\varepsilon} + 2\widetilde{b}^2\widetilde{\varepsilon}^2 + 2\widetilde{b}^3 + \widetilde{b}^2\widetilde{\varepsilon} - 2\widetilde{\varepsilon}^2 + 4\widetilde{\varepsilon} - 2}\,. \tag{4.7d}$$

Hence, the general expression for the scaled electric field at any point of space is given by:

$$\widetilde{E}_1(\vec{r},\theta) = -(1+\widetilde{A})\cos\theta\hat{r} + (1+\widetilde{A})\sin\theta\hat{\theta}\,, \tag{4.8a}$$

$$\widetilde{E}_2(\vec{r},\theta) = -\left(1+\widetilde{B}-2\widetilde{C}\frac{\widetilde{b}^2}{r^3}\right)\cos\theta\hat{r} + \left(1+\widetilde{B}+\widetilde{C}\frac{\widetilde{b}^2}{r^3}\right)\sin\theta\hat{\theta}\,, \tag{4.8b}$$

$$\widetilde{E}_3(\vec{r},\theta) = \left(-1+2\widetilde{D}\frac{\widetilde{b}^2}{r^3}\right)\cos\theta\hat{r} + \left(1+\widetilde{D}\frac{\widetilde{b}^2}{r^3}\right)\sin\theta\hat{\theta}\,. \tag{4.8c}$$

After simplification we obtain:

$$\widetilde{E}_1(\vec{r},\theta) = (1+\widetilde{A})\left(-\cos\theta\hat{r} + \sin\theta\hat{\theta}\right)\,, \tag{4.9a}$$

$$\widetilde{E}_2(\vec{r},\theta) = (1+\widetilde{B})\left(-\cos\theta\hat{r} + \sin\theta\hat{\theta}\right) + \widetilde{C}\frac{\widetilde{b}^2}{r^3}\left(2\cos\theta\hat{r} + \sin\theta\hat{\theta}\right)\,, \tag{4.9b}$$

$$\widetilde{E}_3(\vec{r},\theta) = \left(-\cos\theta\hat{r} + \sin\theta\hat{\theta}\right) + \widetilde{D}\frac{\widetilde{b}^2}{r^3}\left(2\cos\theta\hat{r} + \sin\theta\hat{\theta}\right)\,, \tag{4.9c}$$

where Eq. (4.9b) implies a uniform electric field inside the cavity. To understand this model better, one can look at a couple of simple experimental models in the following.

Giant unilamelar vesicles (GUVs)

Giant unilamellar vesicles (GUVs) are spherical vesicles bound by a single bilayer membrane containing an aqueous solution. Their diameter is of the order of $10\mu m$ [76]. They are in vitro used as model systems for biological membranes. For a typical GUV, the scaled parameters are obtained as; $a = 5\mu m$, $\widetilde{b} = 1 + 10^{-3}$, $\varepsilon_w = 80$, $\varepsilon_M = 4$, and $\widetilde{\varepsilon} = \frac{\varepsilon_M}{\varepsilon_w} = \frac{1}{20}$. Inserting these numerical values into the Eq. (4.7) leave us the numerical values of the scaled coefficients as: $\widetilde{A} = -0.012$, $\widetilde{B} = 6.24$, $\widetilde{C} = -6.24$, $\widetilde{D} = 0.007$. Therefore, substituting the scaled coefficients into Eq. (4.9) the scaled electric field at any point in space are derived as:

$$\widetilde{E}_1(\vec{r},\theta) = -0.988\mathbf{z}\,, \tag{4.10a}$$

$$\widetilde{E}_2(\vec{r},\theta) = -7.24\mathbf{z} - \frac{6.24}{\widetilde{r}^3}\left(2\cos\theta\mathbf{r} + \sin\theta\boldsymbol{\theta}\right)\,, \tag{4.10b}$$

$$\widetilde{E}_3(\vec{r},\theta) = -\mathbf{z} + \frac{0.007}{\widetilde{r}^3}\left(2\cos\theta\mathbf{r} + \sin\theta\boldsymbol{\theta}\right)\,. \tag{4.10c}$$

where $\mathbf{z} = \cos\theta\mathbf{r} - \sin\theta\boldsymbol{\theta}$.

Mitochondra

Mitochondria are double membrane-bound organelles which are found in all eukaryotic organisms. They commonly are between 0.75 and $3\mu m$ in diameter [77]. For a typical mitochondria the scaled parameters are; $a = 0.5\mu m$, $\widetilde{b} = 1 + 10^{-2}$, $\varepsilon_w = 80$, $\varepsilon_M = 4$, and $\widetilde{\varepsilon} = \frac{1}{20}$ [78]. Inserting these numerical values into Eq. (4.7), the scaled coefficients are; $\widetilde{A} = -0.11$, $\widetilde{B} = 5.54$, $\widetilde{C} = -5.54$, and $\widetilde{D} = 0.06$. By making use of Eq. (4.9), the scaled electric field in each region is obtained as:

$$\widetilde{E}_1(\vec{r},\theta) = -0.89\mathbf{z}\,, \tag{4.11a}$$

$$\widetilde{E}_2(\vec{r},\theta) = -6.54\mathbf{z} - \frac{5.54}{\widetilde{r}^3}\left(2\cos\theta\mathbf{r} + \sin\theta\boldsymbol{\theta}\right)\,, \tag{4.11b}$$

$$\widetilde{E}_3(\vec{r},\theta) = -\mathbf{z} + \frac{0.61}{\widetilde{r}^3}\left(2\cos\theta\mathbf{r} + \sin\theta\boldsymbol{\theta}\right)\,. \tag{4.11c}$$

In conclusion, we are allowed to assume a uniform electric field inside the cavity when a uniform external external electric field is applied. The only effect of the cavity is an attenuation of the value of the field which is of the order of 1%-10%.

4.3 Confined Flexoelectric Fluid Membrane Vesicles in the Presence of an Applied Electric Field

In Sec. 2.1, the structure of lipid bilayers that are the essential part of the walls of cells and its compartments was introduced. They consist of two layers of phospholipids that can form intricate structures. The mitochondrion, for example, is a system built by two of such membranes: the highly folded inner membrane and the confining outer one. The mitochondria provide the energy to the cells via the adenosine triphosphate (ATP) molecules. The folds called, *cristae*, increase the area of the inner membrane to enhance the ability of mitochondria to produce ATP [79]. Mitochondria *in vivo* can have diverse shapes from large tubes to small sphere. *In vitro* they are ellipsoidal or spherical [80].

As an abstract model of such systems, one can study a fluid membrane vesicle inside a spherical outer membrane. The inner membrane is modelled as an elastic fluid surface, whereas the outer one is assumed to be much stiffer. This system has stimulated several studies only recently [1, 2, 76, 81–83]. For instance, Kahraman et al. [2] numerically obtained the morphology of spherically confined fluid membranes. They indicated that the transformation of axisymmetric invaginations to ellipsoidal invaginations happens when increasing the surface area, followed by a transition to a stomatocyte.

As another research review on this subject, one can mention the research by Bouzar et al. [36] on a spherically confined toroidal membrane. This study demonstrates a shape transition from spherical to a toroidal configuration, for different values of volume and area. It also displays that a change in the topology can be energetically favourable.

In the following, we will switch on an external uniform electric field and investigate the folding patterns of a spherically confined flexoelectric membrane due to external stress.

4.3.1 Theoretical Model

In Sec. 3.2 the total energy of a flexoelectric fluid membrane in the presence of an electric field, Eq. (3.4), was introduced to find equilibrium solutions and to identify the energy minima. Here, the main aim is to capture the folding pattern of a closed flexoelectric fluid membrane of constant volume and area surrounded by spherical confinement in the presence of an electric field. Since the energy scales of the surface and pressure contributions are much larger than the bending energy [22], these terms are included as constraints on the total surface area $\bar{A}$ and enclosed volume $\bar{V}$ of the membrane vesicle. For simplification, the two quantities with the corresponding area A_0 and volume V_0 of the confining container are scaled [1, 2]:

$$a = \bar{A}/A_0 \quad \text{and} \quad v = \bar{V}/V_0 \,. \tag{4.12}$$

Flexoelectricity adds another contribution to the total energy when an external electric field $\mathbf{E}_{\text{ext}}$ is present. Following Steigmann and Agrawal, the corresponding energy of the flexoelectric membrane is given by [32]:

$$E_{\text{f}} = \int_{\Omega} \left[\frac{1}{2D} [(\mathbf{E}_{\text{ext}} \cdot \mathbf{n})^2 - |\mathbf{E}_{\text{ext}}|^2] \right] \mathrm{d}A \,, \tag{4.13}$$

where $\mathbf{n}$ is the normal vector of the membrane surface and $D = \chi_\perp - \frac{c_2^2}{k_3}$ the material constant which indicates the strength of the flexoelectric effect (see Sec. 3.1).

In the following, a uniform electric field, which is pointing in the antiparallel $\mathbf{z}$-direction, $\mathbf{E}_{\text{ext}} = -E_{\text{ext}}\mathbf{z}$ will be considered. In Sec. 3.2, total energy was found:

$$E_{\text{tot}} = \int_\Omega dA \left(\frac{\kappa}{2}(2K - C_0)^2 + \overline{\kappa} K_G + \sigma + \frac{1}{2D}[(\mathbf{E}_{\text{ext}} \cdot \mathbf{n})^2 - |\mathbf{E}_{\text{ext}}|^2] \right) + \int dVP \quad (4.14)$$

In equilibrium, lipids will not exchange between the membrane and the solution. This implies that the area is constrained. The pressure difference between the inside and the outside of the membrane must be constant in equilibrium. The resulting forces lead the volume v inside the vesicle to remain invariant as well. Thus, volume and area constraints enter the energy expression *via* the Lagrange multipliers σ and P. One can also consider the flexoelectric membrane to be flat without any other constraints, which results in a vanishing spontaneous curvature ($C_0 = 0$). It is then possible to reformulate the total energy of the system:

$$E = \int dA \left(\frac{\kappa}{2}(2K)^2 + \sigma + \frac{1}{2D}[(\mathbf{E}_{\text{ext}} \cdot \mathbf{n})^2 - |\mathbf{E}_{\text{ext}}|^2] \right) + \int dVP \,. \quad (4.15)$$

For the sake of simplicity, one can define a dimensionless electric field parameter:

$$e = \frac{E_{\text{ext}}^2 R^2}{D\kappa} \,, \quad (4.16)$$

where R is the radius of the confining sphere. This finally allows writing the scaled total energy of a free flexoelectric membrane vesicle as:

$$\tilde{E}_{\text{tot}} = \int_\Omega u \, \mathrm{d}\tilde{A} = \int_\Omega \left[2\tilde{K}^2 + \frac{1}{2} e[(\mathbf{z} \cdot \mathbf{n})^2 - 1] \right] \mathrm{d}\tilde{A} + \text{constraints} \,, \quad (4.17)$$

where all lengths are scaled with R. The expressions for the constraints on area and volume depend on the numerical solution methods, as explained in the Appendix. C. Inverting the direction of the electric field does not change the equilibrium shapes since $\mathbf{E}_{\text{ext}}$ enters the equations quadratically.

To include the effect of the confinement, one can model the spherical cavity as a rigid container. A simple calculation shows that a uniform electric field, which is applied at infinity, Sec. 4.2, stays uniform inside the container as long as the whole system—except the membrane vesicle which does not contribute due to the neglection of the self-field—consists of isotropic dielectric media [75]. This rather crude approximation allows obtaining a first idea of the shapes that flexoelectric membrane vesicles can adopt in a spherical confinement. To make contact with more realistic experimental setups, one would have to take into account an electrolyte in the interior of the container.

Because of the nonlinearity of Eq. (4.15), a simple solution cannot be found. To minimize the energy of the system, the first variation of the total energy, as explained in the Chp. 3, is essential. There are two possibilities to proceed: numerical simulations or Runge-Kutta integration for the axisymmetric case. If we suppose that the folding of the flexoelectric membrane is axially symmetric concerning the z-axis, we can make use of the angle-arc-length parametrization $\psi(s)$ (see Sec. 3.3.1). In this parametrization, $\psi(s)$ is the angle between the tangent vector and the x axis, whereas s denotes the arc length (see Figure. 4.2, and Appendix. C).

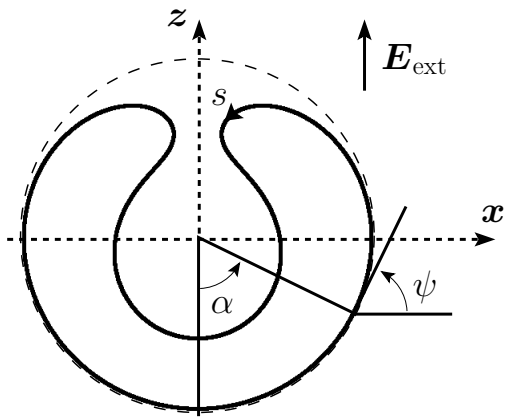

Figure 4.2: Parametrization of the axially symmetric flexoelectric fluid membrane in spherical confinement. The solid black line represents the cross-section of the axisymmetric flexoelectric membrane. The dashed line indicates the spherical confinement. s is the arc-length, ψ is the angle between the x axis and the tangent of the flexoelectric membrane and α represents the detachment angle of the flexoelectric membrane from the confinement. The flexoelectric free membrane consists of two segments, a spherical segment in contact with the confinement (bottom part) and an upper free segment whose shape is determined by solving the Hamilton equation (4.26) together with the appropriate boundary conditions (4.27).

In this parametrization the area element dA is given by:

$$dA = 2\pi\rho ds \tag{4.18}$$

and the volume element dV:

$$dV = \pi\rho^2 \sin\psi ds \tag{4.19}$$

The mean curvature is obtained as:

$$K = -\frac{1}{2}\left(\dot{\psi} + \frac{\sin\psi}{\rho}\right), \tag{4.20}$$

where the curvature in the meridian direction is $c_\perp = -\dot{\psi}$, and the curvature along the parallel direction is $c_\parallel = -\frac{\sin\psi}{\rho}$. The flexoelectric energy term simplifies to:

$$\frac{-1}{2D}\left(\mid \mathbf{E}_{\text{ext}} \mid^2 -(\mathbf{E}_{\text{ext}}\cdot\mathbf{n})^2\right) = \frac{-{E_{\text{ext}}}^2}{2D}\sin^2\psi\,. \tag{4.21}$$

Inserting Eqs. (4.18), (4.19), (4.20), and (4.21) into Eq. (4.15) allows to formulate the scaled energy functional of the free part of an axisymmetric flexoelectric confined membrane with purely tangential polarizations as follows:

$$\begin{aligned}\tilde{E} &:= \frac{E}{\pi\kappa} = \int_{\underline{s}}^{\bar{s}} ds\tilde{L} \\ &= \int_{\underline{s}}^{\bar{s}} ds\left[\rho\left(\dot{\psi}+\frac{\sin\psi}{\rho}\right)^2 + 2\tilde{\sigma}\rho + \lambda_\rho(\dot{\rho}-\cos\psi) + \lambda_z(\dot{z}-\sin\psi) + \tilde{P}\rho^2\sin\psi - \rho e\sin^2\psi\right],\end{aligned} \tag{4.22}$$

where $\tilde{\sigma} = \frac{\sigma R^2}{\kappa}$ and $\tilde{P} = \frac{PR^3}{\kappa}$ are the scaled surface tension and pressure, respectively. The Lagrange multiplier functions λ_ρ and λ_z fix the geometrical constraints $\dot{z} = \sin\psi$ and $\dot{\rho} = \cos\psi$ along the profile. In the integral, $\underline{s}$ represents the arc-length at the contact point and $\bar{s}$ corresponds to the arc-length at the z-axis where the tangent of the membrane is parallel to x. All lengths are scaled with the radius R of the confining sphere. The dimensionless electric field parameter e is defined as:

$$e = \frac{E_{\text{ext}}^2 R^2}{D\kappa}\,, \tag{4.23}$$

which can be positive or negative depending on the flexodielectric constant, D. If the flexoelectric effect is weak, e is positive, and if the flexoelectric effect is strong e is negative [32].

4.3.2 Hamilton Equations and Boundary Conditions

To simplify the numerical integration, one can resort to the Hamiltonian formulation of the problem.

Hamilton equations

In this respect, the conjugate momenta of the system are:

$$p_\psi = \frac{\partial \tilde{L}}{\partial \dot{\psi}} = 2\rho\left(\dot{\psi} + \frac{\sin\psi}{\rho}\right), \tag{4.24a}$$

$$p_\rho = \frac{\partial \tilde{L}}{\partial \dot{\rho}} = \lambda_\rho, \tag{4.24b}$$

$$p_z = \frac{\partial \tilde{L}}{\partial \dot{z}} = \lambda_z . \tag{4.24c}$$

From Eqs. (4.24) and (4.22), one obtains the scaled Hamiltonian *via* the Hamiltonian formalism:

$$\begin{aligned}\widetilde{H} &= \dot{\psi} p_\psi + \dot{\rho} p_\rho + \dot{z} p_z - \tilde{L} \\ &= \frac{p_\psi^2}{4\rho} - p_\psi \frac{\sin\psi}{\rho} - 2\tilde{\sigma}\rho + p_\rho \cos\psi + p_z \sin\psi - \tilde{P}\rho^2 \sin\psi + e\rho\sin^2\psi .\end{aligned} \tag{4.25}$$

Instead of having one fourth-order equation one obtains six first-order ordinary Hamilton equations:

$$\dot{\psi} = \frac{\partial \widetilde{H}}{\partial p_\psi} = \frac{p_\psi}{2\rho} - \frac{\sin\psi}{\rho}, \tag{4.26a}$$

$$\dot{\rho} = \frac{\partial \widetilde{H}}{\partial p_\rho} = \cos\psi, \tag{4.26b}$$

$$\dot{z} = \frac{\partial \widetilde{H}}{\partial p_z} = \sin\psi, \tag{4.26c}$$

$$\dot{p}_\psi = -\frac{\partial \widetilde{H}}{\partial \psi} = \left(\frac{p_\psi}{\rho} + \widetilde{P}\rho^2 - p_z\right)\cos\psi + p_\rho \sin\psi - 2e\rho\sin\psi\cos\psi, \tag{4.26d}$$

$$\dot{p}_\rho = -\frac{\partial \widetilde{H}}{\partial \rho} = \frac{p_\psi}{\rho}\left(\frac{p_\psi}{4\rho} - \frac{\sin\psi}{\rho}\right) + 2\widetilde{\sigma} + 2\widetilde{P}\rho\sin\psi - e\sin^2\psi, \tag{4.26e}$$

$$\dot{p}_z = \frac{\partial \widetilde{H}}{\partial z} = 0 . \tag{4.26f}$$

For $e = 0$ one obtains the classical Hamilton equations of a lipid membrane vesicle as expected [2]. The flexoelectric effect adds terms which are linear in e and simple analytical functions of the surface parametrization. The Hamilton equations can be solved with a standard shooting method [65] subject to boundary conditions which we discuss in the following.

Boundary conditions

The Hamiltonian H does not explicitly depend on the arc length s. Since we have not fixed the total arc length $\bar{s} - \underline{s}$ for the integration, the Hamiltonian is conserved [JS94, CVG07]:

$$\tilde{H} = 0 \,. \tag{4.27a}$$

At the contact point ($s = \underline{s}$) the free part of the flexoelectric membrane detaches from the container and the angle ψ has to equal α since the membrane must not have kinks. At the $\mathbf{z}$ axis ($s = \bar{s}$) the free profile is horizontal, which leaves us with the following boundary conditions:

$$\psi(\underline{s}) = \alpha \,, \qquad \psi(\bar{s}) = \pi \,. \tag{4.27b}$$

As we have seen in Sec. (3.6) by making use of the variation along the contact line, $\partial H_{cl} = 0$, it is possible to peal the last boundary condition out as:

$$\psi(\underline{s}) = 1 + \sqrt{|e_\mathrm{c} - e_\mathrm{f}|}\sin\alpha \,, \tag{4.27c}$$

where e_c is the electric field parameter at the membrane in contact with the confinement and e_f is the electric field parameter of the free membrane. For a uniform external electric field, however, the second term equals zero and we are left with the classical contact curvature condition of the case without electric field.

4.3.3 Uniform Electric Field Stress Tensor

In Sec. 3.2, the generic form of the flexoelectric field stress tensor was derived. With this in mind, it is simple to specialize to a uniform electric field. Since the uniform electric field is oriented antiparallel to the z-axis, $\mathbf{E}_\mathrm{ext} = -E_\mathrm{ext}\mathbf{z}$, one obtains the scaled

multiplier $\tilde{\mathbf{f}}^a$ with the help of Eq. (3.12):

$$\tilde{\mathbf{f}}^a = \mathbf{f}^a - \frac{2}{3}\tilde{P}\mathbf{J}^a - e\left(\frac{1}{2}((\mathbf{z}\cdot\mathbf{n})^2-1)g^{ab})\mathbf{e}_b - [(\mathbf{z}\cdot\mathbf{n})(\mathbf{z}\cdot\mathbf{e}^a)]\mathbf{n}\right) , \tag{4.28}$$

where $\tilde{P} = \frac{PR^3}{\kappa}$, and $e = \frac{E_{\text{ext}}^2 R^2}{D\kappa}$.

Consequently, the part of the stress tensor originating form the external electric field is given by:

$$\mathbf{E}^a = -e\left(\frac{1}{2}((\mathbf{z}\cdot\mathbf{n})^2-1)\mathbf{e}^a - (\mathbf{z}\cdot\mathbf{n})(\mathbf{z}\cdot\mathbf{e}^a)\mathbf{n}\right) , \tag{4.29}$$

The divergence of Eq. (4.29) is written as:

$$\begin{aligned}
\frac{\nabla_a \mathbf{E}^a}{e} &= \left\{\frac{-K}{2}[(\mathbf{z}\cdot\mathbf{n})^2-1]\mathbf{n} + \nabla_a[(\mathbf{z}\cdot\mathbf{n})(\mathbf{z}\cdot\mathbf{e}^a)]\right\}\mathbf{n} \\
&\quad - \frac{1}{2}\nabla_a[1-(\mathbf{z}\cdot\mathbf{n})^2]\mathbf{e}^a + (\mathbf{z}\cdot\mathbf{n})(\mathbf{z}\cdot\mathbf{e}^a)\nabla_a\mathbf{n} , \\
&= \left\{\frac{-K}{2}[(\mathbf{z}\cdot\mathbf{n})^2-1] + \nabla_a[(\mathbf{z}\cdot\mathbf{n})(\mathbf{z}\cdot\mathbf{e}^a)]\right\}\mathbf{n} \\
&\quad - (\mathbf{z}\cdot\mathbf{n})(\mathbf{z}\cdot\mathbf{e}_b)K_a^b\mathbf{e}^a + (\mathbf{z}\cdot\mathbf{n})(\mathbf{z}\cdot\mathbf{e}^a)K_a^b\mathbf{e}_b , \\
&= \left\{\frac{-K}{2}[(\mathbf{z}\cdot\mathbf{n})^2-1] + \nabla_a[(\mathbf{z}\cdot\mathbf{n})(\mathbf{z}\cdot\mathbf{e}^a)]\right\}\mathbf{n} .
\end{aligned} \tag{4.30}$$

Thus, it is feasible to write the effective stress tensor of the flexoelectric membrane as:

$$\begin{aligned}
\tilde{\mathbf{f}}_e^a &= \mathbf{f}^a - \tilde{P}\mathbf{J}^a + \mathbf{E}^a \\
&= \left\{K(K^{ab} - \frac{K}{2}g^{ab}) - [\frac{\tilde{P}}{2}(\mathbf{X}\cdot\mathbf{n}) + \tilde{\sigma} - e(\frac{1}{2}(1-(\mathbf{z}\cdot\mathbf{n})^2))]g^{ab}\right\}\mathbf{e}_b \\
&\quad - \left\{\nabla_a K - \frac{\tilde{P}}{2}(\mathbf{X}\cdot\mathbf{e}^a) - e((\mathbf{z}\cdot\mathbf{n})(\mathbf{z}\cdot\mathbf{e}^a))\right\}\mathbf{n} .
\end{aligned} \tag{4.31}$$

Projection onto the unit vector $\mathbf{l} = l_a\mathbf{e}^a$ perpendicular to the contact line gives the local force density:

$$
\begin{aligned}
l_a\tilde{\mathbf{f}}_e^a &= \left\{\frac{1}{2}(K_\perp^2 - K_\parallel^2) - [\frac{\tilde{P}}{2}(\mathbf{X}\cdot\mathbf{n}) + \tilde{\sigma} - e(\frac{1}{2}(1-(\mathbf{z}\cdot\mathbf{n})^2)]\right\}\mathbf{l} \\
&- \left\{\nabla_\perp K - \frac{\tilde{P}}{2}(\mathbf{X}\cdot\mathbf{l}) - \bar{E}^a((\mathbf{z}\cdot\mathbf{n})(\mathbf{z}\cdot\mathbf{l}))\right\}\mathbf{n} \\
&= \left\{\frac{1}{2}(\dot{\psi}^2 - \frac{\sin^2\psi}{\rho^2}) - [\frac{\tilde{P}}{2}(\mathbf{X}\cdot\mathbf{n}) + \tilde{\sigma} - \frac{e}{2}\sin^2\psi\right\}\mathbf{l} \\
&- \left\{\ddot{\psi} + \frac{\dot{\psi}\cos\psi}{\rho} - \frac{\cos\psi\sin\psi}{\rho^2} - \frac{\tilde{P}}{2}(\mathbf{X}\cdot\mathbf{l}) + e\sin\psi\cos\psi\right\}\mathbf{n}\,,
\end{aligned}
\tag{4.32}
$$

where $\mathbf{z}\cdot\mathbf{n} = -\cos\psi$, and $\mathbf{z}\cdot\mathbf{l} = \sin\psi$ relations. The normal vector $\mathbf{n}$ points towards the outside of the vesicle.

Applied forces

The integral of the flux through an arbitrary contour γ gives the force as below:

$$
\begin{aligned}
-\mathbf{F}_{\text{ext}} &= -\mathbf{z}\cdot\oint_\gamma ds l_a\tilde{\mathbf{f}}_e^a \\
&= -\oint_\gamma ds\left[\frac{1}{2}(\dot{\psi}^2 - \frac{\sin^2\psi}{\rho^2}) - [\frac{\tilde{P}}{2}(\mathbf{X}\cdot\mathbf{n}) + \tilde{\sigma} - \frac{e}{2}\sin^2\psi]\right](\mathbf{z}\cdot\mathbf{l}) \\
&- \left[\ddot{\psi} + \frac{\dot{\psi}\cos\psi}{\rho} - \frac{\cos\psi\sin\psi}{\rho^2} - \frac{\tilde{P}}{2}(\mathbf{X}\cdot\mathbf{l}) + e\sin\psi\cos\psi\right](\mathbf{z}\cdot\mathbf{n}) \\
&= -\oint_\gamma ds\left[\frac{1}{2}(\dot{\psi}^2 - \frac{\sin^2\psi}{\rho^2}) - [\frac{\tilde{P}}{2}(\mathbf{X}\cdot\mathbf{n}) + \tilde{\sigma} - \frac{e}{2}\sin^2\psi]\right]\sin\psi \\
&+ \left[\ddot{\psi} + \frac{\dot{\psi}\cos\psi}{\rho} - \frac{\cos\psi\sin\psi}{\rho^2} - \frac{\tilde{P}}{2}(\mathbf{X}\cdot\mathbf{l}) + e\sin\psi\cos\psi\right]\cos\psi
\end{aligned}
\tag{4.33}
$$

Calculation of $\ddot{\psi}$:

It is possible to calculate the second derivative of $\ddot{\psi}$, by taking the derivative of Eq. (4.26a) $\dot{\psi} = \frac{p_\psi}{2\rho} - \frac{\sin\psi}{\rho}$:

$$
\begin{aligned}
\ddot{\psi} &= \frac{\dot{p}_\psi}{2\rho} - \frac{p_\psi}{2\rho^2}\cos\psi - \frac{\dot{\psi}\cos\psi}{\rho} + \frac{\sin\psi\cos\psi}{\rho^2}, \\
&= \frac{1}{2\rho}(\tilde{P}\rho^2 - p_z)\cos\psi + \frac{p_\rho}{2\rho}\sin\psi - e\sin\psi\cos\psi - \frac{\dot{\psi}\cos\psi}{\rho} + \frac{\sin\psi\cos\psi}{\rho^2}\,.
\end{aligned}
\tag{4.34}
$$

One has to take into account Eq. (4.26), $\tilde{H} = 0$, to find $\tilde{p}_\rho$.

$$\begin{aligned}\ddot{\psi}\cos\psi = \frac{1}{2\rho}(\tilde{P}\rho^2 - p_z) - \frac{p_\psi^2 \sin\psi}{8\rho^2} + \frac{p_\psi \sin^2\psi}{2\rho^2} + \tilde{\sigma}\sin\psi \\ - \frac{e\sin^3\psi}{2} - e\sin\psi\cos^2\psi - \frac{\dot{\psi}\cos^2\psi}{\rho} + \frac{\sin\psi\cos^2\psi}{\rho^2}\ .\end{aligned} \tag{4.35}$$

$\ddot{\psi}$ at the contact line, where $\frac{\sin\psi}{\rho} = 1$, is:

$$\begin{aligned}\ddot{\psi}_{c.l}\cos\psi &= \frac{1}{2\rho}(\tilde{P}\rho^2 - p_z) + \rho\tilde{\sigma} - \frac{e\rho}{2}(\rho^2 + 2\cos^2\psi), \\ &= \frac{1}{2\rho}(\tilde{P}\rho^2 - p_z) + \rho\tilde{\sigma} - \frac{e\rho}{2}(2 - \rho^2)\ .\end{aligned} \tag{4.36}$$

Therefore, p_z at the equator $\psi = \frac{\pi}{2}$ is as following.

$$p_z = \left(\tilde{P} + 2\tilde{\sigma} - e\right)\ . \tag{4.37}$$

where p_z at $\rho = 1$ is calculated. Inserting Eq. (4.35) into Eq. (4.33), the external force is obtained as:

$$\mathbf{F}_{\text{ext}} = \frac{1}{2}\oint_\gamma ds\left\{-\tilde{P}(\mathbf{X}\cdot\mathbf{n})\sin\psi + \tilde{P}\rho - \frac{p_z}{\rho} - \tilde{P}(\mathbf{X}\cdot\mathbf{l})\cos\psi\right\}\ , \tag{4.38}$$

At the circular contact line; $c_\perp = c_\parallel = 1$, $\mathbf{X}\cdot\mathbf{n} = 1$, and $\mathbf{X}\cdot\mathbf{l} = 0$, it is possible to write force as:

$$\mathbf{F}_{\text{ext}} = -\frac{1}{2}\oint_\gamma ds\left(\frac{p_z}{\rho}\right)\ . \tag{4.39}$$

One can obtain the projections as:

$$\rho\cdot l_a\mathbf{f}_e^a = -\left(\frac{\tilde{P}}{2} + \tilde{\sigma}\right)\sin\psi + \ddot{\psi}\cos\psi + e\left(\sin\psi\cos^2\psi - \frac{\sin^3\psi}{2}\right)\ . \tag{4.40}$$

$$\mathbf{z}\cdot l_a\mathbf{f}_e^a = -\left(\frac{\tilde{P}}{2} + \tilde{\sigma}\right)\cos\psi - \ddot{\psi}\sin\psi + e\left(\frac{3}{2}\sin^2\psi\cos\psi\right)\ . \tag{4.41}$$

4.4 Results

To study the axially symmetric folding patterns of the spherical confined flexoelectric fluid membranes in the presence of the uniform electric field, one can suppose that the external electric field, $\mathbf{E}_{\text{ext}}$, in the vicinity of the system is constant, and locates anti-parallel to z-axis. This section aims to search for axisymmetric equilibrium solutions of spherically confined flexoelectric fluid vesicles as a function of their surface area $\bar{A}$, and the volume $\bar{V}$ by making use of the continuum model described in detail above. One can examine the system based on the dimensionless scaled area A_0 and scaled volume V_0 of the confining container [1, 2]:

$$a = \bar{A}/A_0 \quad \text{and} \quad v = \bar{V}/V_0 \,. \tag{4.42}$$

in which A_0 and V_0 are the area and the volume of the confining sphere, respectively. Figure. 4.3 exhibits the cut of the system for $a = 1.2$, and $v = 0.8$ in the absence of an electric field.

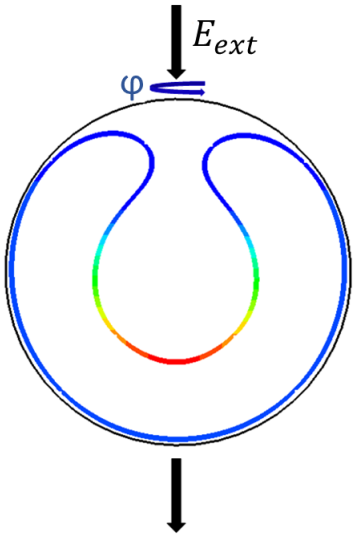

Figure 4.3: Runge-Kutta equilibrium solution for a flexoelectric fluid membrane (coloured line) inside a spherical container (black solid circle) with scaled area a = 1.2 and scaled volume v = 0.8 in the absence of an electric field, $\mathbf{E}_{\text{ext}} = 0$.

This system has been treated before in the absence of an electric field by Kahraman et al. (see details in [1, 2]). Flexoelectricity adds another term to the total energy in the presence of an external electric field $\mathbf{E}_{\text{ext}}$. It is trivial that as soon as an area becomes slightly larger than one (*i.e.*, $a > 1$), the flexoelectric fluid membrane will not fit into the confinement and starts to detach from the confinement. This leads the flexoelectric membrane to fold inward. This is only possible when the volume enclosed by the vesicle is smaller than the confining volume. Since the system is highly nonlinear, the analytical treatment of this problem is not accessible. We will thus resort to numerical calculations in the following.

Numerical solution methods

Equilibrium solutions are determined by minimising Eq. (4.17) for fixed parameters a, v, and e. Here, two different numerical methods are used: (i) Axisymmetric shapes without self-contact can be found with the help of a Hamiltonian formulation (see Sec. 4.3.2). One, then, can solve the resulting differential equations with a traditional shooting method. The cavity is handled as a hard constraint. Volume and area are conserved with the help of Lagrange multipliers. This method searches for the simplest axisymmetric shapes, which consist of one part in contact with the container and one free part. (ii) The finite element method is the second approach and can search for more intricate configurations, including symmetry breaking and self-contacts. In this method, the surface of the flexoelectric membrane is discretized into a triangular mesh. A discretized version of Eq. (4.17) is used to determine the forces that act on each node. To equilibrate the system, one can add a damping force on the nodes and integrate Newton's equations of motion in time. In the simulations, the container is modelled as a soft constraint with a quadratic repulsive force. The constraints on area and volume are implemented via a penalty method.

The details of both solution methods with the flexoelectric contribution can be found in Appendix. C [2]. Flexoelectricity appends additional terms to the differential equations of method (i). These are linear in e and simple analytical functions of the surface parametrization. A subtlety, however, lies in the boundary conditions. A variation of the contact line as was, for example, done for the non-electric case in Refs. [66, 69] yields an additional term in the contact curvature condition (see Sec. 4.3.2). For a uniform external electric field, however, this term equals zero. To employ method (ii), one needs to determine the local flexoelectric force on the membrane. Its continuous version can be found in Ref. [32] and is discretized and added to the forces that act on each node. The following sections focus on the results obtained by the two methods.

4.4.1 Solutions from the Classical Shooting Method

To determine the equilibrium profiles of the flexoelectric membrane in the presence of the electric field the Hamilton equations, Eq. (4.24), are integrated with a fourth-order Runge-Kutta method. For a fixed $\tilde{\sigma}$ and $\tilde{P}$ and a trial angle α, we search for shapes which fulfil all of the boundary conditions Eq. (4.22) (see also Appendix. C for more details). When a profile is found, we calculate its area and volume *a posteriori*. By scanning the parameter space $(\tilde{\sigma}, \tilde{P})$ we obtain vesicles with variable area and volume.

4.4.1.1 Influence of the Electric Field

In this section, we will scrutinize the response of the axisymmetric flexoelectric fluid membrane to different strengths of the flexoelectric effect. For moderate values of the parameters a, v, and e, the equilibrium solutions consist of an axisymmetric invagination connected to the contacting part of the membrane *via* a neck. To study the behavior of the system, one can first consider different values of e with area and volume fixed to $(a, v) = (1.2, 0.8)$ (see Fig. 4.4) which were found by the shooting method. The sign of the electric field parameter, Eq. (4.16), depends on the sign of D,

which, in turn, is determined by the strength of the flexoelectric effect. The latter is encoded in the constant c_2. When the flexoelectric effect is weak, $c_2^2 < k_3\chi_\perp$, and e is positive, whereas e is negative for $c_2^2 > k_3\chi_\perp$. An inspection of Eq. (4.17) reveals that the flexoelectric energy density is minimized when $e(\mathbf{z}\cdot\mathbf{n})^2$ is as small as possible. For positive e this term is minimized when the surface normal $\mathbf{n}$ is perpendicular to $\mathbf{z}$ leading to elongation in the direction of the electric field. When the flexoelectric effect is strong, the surface normal prefers to be parallel to $\mathbf{z}$ as far as possible. This explains the elongation of the invagination perpendicular to $\mathbf{E}_{\text{ext}}$ for $e < 0$.

Weak flexoelectric effect:

Figure. 4.4 shows axisymmetric shapes for $e = 0, 0.5, 1, 5$ and 10 which were obtained with the shooting method. An electric field parameter of the order of 0.5 and 1 does not influence the resulting shape dramatically. One can observe, however, that the circle at which the vesicle detaches from the container depends crucially on the value of e (dots in Figure. 4.4). Therefore, the flexoelectric membrane with weak flexoelectric effect, $e > 0$, is elongated vertically along with the electric field orientation (see the coloured profiles in Figure. 4.4) in comparison to the reference double confined membrane which is equilibrated in the absence of an external field (see the black profile in Figure. 4.4).

Even though a modification of the membrane along the field direction in response to the electric field is barely noticeable for weak flexoelectricity, the change of the position at which membrane starts to detach from the confinement is pretty clear (see the two points in the profiles with $e = 0.5$ (the solid magenta curve) and $e = 1$ (the cyan solid curve) in Figure 4.4). Consequently, with slightly increasing the strength of the flexoelectric field, the detachment angle is decreasing. Besides, when increasing the

flexoelectricity strength effect, the free membrane folds inward heavily, and the neck starts to open (see Figure. 4.4).

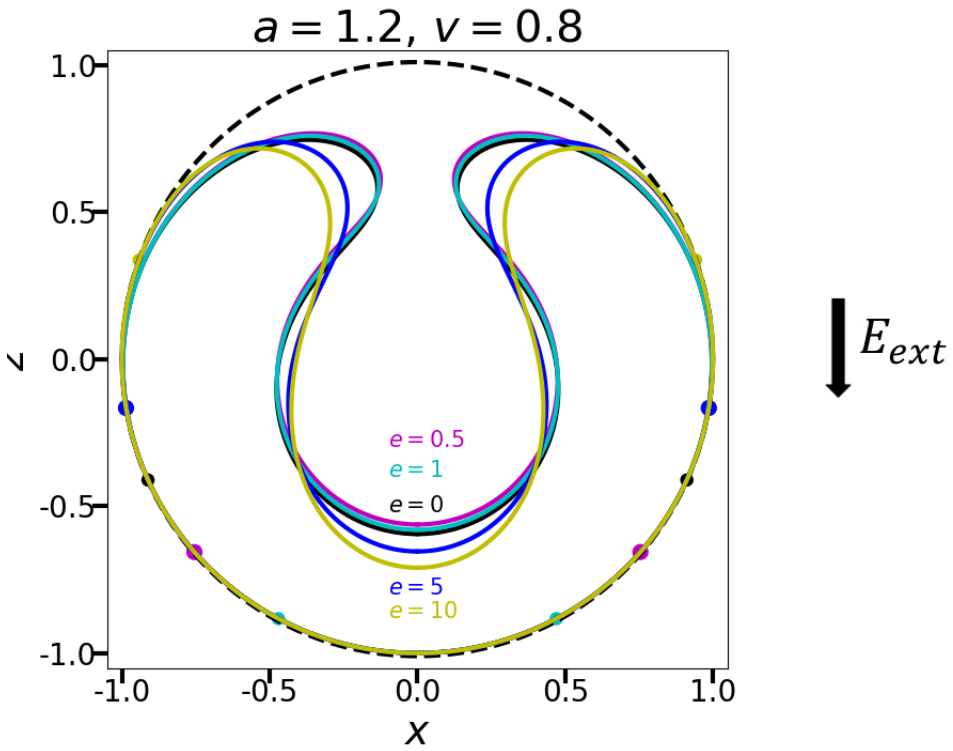

Figure 4.4: Slices of numerical equilibrium solutions of spherically confined flexoelectric fluid membrane vesicles in an external uniform electric field with fixed area and volume $(a, v) = (1.2, 0.8)$ for different strengths of $e > 0$. The flexoelectric membrane is composed of two segments, one completely in contact with the confinement (below the two points), and the other, the free part, (above the two points) (a) $e = 0$ (solid black line), (b) $e = 0.5$ (solid magenta line), (c) $e = 1$ (solid cyan line), (d) $e = 5$ (solid blue line), and $e = 10$ (yellow dash line).The dots indicate, at which point the membrane starts to detach from the container. All the slices are obtained with the shooting method.

Strong flexoelectric effect:

Figure. 4.5 shows axisymmetric shapes for $e = 0, -0.5, -1, -5$ and -10 which were obtained with the shooting method. An electric field parameter of the order of -0.5 and -1 does not influence the resulting shape dramatically. One can observe, however, that the circle at which the vesicle detaches from the container depends crucially on the value of e (dots in Figure. 4.4) as we have already seen for positive e. The flexoelectric

membrane with strong flexoelectric effect, $e < 0$, is vertically compressed along the electric field direction (see the coloured profiles in Figure. 4.5) in comparison with the reference membrane which is equilibrated in the absence of an external electric field (see the black profile in Figure. 4.5).

Similar to the previous case, one does not observe a strong deformation of the membrane along the field direction for e close to zero. However, the change of the position at which the membrane starts to detach from the confinement is again evident (see the two points in the profiles with $e = -0.5$ (red dashed curve) and $e = -1$ (magenta dashed curve) in Figure. 4.5. Thus, by slightly increasing the strength of the flexoelectric effect, the detachment angle increases and the free part of the membrane folds upward exhibiting an increasingly narrower neck (see Figure. 4.5).

For a better comparison, let us look at the response of the confined flexoelectric fluid membrane at constant $|e|$ (see Figures. 4.6, and 4.7). One finds that the membrane with a weak flexoelectric effect detaches earlier than the membrane with a strong effect; this behaviour is consistent. For the low strength value, the membrane starts to detach even earlier than the reference membrane (see Figure. 4.6), and for the high strength, the detachment initiates above reference membrane (see Figure. 4.7).

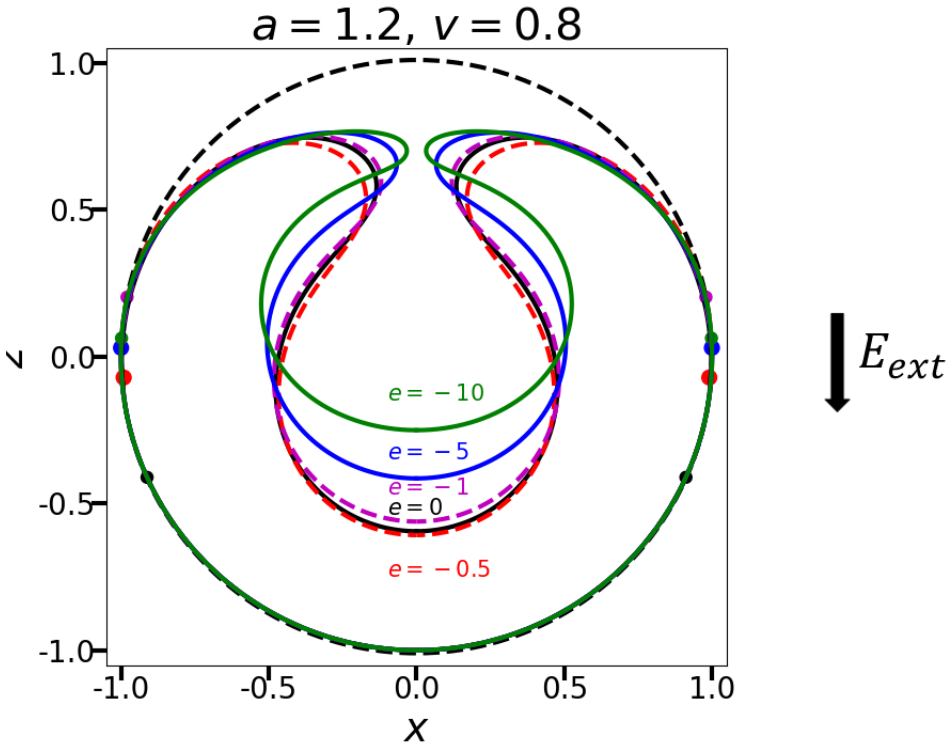

Figure 4.5: Slices of numerical equilibrium solutions of spherically confined flexoelectric fluid membrane vesicles in an external uniform electric field with fixed area and volume $(a, v) = (1.2, 0.8)$ for different strengths of $e < 0$. (a) $e = 0$ (solid black line), (b) $e = -0.5$ (red dashed line), (c) $e = -1$ (solid magenta line), and (d) $e = -5$ (solid blue line), and $e = -10$ (solid green line). The dots indicate at which point the membrane starts to detach from the container. All the slices are obtained with the shooting method.

When one increases the flexoelectric effect such that $e = \pm 50$, or even ± 100, it is not possible to find any profile for the specific values $(a, v) = (1.2, 0.8)$. The results of the Runge- Kutta calculations for these values are limited to a narrow region of a and v values, which will be discussed further in the following sections. This method does not only find the minimum solutions that are the interest of this manuscript, but it also finds the maximum ones. One, thus, has to apply full-numerical treatments (FES) to identify minimum solutions, to find all axisymmetric solutions and beyond, and to understand them precisely.

4.4.1.2 Solutions of Constant Area

To study the effect of the area of the confined vesicle, we determine the axisymmetric solutions of constant a by changing its volume.

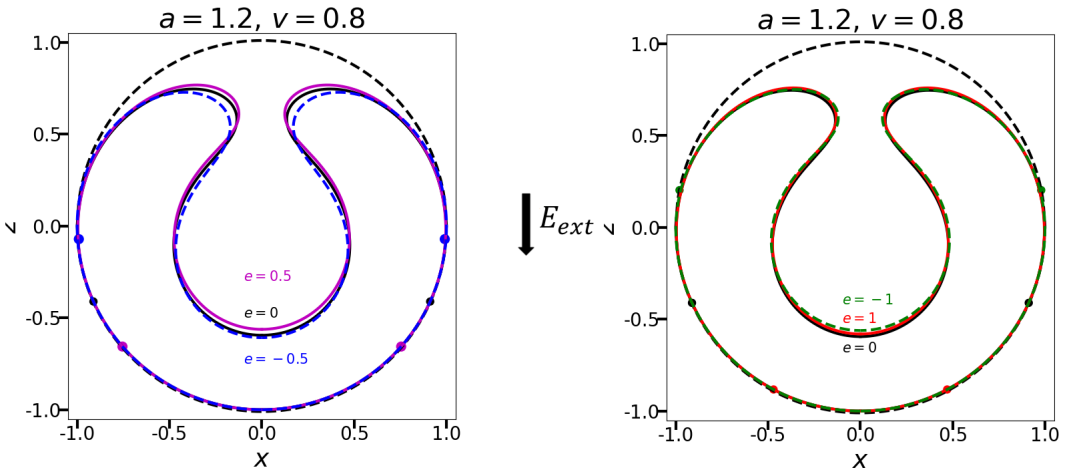

Figure 4.6: Response of flexoelectric fluid membrane with $(a, v) = (1.2, 0.8)$ for small values of $|e|$. The black curve indicates the flexoelectric membrane in the absence of an electric field.

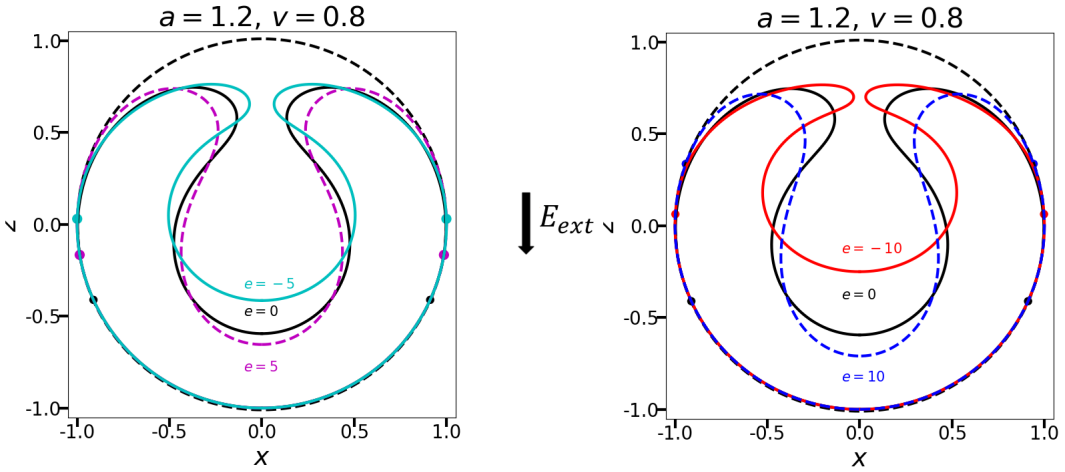

Figure 4.7: Response of flexoelectric fluid membrane with $(a, v) = (1.2, 0.8)$ for moderate values of $|e|$. The black curve indicates the flexoelectric membrane in the absence of an electric field.

Solutions of weak flexoelectric effect:

In the following examples for a small area, $a = 1.1$, and positive electric field parameter

$e > 0$ are given. Figure. 4.8 shows flexoelectric membranes deformations for $a = 1.1$, and $e = 5$ with different volumes of $v = 0.8$, and $v = 0.9$.

Figure. 4.9 shows flexoelectric membranes deformations for $a = 1.1$, and $e = 10$ with different volumes of $v = 0.8$, and $v = 0.9$. Similar shapes are found for moderate values of area and volume as long as of $e > 0$ is small enough.

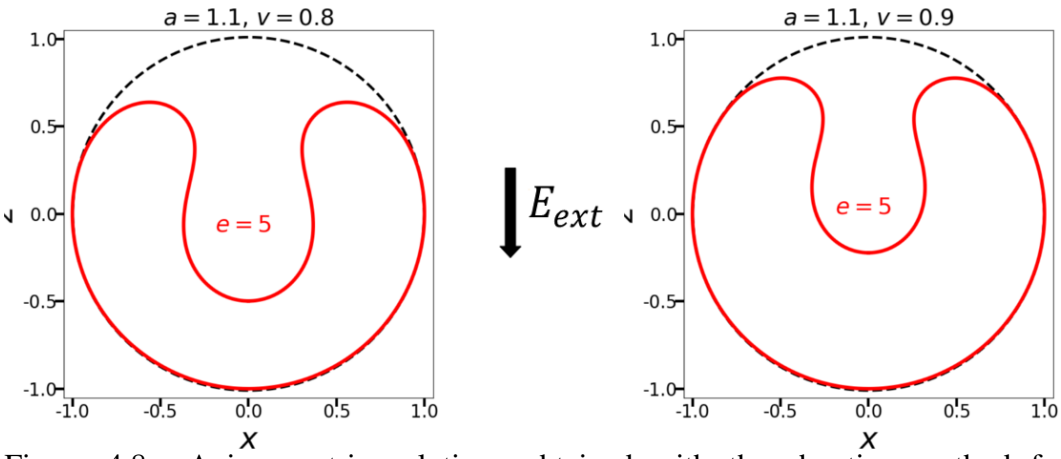

Figure 4.8: Axisymmetric solutions obtained with the shooting method for a flexoelectric fluid membrane inside a spherical container with scaled area $a = 1.1$ and scaled volumes of $v = 0.8$, and $v = 0.9$ for $e = 5$.

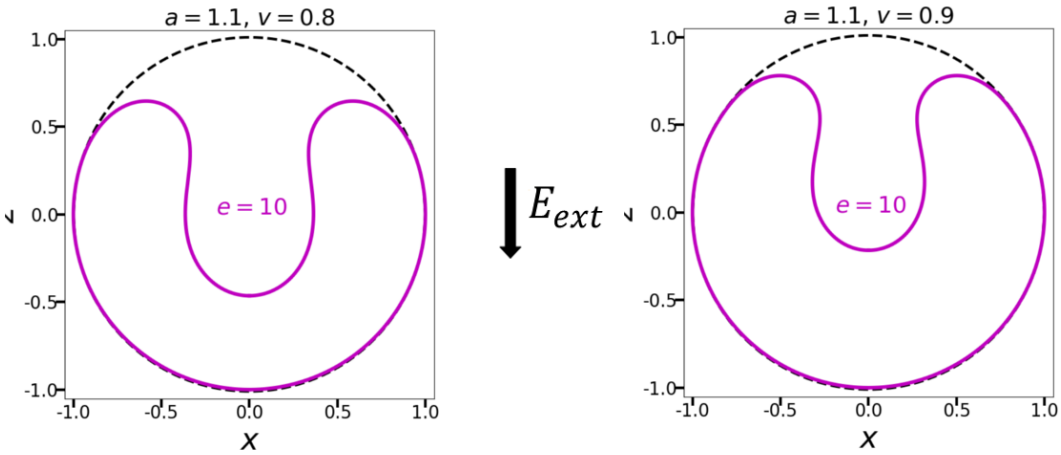

Figure 4.9: Axisymmetric solutions obtained with the shooting method for a flexoelectric fluid membrane inside a spherical container with scaled area $a = 1.1$ and scaled volumes of $v = 0.8$, and $v = 0.9$ for $e = 10$. For $e = 10$ one observes an additional detachment of the membrane in the finite element simulations (see Figures. 4.19c and 4.19d), which is not taken into account in the shooting method.

For $e > 0$, the invagination is axisymmetric and orients itself parallel to the electric field.

Solutions of strong flexoelectric effect:

Here, examples for a small area, $a = 1.1$, and negative electric field parameter $e < 0$ are discussed. Figure. 4.10 displays flexoelectric membranes deformations for $a = 1.1$, and $e = -5$ with different volumes of $v = 0.6$, $v = 0.7$, $v = 0.8$, and $v = 0.9$.

Figure. 4.11 displays flexoelectric membranes deformations for $a = 1.1$, and $e = -10$ with different volumes of $v = 0.6$, $v = 0.7$, $v = 0.8$, and $v = 0.9$. Similar shapes can be found for moderate values of area and volume as long as $e < 0$ is small enough.

For $e < 0$, the invagination is axisymmetric and orients itself perpendicular to the electric field. The Eq. (4.17) indicates that the flexoelectric energy density is minimized when $e(\mathbf{z} \cdot \mathbf{n})^2$ is as small as possible. When the flexoelectric effect is strong, the surface normal prefers to be parallel to $\mathbf{z}$ as far as possible. This explains the elongation of the invagination perpendicular to $\mathbf{E}_{\text{ext}}$ for $e < 0$. For larger values of $e < 0$ one observes a new detachment of the membrane in contact with the container in the finite element simulations (see Figs. 4.19c and 4.19d), which we cannot capture with our simple shooting method.

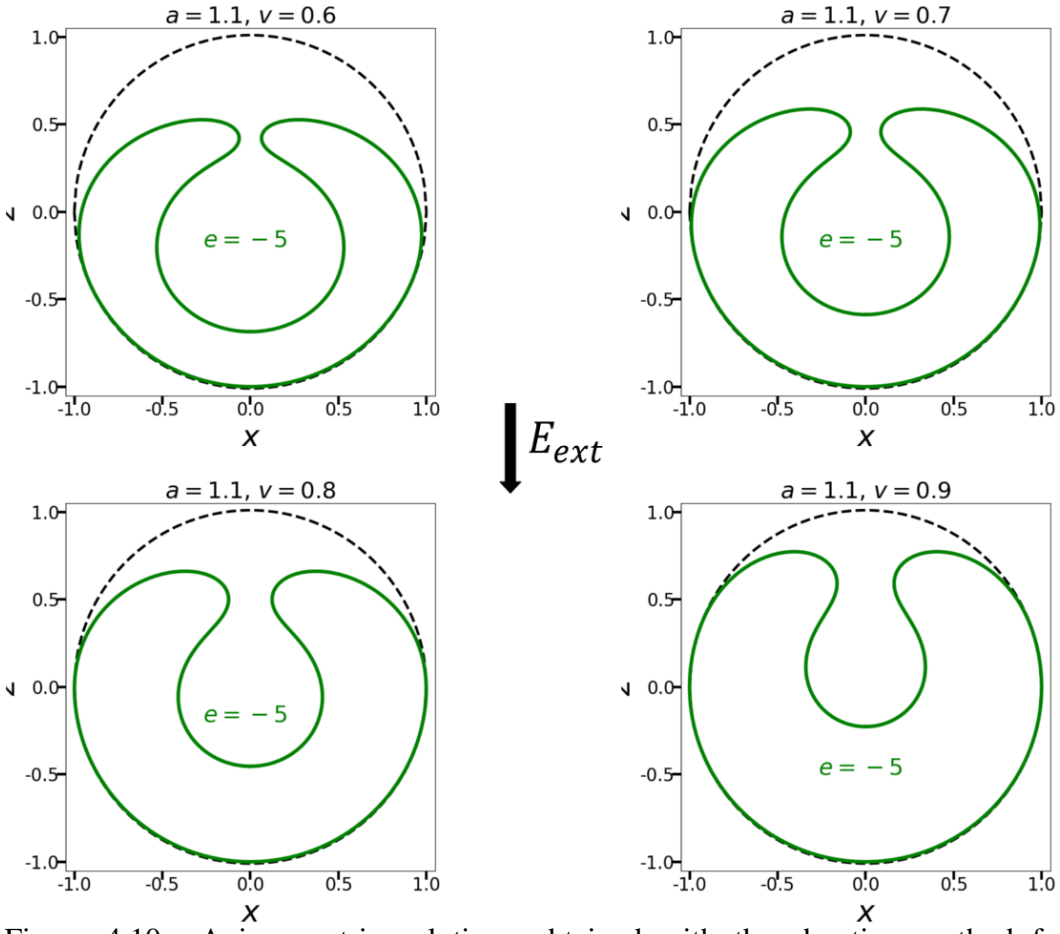

Figure 4.10: Axisymmetric solutions obtained with the shooting method for a flexoelectric fluid membrane inside a spherical container with scaled area $a = 1.1$ and scaled volumes of $v = 0.6$, $v = 0.7$, $v = 0.8$, and $v = 0.9$ for $e = -5$. For $e = -5$ one observes an additional detachment from the bottom of the membrane in the finite element simulations, which we could not find with our simple shooting method.

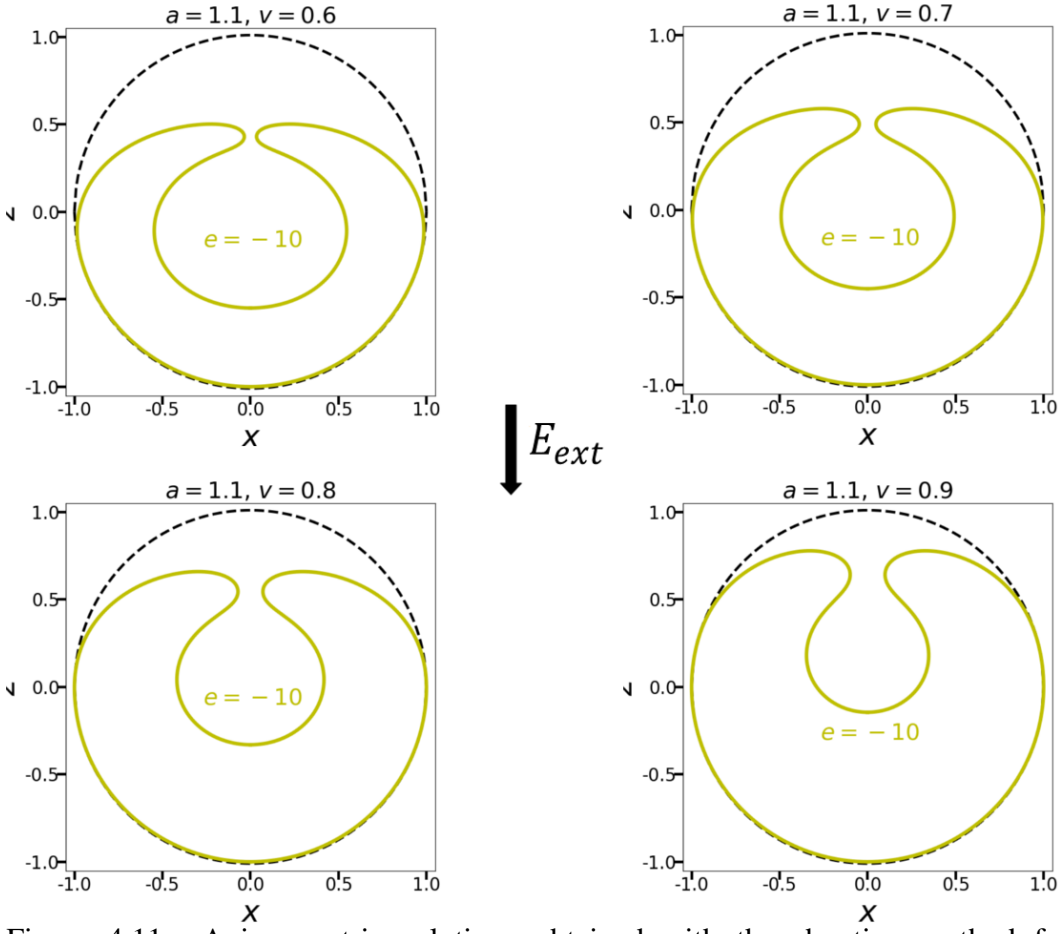

Figure 4.11: Axisymmetric solutions obtained with the shooting method for a flexoelectric fluid membrane inside a spherical container with scaled area $a = 1.1$ and scaled volumes of $v = 0.6$, $v = 0.7$, $v = 0.8$, and $v = 0.9$ for $e = -10$. For $e = -10$ one also observes an additional detachment from the bottom of the membrane in the finite element simulations (see Figs. 4.19c and 4.19d), which we could not find with our simple shooting method.

4.4.1.3 Solutions of Constant Volume

In this section, we will see how a vesicle of constant volume $v = 0.8$ deforms when changing the values of e and a.

Solutions of weak flexoelectric effect:

In the following shape deformations for a fixed volume, $v = 0.8$, and positive electric field parameter $e > 0$ are shown for different values of vesicle area. These shape deformations were again obtained by the shooting method.

Figure. 4.12 exhibits flexoelectric membranes deformations for $v = 0.8$, and $e = 5$ with increasing area in the range of $a = 1.0$, $a = 1.1$, $a = 1.2$, and $a = 1.3$. The folding patterns for the moderate value of surface growth are found to be axisymmetric and orient themselves parallel to the electric field within the numerical errors. As the area is increased, the inner membrane folds further inwards and gets more deformed, while the neck contracts.

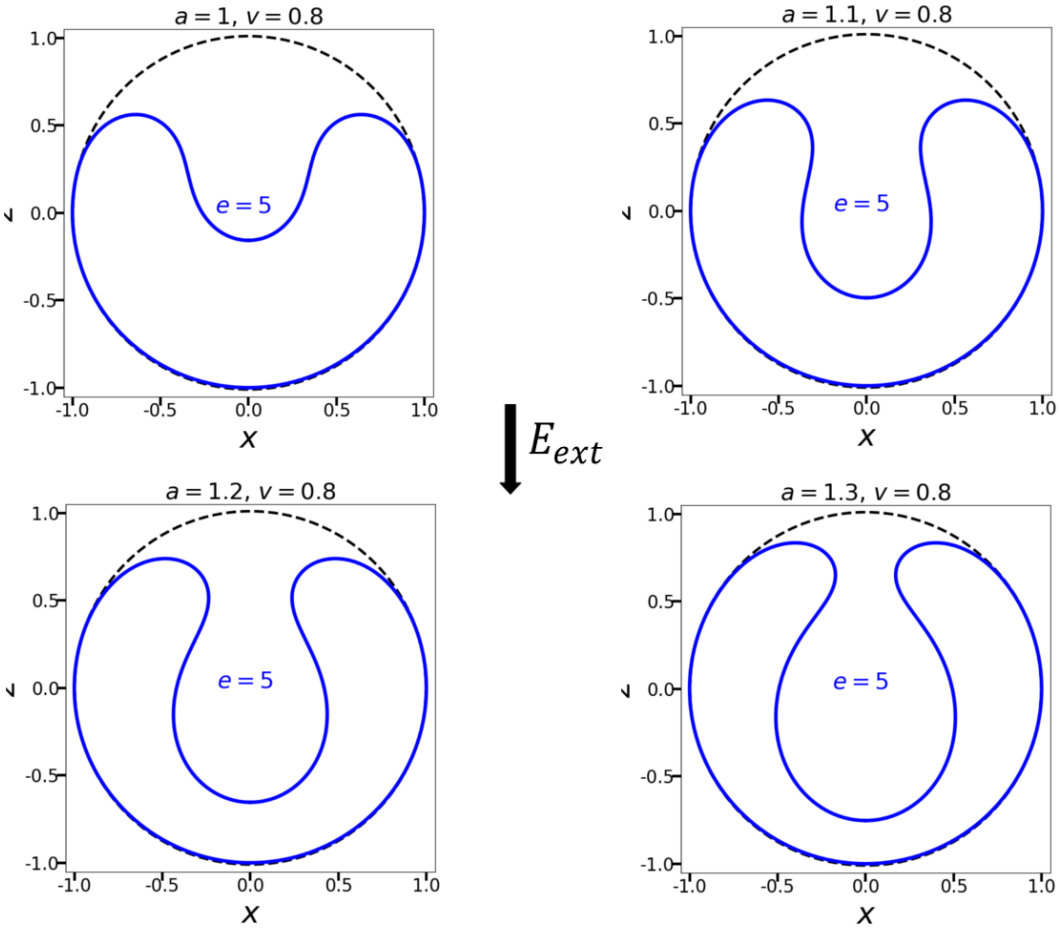

Figure 4.12: Axisymmetric solutions obtained with the shooting method for a flexoelectric fluid membrane inside a spherical container for fixed volume of $v = 0.8$ with increasing area in the range of $a = 1.0$, $a = 1.1$, $a = 1.2$, and $a = 1.3$ for $e = 5$. For $e = 5$ one observes an additional detachment from the equator of the membrane in the finite element simulations (see Figures. 4.19c and 4.19d), which we could not find with our simple shooting method.

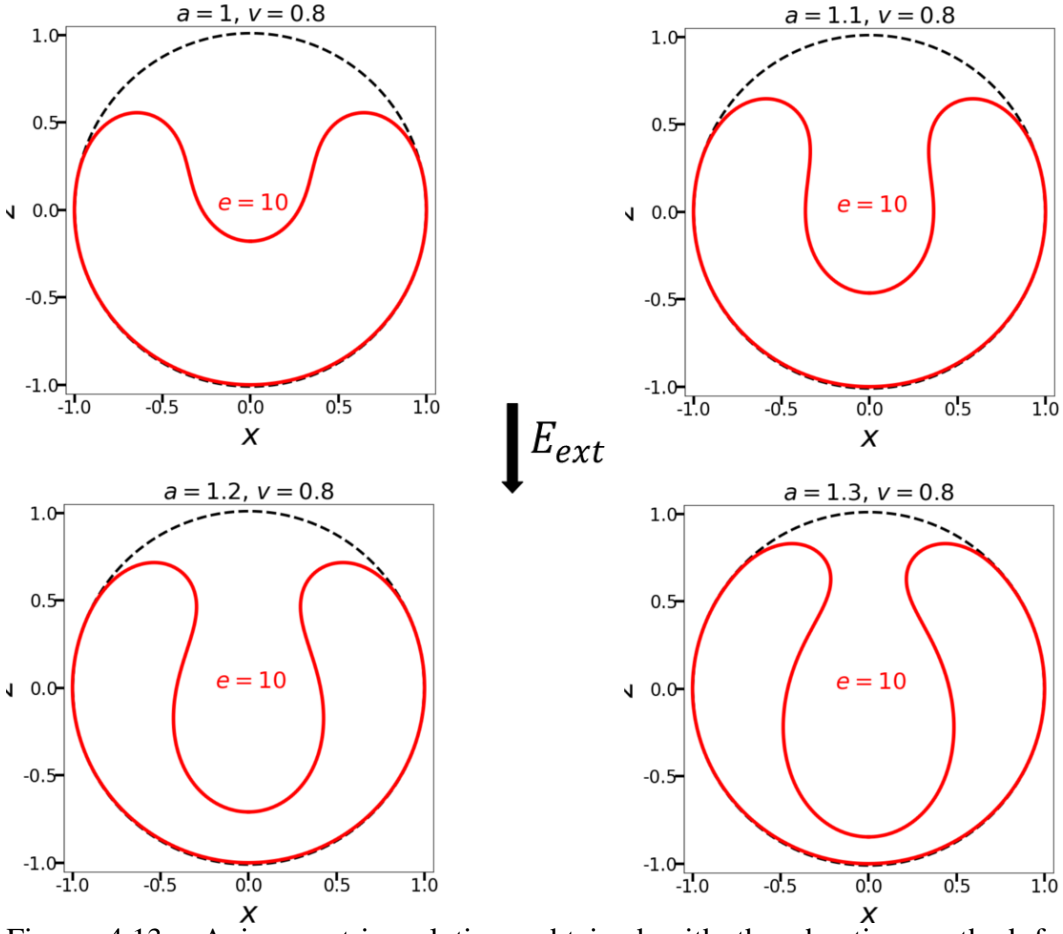

Figure 4.13: Axisymmetric solutions obtained with the shooting method for a flexoelectric fluid membrane inside a spherical containerfor fixed volume of $v = 0.8$ with increasing area in the range of $a = 1.0$, $a = 1.1$, $a = 1.2$, and $a = 1.3$ for $e = 10$. For $e = 10$ one observes an additional detachment from the equator of the membrane in the finite element simulations (see Figures. 4.19c and 4.19d), which we could not find with our simple shooting method.

Figure. 4.13 shows flexoelectric membranes deformations for $v = 0.8$, and $e = 10$ with increasing area in the range of $a = 1.0$, $a = 1.1$, $a = 1.2$, and $a = 1.3$.

One can observe, however, that as the electric field increases, the inner flexoelectric membrane folds inwards further while the neck contracts.

Solutions of strong flexoelectric effect:

Figure. 4.14 confined membrane vesicles with $v = 0.8$, and $e = -5$ with increasing

area in the range of $a = 1.0$, $a = 1.1$, $a = 1.2$, and $a = 1.3$. The deformation for these moderate values of surface growth is again axisymmetric. As the area is increased, the inner flexoelectric membrane folds outward further and gets more folded, and the neck decreases.

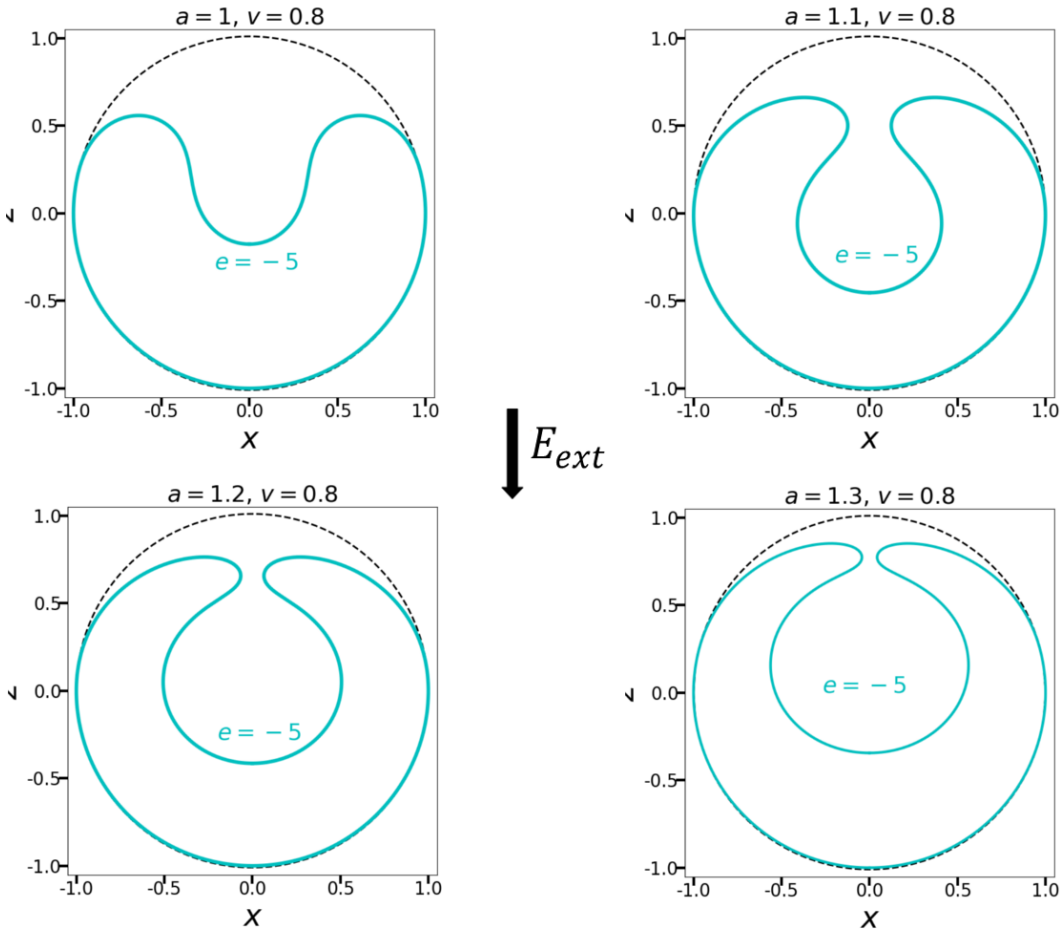

Figure 4.14: Axisymmetric solutions obtained with the shooting method for a flexoelectric fluid membrane inside a spherical container for fixed volume $v = 0.8$ with increasing area in the range of $a = 1.0$, $a = 1.1$, $a = 1.2$, and $a = 1.3$ for $e = -5$. For $e = -5$ one can observe an additional detachment from the bottom of the vesicle in the finite element simulations (see Figures. 4.19c and 4.19d), which we could not obtain with our simple shooting method.

Figure. 4.15 shows flexoelectric membranes deformations for $v = 0.8$, and $e = -10$ with increasing area in the range of $a = 1.0$, $a = 1.1$, $a = 1.2$, and $a = 1.3$. As the electric field increases, the inner flexoelectric membrane folds more and more outward

whereas the neck contracts.

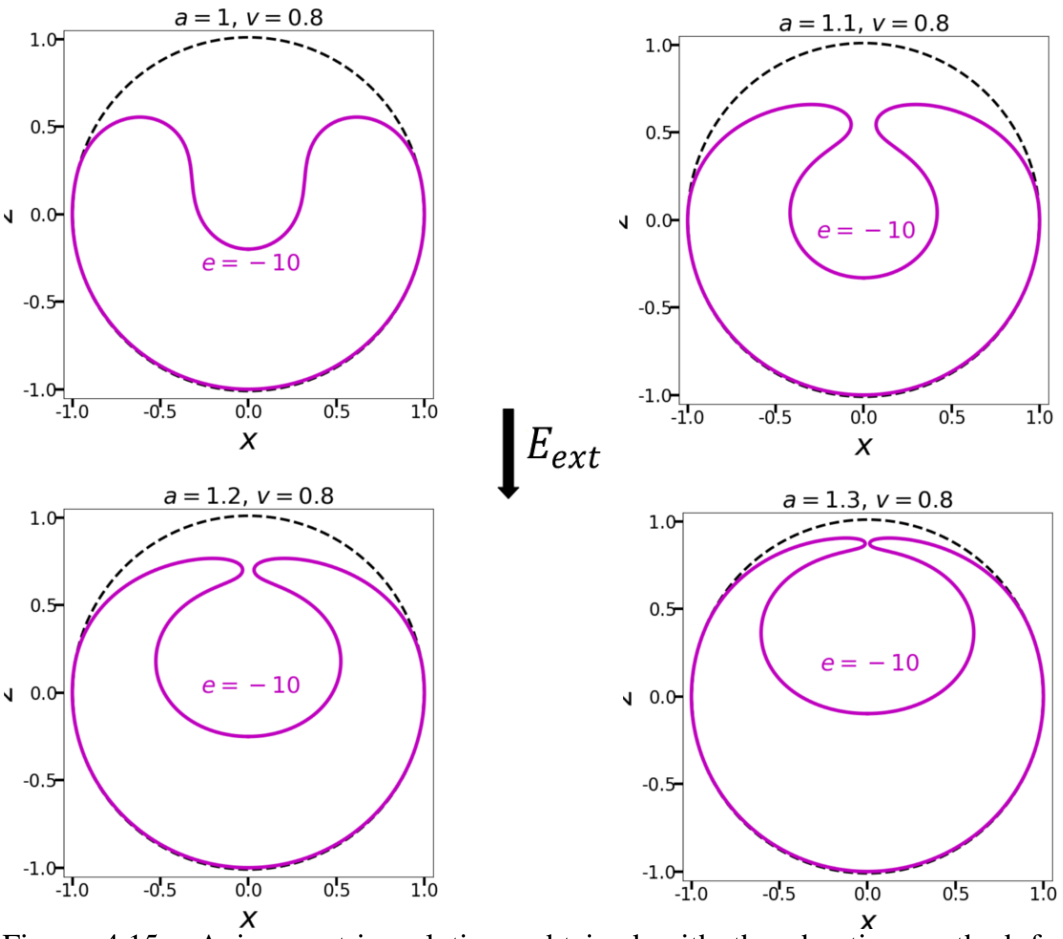

Figure 4.15: Axisymmetric solutions obtained with the shooting method for a flexoelectric fluid membrane inside a spherical container for fixed volume $v = 0.8$ and $a = 1.0$, $a = 1.1$, $a = 1.2$, and $a = 1.3$ for $e = -10$. For $e = -10$ one again observes an additional detachment from the bottom of the membrane in the finite element simulations (see Figures. 4.19c and 4.19d), which we could not obtain with our simple shooting method.

4.4.1.4 Morphological Phase Diagram from Shooting Method

The previous sections have given us a general idea of how the vesicle behaves as a function of the parameters a, v, and e. With this in mind, one can now take a look at the following phase diagrams, display the behavior of the system in more detail.

Phase diagram for small $|e| < 1$

Figure. 4.16 recalls the axisymmetric results for the system without electric field, $e = 0$, which was obtained in Refs. [1, 2]. In the green region, one finds axisymmetric solutions with the shooting method. In the pink region below, the finite element solutions are also axisymmetric but display a more complicated configuration with several free parts or self-contact, for example. In the yellow area above, the finite element solutions display even more intricate shapes with several self-contacts. For a small absolute value of the electric field parameter $|e| < 1$, shifting of the lower boundary separating the axisymmetric (green region in Figure. 4.16) and the axisymmetric - with - detachment (pink region in Figure. 4.16) region is observed in the phase diagram. Figure. 4.16 shows downward and upward shifting of the lower boundary of the axisymmetric region for strong, $e < 0$, and weak, $e > 0$, flexoelectric effect respectively.

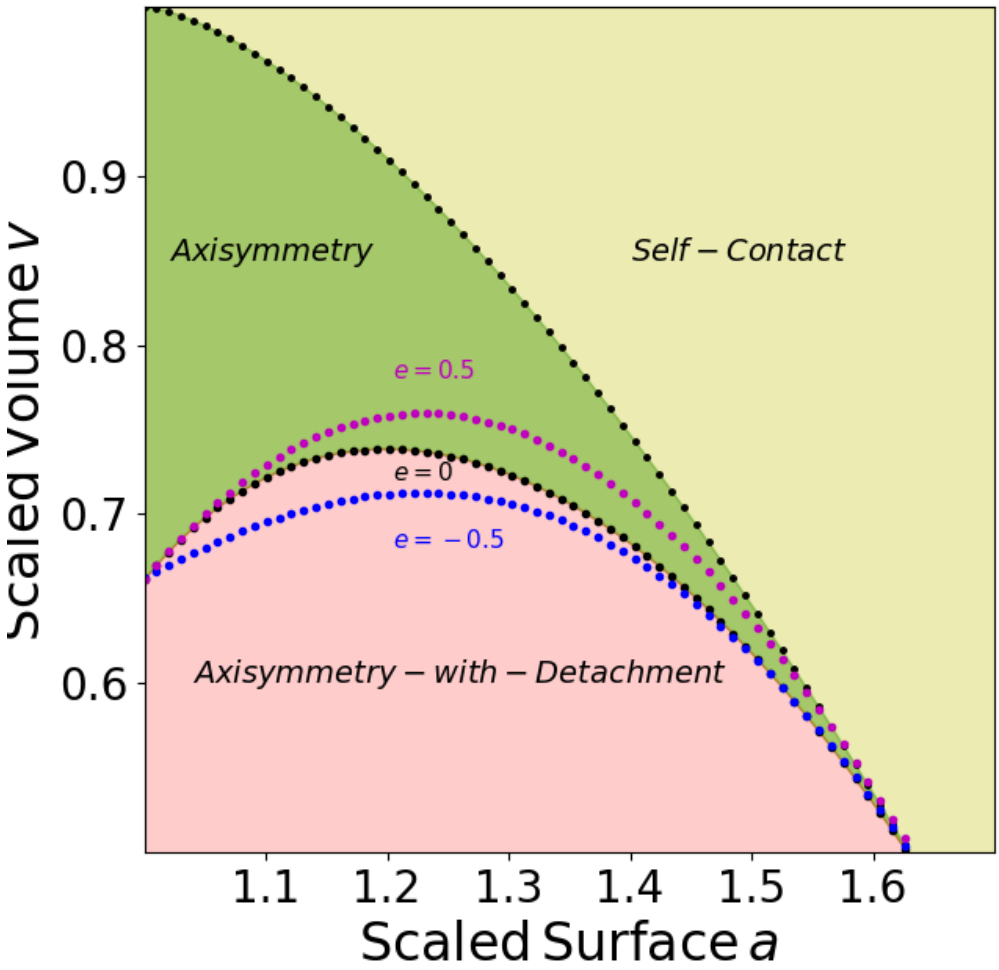

Figure 4.16: Morphological phase diagram (a, v) is displaying the axisymmetric extrema (green region) which obtained with the shooting method. Besides, it exhibits the axisymmetric - with - detachment (pink area), and self-contact (yellow zone) which were found with the finite element method. The magenta curve, which shows the lower boundary of the axisymmetric region of electric field parameter of $e = 0.5$, is shifting upward. Whereas, the blue curve which sets out the lower boundary of the axisymmetric region of electric field parameter of $e = -0.5$, is shifting downward. However, the upper boundary of the axisymmetric area for the small absolute value of electric field parameter $|e| < 1$ stays approximately the same as the upper boundary of the region without electric field.

Phase diagram for moderate values of $e > 0$

If one increases the electric field parameter, our simple shooting method predicts a shift of the axisymmetric area for moderate positive value of e. Not only the axisymmetric region decreases in size but also a change in the upper boundary

appears. To investigate our solutions, one can take a look at each two-dimensional vertical slice of the membrane's profile and compare it with the finite element results. Figure. 4.17 investigates the change in the morphological phase diagram of the axisymmetric region for electric field parameter $e = 5$ (blue dotted curves) in comparison with the axisymmetric area of $e = 0$ (green area).

With this in mind, let us consider a few vertical slices obtained from the shooting method without electric field, one obtains a perfect spherical invagition ("a sphere inside a sphere") with a vanishing neck along the black dotted boundary. However, as shown in Figure. 4.17 the flexoelectric effect induces an axisymmetric elongation which implies that the upper (blue dotted) boundary is shifted. When moving along the upper boundary and slightly increasing the area of the membrane larger than the area of the container at $(a, v) = (1.16, 0.94)$, one can observe a folding inward parallel to the direction of the electric field. At the kink, when the axisymmetric region stops, one can take a look at $(a, v) = (1.48, 0.66)$. An inspection of the shape reveals that the membrane starts to touch the container at this point. At $(a, v) = (1, 0.73)$ a simple axisymmetric invagination is obtained.

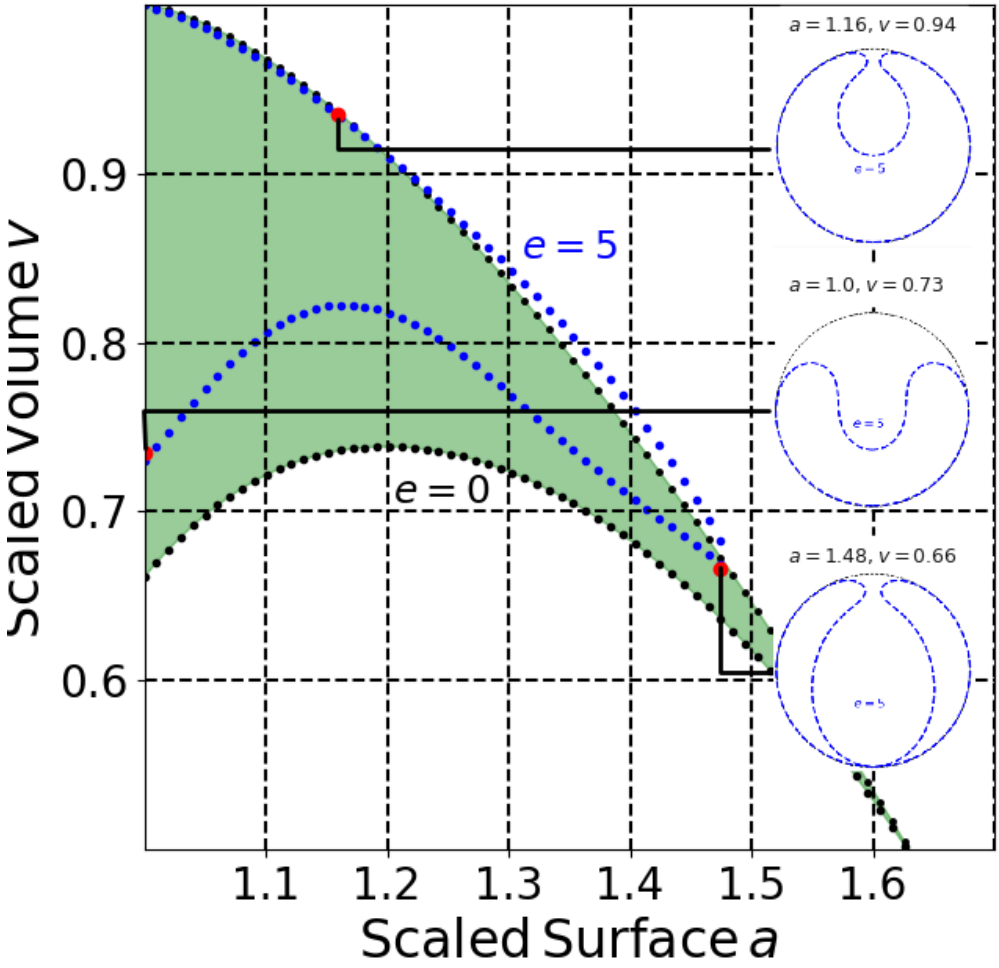

Figure 4.17: Shift of the axisymmetric area for the electric field parameter of $e = 5$ in the morphological phase diagram with vertical slices of the shapes found with the shooting method. The green shaded region displays simple axisymmetric solutions in the absence of electric field $e = 0$. Moreover, the dotted blue curved zone shows axisymmetric results for the electric field parameter of $e = 5$ (see also the main text).

The axisymmetric region is shifting more and more and decreasing more and more when the positive value of the electric field parameter is increased. To gain more insight into the behaviour of the system, let us look at the system with an electric field parameter of $e = 10$. Figure. 4.18 displays the change in the morphological phase diagram of the axisymmetric area for electric field parameter $e = 10$ (red dotted curves) in comparison to the axisymmetric area of $e = 0$ (green shaded region). In Fig. 4.18 the axisymmetric region (red dotted curves) is smaller compared to the axisymmetric

area of $e = 5$ in Figure. 4.17, (blue dotted curves), with a change in the upper boundary for electric field parameter $e = 10$.

With this in mind, let us consider a few two-dimensional vertical profiles obtained from the shooting method. At $(a, v) = (1.13, 0.95)$, the system displays a simple axisymmetric. The flexoelectric effect induces an axisymmetric elongation. When moving to the end of the upper boundary and increasing the area of the membrane to a value that is larger than the area of the container at $(a, v) = (1.39, 0.77)$, one can observe a folding inward parallel to the direction of the electric field which forces the membrane to touch the container. At the kink, when the axisymmetric region stops, one can take a look at $(a, v) = (1.29, 0.73)$ where the membrane still touches the container displaying a bigger neck. At $(a, v) = (1, 0.78)$ a simple axisymmetric invagination is found.

For large positive and negative values of the electric field parameter, it was only possible to find a narrow axisymmetric region from shooting method, which is why one needs to switch to the finite element method to obtain further solutions.

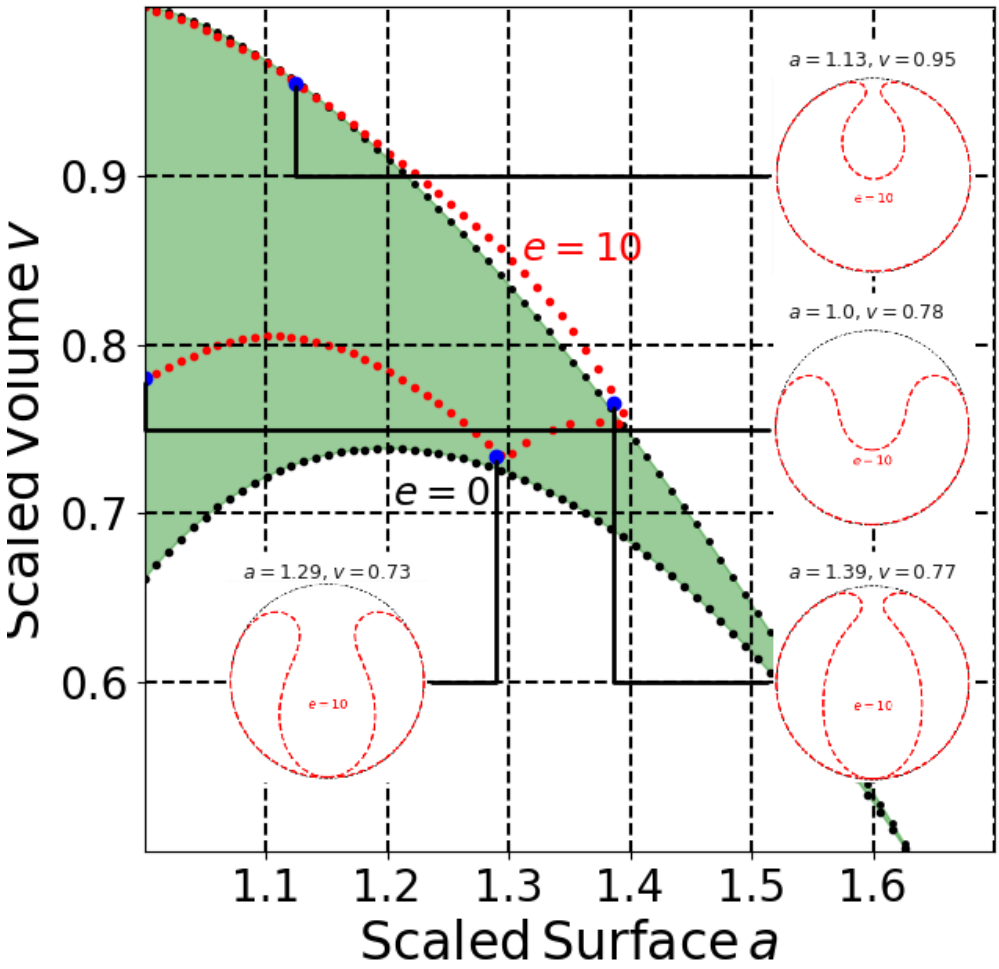

Figure 4.18: Shift of the axisymmetric area for the electric field parameter of $e = 10$ in the morphological phase diagram with vertical slices of the shapes found with the shooting method. The green shaded region displays simple axisymmetric solutions in the absence of electric field $e = 0$. Moreover, the dotted red curved zone shows axisymmetric results for the electric field parameter of $e = 10$ (see also the main text).

4.4.2 Finite Element Solutions

In the previous section, equilibrium solutions were obtained by minimising Eq. (4.17) for fixed parameters a, v, and e with our simple shooting method. Axisymmetric shapes without self-contact were determined with the help of a Hamiltonian formulation. The resulting differential equations are solved with a classical Runge-Kutta method. The container was treated as a hard constraint. Area and volume were conserved with the

help of Lagrange multipliers. The simplest axisymmetric shapes consisting of one free segment, and one portion in contact with the container were obtained. This method has its limitations, for instance, it is not possible to isolate minima solutions, and the shapes with more and complicated folding pattern.

To isolate minimum solutions, one needs to apply full-numerical treatments. When geometries become more complex, including symmetry breaking and self-contacts, the finite element simulations (FES) technique as a fully three-dimensional approach is more practical. In this approach, the first step is designing the initial mesh. For this purpose, one has to discretise the flexoelectric fluid membrane surface into a triangular mesh. This FE method was adjusted to fluid membranes by Klug et al. [84, 85]. A discretised version of Eq. (4.17) is used to determine the forces that act on each node. To equilibrate the system, we add a damping force on the nodes and integrate Newton's equations of motion in time. In the simulations, the container is modelled as a soft constraint with a quadratic repulsive force. The constraints on area and volume are implemented via a penalty method (for more detail see Appendix. C).

For moderate values of the parameters a, v, and e, the equilibrium solutions consist of an axisymmetric invagination connected to the contacting part of the membrane *via* a neck as we have already seen before (see Figure. 4.19). To get an insight into the behaviour of the system, first, different values of e with area and volume fixed to $(a, v) = (1.2, 0.8)$ are considered, which yields the shapes shown in Figure. 4.19. The *free* vesicle without electric field adopts the form of an oblate-discocyte as the global energy minimum [86] [5] . Figure. 4.19a exhibits the *confined* equilibrium result which

[5] For the free vesicle with $e = 0$ one also finds two local minima with higher bending energy: a stomatocyte and a prolate configuration. The energies of stomatocyte and oblate-discocyte are comparably close. However, the energy barrier between these shapes is high enough to avoid a transition due to thermal energy [86].

can be similar to a stomatocyte [1, 2]. The flexoelectric effect induces an elongation of the invagination. Depending on the sign of e this deformation is either parallel or perpendicular to the direction $\mathbf{z}$ of the external electric field (see Figures. 4.19b-4.19d and discussion in the previous sections) [6] .

[6] When the electric field is not directed along the invagination at the beginning of a simulation, the mesh reorients during equilibration until symmetry axis and electric field coincide.

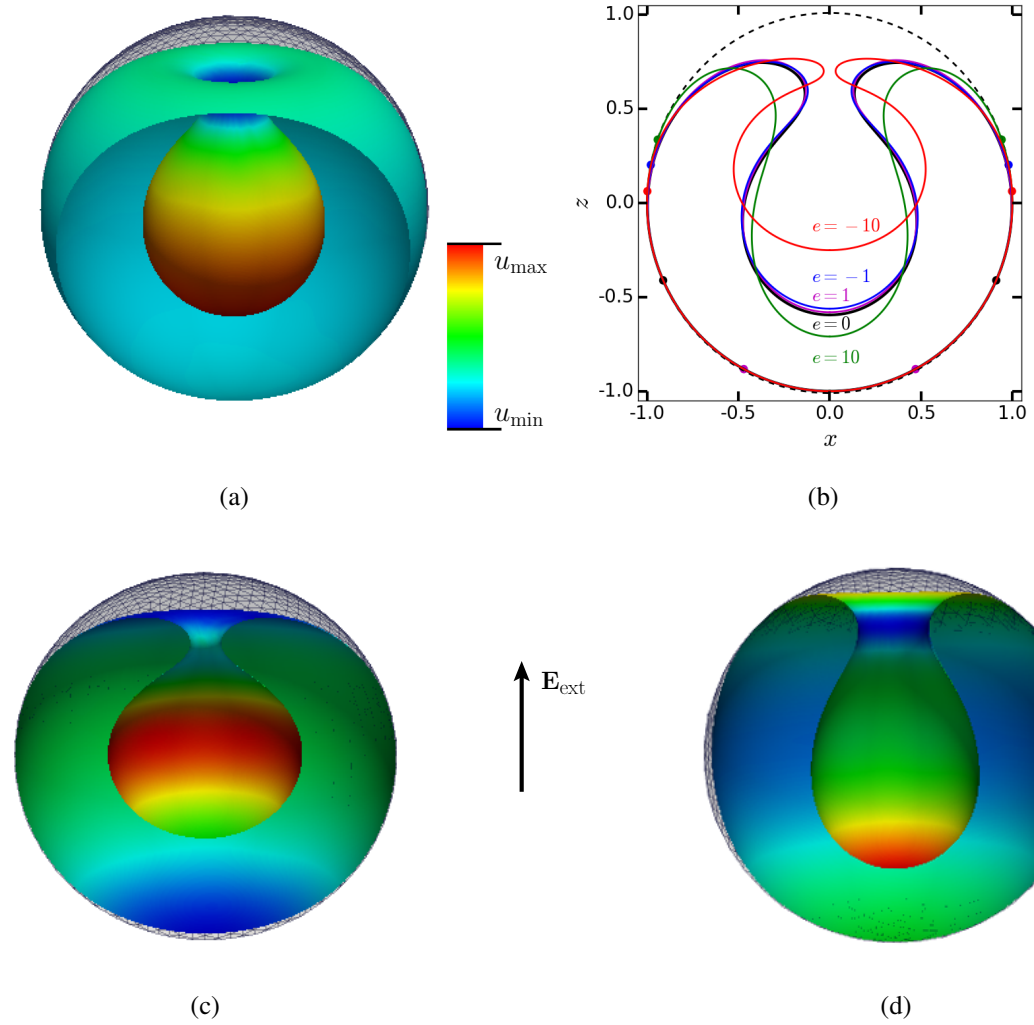

Figure 4.19: Numerical equilibrium results of a spherically confined membrane vesicle in an external uniform electric field with area $a = 1.2$ and volume $v = 0.8$ for different values of the electric field parameter e. (a) Finite element simulation solution for $e = 0$ [1, 2]. (b) The shooting method's axisymmetric solutions for $e = 0, \pm 1$ and ± 10. The membrane is formed of two segments, one in contact with the confinement and one which is free. The detachment points are indicated with dots. The solutions for $e = 0$ and $e = \pm 1$ coincide with the results from finite element simulations within the numerical error. For $e = \pm 10$ one observes an additional detachment of the membrane in the finite element simulations (see Figures. 4.19c and 4.19d), which is not considered in the shooting method. (c) Finite element simulation solution for $e = -10$. (d) Finite element simulation solution for $e = 10$. Colours in (a), (c), and (d) indicate the values of the scaled total energy density ranging from $u_{\min}$ to $u_{\max}$ with $(u_{\min}, u_{\max}) = (0, 10)$ in (a), $(2, 14)$ in (c), and $(-5, 10)$ in (d). The external electric field in (b)-(d) is aligned along the symmetry axis.

For larger values of $|e|$ one observes a new detachment of the membrane in contact with the container in the finite element simulations (see Figures. 4.19c and 4.19d), which

we cannot capture with our simple shooting method. The corresponding solutions thus have to be treated with prudence and should always be confirmed by finite element simulations.

4.4.2.1 Morphological Phase Diagram from Finite Element Simulation

With this in mind, one can now take a look at Figure. 4.20, which exhibits phase diagrams of our system. Figure. 4.20a recalls the results for the system without an external electric field, which was studied in Refs. [1, 2]. The vertical slices were obtained from finite element simulations. In the green region, one finds axisymmetric results with the shooting method. In the pink region below, the solutions are also axisymmetric but show a more intricated configuration with several free segments or self-contact, for instance. Figure. 4.20b presents the corresponding part of the phase diagram for $e = \pm 10$, where the above-mentioned detachment of the membrane takes place (slices of detached shapes highlighted with confining circle in blue).

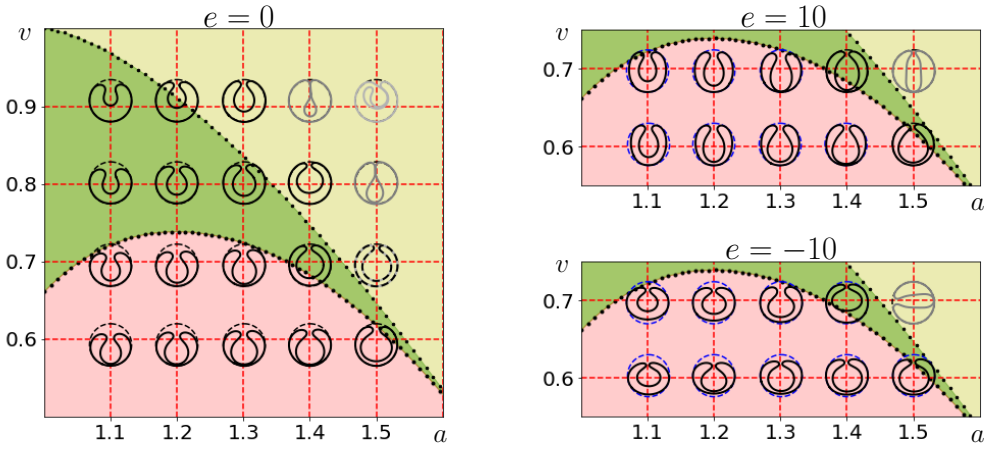

(a) (b)

Figure 4.20: Morphological phase diagrams with vertical slices of the shapes from finite element simulations (a) for $e = 0$ as obtained in Ref. [1] and (b) for $e = \pm 10$. The dotted lines and coloured regions in all figures were obtained for $e = 0$. In (b) they are duplicated for a better comparison with the detached vesicle shapes (see also main text).

4.4.2.2 Strong Electric Field and Symmetry Breaking

A flexoelectric membrane vesicle in a spherical cavity without electric field ($e = 0$) can be forced to break axisymmetry by increasing its area above a critical value (corresponding approximately to the upper black curve in Figure. 4.20) [1]. Consider, for instance, the vertical slices in Figure. 4.20a at constant volume $v = 0.7$. Below $a = 1.5$ the equilibrium solutions are axisymmetric. For $a = 1.5$, a metastable ellipsoidal state is observed. The corresponding ground state breaks axisymmetry with an invagination which is reminiscent of a prolate (comparable to the one of $(a, v) = (1.5, 0.8)$ in Figure. 4.20a). For $e = \pm 10$ similar shapes are observed which orient themselves parallel ($e > 0$) or perpendicular ($e < 0$) to the electric field (see again Figure. 4.20b). However, the neck connecting the invagination with the rest of the vesicle is not a slit with self-contact but exhibits an ellipsoidal cross-section.

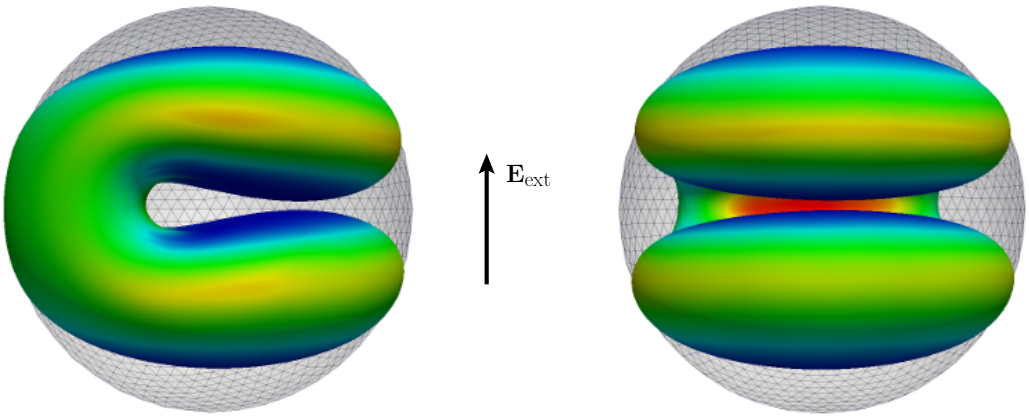

(a) (b)

Figure 4.21: Symmetry breaking for $a = 1.1$, $v = 0.7$ and $e = -50$ (from finite element simulations). The invagination of the membrane is not axisymmetric but deforms into a large elongated slit reminiscent of shapes that can be found with the ADE model for confined membranes without electric field (see Ref. [3] and references therein). (a) Side view and (b) top view of the invagination. The electric field is oriented vertically in (a) and (b). The color code of the profiles is the same as in Figure. 4.19 with $(u_{\min}, u_{\max}) = (0, 54)$.

A stronger coupling between the membrane and an external electric field provokes symmetry breaking at lower values of a. Figure. 4.21 shows one example for small area $a = 1.1$ and high *negative* electric field parameter $e = -50$. Similar shapes can be found for other areas and volumes as long as the absolute value of $e < 0$ is large enough. The invagination is slit-like and orients itself perpendicular to the electric field. The minimisation of the flexoelectric energy density, $e(\mathbf{z} \cdot \mathbf{n})^2$, now leads to almost flat membrane parts since this term dominates the bending energy term for high $|e|$.

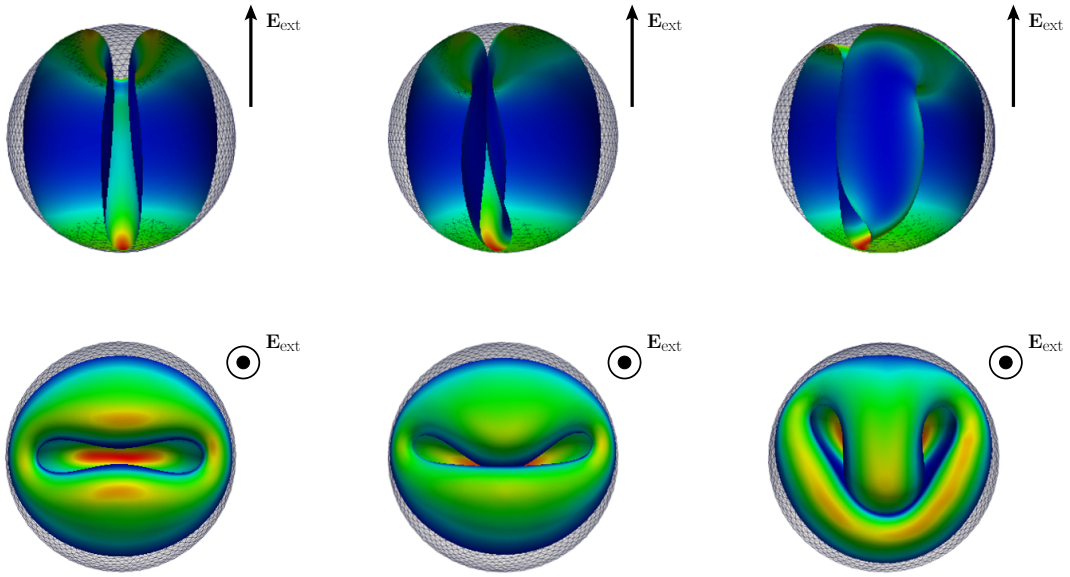

(a) (b) (c)

Figure 4.22: Symmetry breaking for constant volume $v = 0.7$, electric field parameter $e = 100$ and increasing area. Equilibrium solutions of finite element simulations with (a) $a = 1.3$, (b) $a = 1.4$, and (c) $a = 1.5$. (*top*) Side view and (*bottom*) top view of the invagination. The direction of the electric field is exhibited in every figure. The color code of the profiles is the same as in Figure. 4.19 with $(u_{\min}, u_{\max}) = (-50, 30)$ in (a), $(-50, 38)$ in (b), and $(-50, 31)$ in (c).

A high *positive* electric field parameter has a similar effect on the membrane vesicle. Figure. 4.22 shows how the electromechanical coupling induces a symmetry breaking for $e = 100$ and constant volume $v = 0.7$. The transition is similar to the

axisymmetric-to-prolate transition of $e = 0$ but happens already between $a = 1.2$ and 1.3. Figure. 4.22a shows the ground state for $a = 1.3$. The system contains two symmetry planes. The slit-like invagination is parallel to $\mathbf{E}_{\text{ext}}$ as expected. For $a = 1.4$ large portions of the membrane come into contact. One of the planar symmetries is broken (see Figure. 4.22b). A further increase of a deforms the slit-like neck even further (see Figure. 4.22c).

Chapter 5

CONCLUSIONS AND FUTURE DIRECTIONS

5.1 Conclusions

In this thesis, we have seen how flexoelectric membranes respond to external constraints. In the following, the essential accomplishments of this study will be summed up:

- A framework for flexoelectric lipid bilayers in the presence of an external electric field is developed, leading to geometrical expressions for the stress tensor and the shape equation. This model is generic; however, we have restricted our discussion to one particular system: a spherically confined flexoelectric membrane vesicle in a uniform electric field. The resulting shapes are presented and the transition lines, that shift due to the presence of an electric field, are shown. The folding patterns that the bilayer membrane can adopt could be of interest to biophysical and technological applications alike.
- To find equilibrium configurations as a function of area, volume and the coupling with the electric field, two numerical methods were exploited. Despite some rather crude approximations such as assuming a constant electric field, we have found exciting shape transformations and symmetry breaking.
- When the area of the vesicle is larger than the area of the spherical confinement, the membrane has to form an invagination inside the container. This is only possible when the volume enclosed by the vesicle is smaller than the confining volume. For moderate values of the parameters a, v, and e, the equilibrium

solutions consist of an axisymmetric invagination connected to the contacting part of the membrane *via* a neck. To gain more insight into the behavior of the system, we have considered different values of e with area and volume fixed to $(a, v) = (1.2, 0.8)$. It turns out that the flexoelectric effect induces an elongation of the invagination. Depending on the sign of e this deformation is either parallel or perpendicular to the direction of the external electric field. An electric field parameter of the order of ± 1 does not influence the resulting shape dramatically. One can observe, however, that the circle at which the vesicle detaches from the container depends crucially on the value of e. A word of caution is due here. For larger values of $|e|$ one observes an additional detachment of the membrane in contact with the container, which cannot be captured with the simple shooting method. The corresponding solutions thus have to be treated with prudence and should always be confirmed by finite element simulations.

- When the electric field parameter is large, complex folding patterns that result from the interplay of the confinement and the flexoelectric effect were obtained. Self-contacts, as observed in this work, can potentially lead to a transition from a spherical to a toroidal vesicle topology *via* membrane fusion. This question was studied for the system without electric field in Ref. [36]. It turns out that the spherical topology is preferred for typical values of the material parameters. Flexoelectricity could potentially facilitate topology changes. For a definite statement, however, one would have to study confined flexoelectric fluid membrane vesicles of toroidal topology in detail for $e \neq 0$.
- The morphological phase diagram of the system displays three different regions: simple axisymmetric solutions, axisymmetric-with-detachment, and more complicated configurations with several free parts or self-contact.
- To confirm that the obtained shapes are stable and do not rupture due to the

stresses induced by the electric field in experiments, one has to check whether the resulting surface tension is below the membrane's rupture tension. This question can be addressed qualitatively by comparing the membrane stresses due to the area constraint and the external electric field. The latter is linear in the electric field parameter e whereas the former is linear in the scaled surface tension $\tilde{\sigma} = \frac{\sigma R^2}{\kappa}$, where σ is the unscaled surface tension and R is the radius of the confining sphere. One expects a maximum surface tension of the order of a few mN/m, which is approximately the rupture tension for a fluid phospholipid bilayer [15]. Inserting typical values for the other parameters, $R = 0.5\,\mu$m and $\kappa = 20 k_B T$, one obtains $\tilde{\sigma} \approx 3000$ which is much larger than the values of e that we consider. However, when R is reduced to $0.1\mu m$, the normalised tensions from the area constraint and the electric field become comparable. An experimental check of our results would have to take this into account to avoid membrane rupture.

5.2 Future Directions

Experiments on confined fluid membrane vesicles are still sparse. The case without electric field has been studied together with numerical simulations in Ref. [76]. One can find a large amount of literature on unconfined vesicles in spatially uniform electric fields. DC pulses can, for instance, lead to elongation [87], wrinkling [88] or even bursting [89] of the vesicle for strong electric fields. I am not aware of an experimental study of the confined system, but the hope is that the results of this thesis arouse interest in this subject.

In this work, we have focused on the effects of polarization and assumed free charges to be absent. These would have to be included to get closer to real experimental conditions, where charges accumulate near the membrane [87, 90]. Moreover, it would be interesting to apply the model to other systems in more complicated electric

fields. A dynamic study could be very fertile as well given experimental observations that show dynamic transitions of membranes induced by electric fields [90, 91].

REFERENCES

[1] O. Kahraman, N. Stoop, and M. M. Müller, "Morphogenesis of membrane invaginations in spherical confinement," *EPL (Europhysics Letters)*, vol. 97, no. 6, p. 68008, 2012.

[2] ——, "Fluid membrane vesicles in confinement," *New Journal of Physics*, vol. 14, no. 9, p. 095021, 2012.

[3] B. Kavčič, A. Sakashita, H. Noguchi, and P. Ziherl, "Limiting shapes of confined lipid vesicles," *Soft matter*, vol. 15, no. 4, pp. 602–614, 2019.

[4] T. Wakatsuki, M. S. Kolodney, G. I. Zahalak, and E. L. Elson, "Cell mechanics studied by a reconstituted model tissue," *Biophysical journal*, vol. 79, no. 5, pp. 2353–2368, 2000.

[5] G. I. Zahalak, J. E. Wagenseil, T. Wakatsuki, and E. L. Elson, "A cell-based constitutive relation for bio-artificial tissues," *Biophysical journal*, vol. 79, no. 5, pp. 2369–2381, 2000.

[6] C. D. McCaig, A. M. Rajnicek, B. Song, and M. Zhao, "Controlling cell behavior electrically: current views and future potential," *Physiological reviews*, vol. 85, no. 3, pp. 943–978, 2005.

[7] J. Voldman, "Electrical forces for microscale cell manipulation," *Annu. Rev. Biomed. Eng.*, vol. 8, pp. 425–454, 2006.

[8] D. Chang, *Guide to electroporation and electrofusion*. Academic Press, 1991.

[9] C. A. Jordan, E. Neumann, and A. E. Sowers, *Electroporation and electrofusion in cell biology*. Springer Science & Business Media, 2013.

[10] U. Zimmermann and G. A. Neil, *Electromanipulation of cells*. CRC press, 1996.

[11] U. Zimmermann, G. Pilwat, and H. Pohl, "Electric field-mediated cell fusion," *Journal of Biological Physics*, vol. 10, no. 1, pp. 43–50, 1982.

[12] U. Zimmermann, J. Vienken, and G. Pilwat, "Development of drug carrier systems: electrical field induced effects in cell membranes," *Journal of Electroanalytical Chemistry and Interfacial Electrochemistry*, vol. 116, pp. 553–574, 1980.

[13] R. Dimova, N. Bezlyepkina, M. D. Jordö, R. L. Knorr, K. A. Riske, M. Staykova, P. M. Vlahovska, T. Yamamoto, P. Yang, and R. Lipowsky, "Vesicles in electric fields: some novel aspects of membrane behavior," *Soft Matter*, vol. 5, no. 17, pp. 3201–3212, 2009.

[14] R. Capovilla and J. Guven, "Geometry of lipid vesicle adhesion," *Physical Review E*, vol. 66, no. 4, p. 041604, 2002.

[15] E. Evans, V. Heinrich, F. Ludwig, and W. Rawicz, "Dynamic tension spectroscopy and strength of biomembranes," *Biophysical journal*, vol. 85, no. 4, pp. 2342–2350, 2003.

[16] E. Evans and W. Rawicz, "Entropy-driven tension and bending elasticity in condensed-fluid membranes," *Physical review letters*, vol. 64, no. 17, p. 2094, 1990.

[17] W. Helfrich, "Elastic properties of lipid bilayers: theory and possible experiments," *Zeitschrift für Naturforschung C*, vol. 28, no. 11-12, pp. 693–703, 1973.

[18] F. Jülicher and R. Lipowsky, "Shape transformations of vesicles with intramembrane domains," *Physical Review E*, vol. 53, no. 3, p. 2670, 1996.

[19] F. Jülicher and U. Seifert, "Shape equations for axisymmetric vesicles: a clarification," *Physical Review E*, vol. 49, no. 5, p. 4728, 1994.

[20] R. Lipowsky and E. Sackmann, *Structure and dynamics of membranes: I. from cells to vesicles/II. generic and specific interactions*. Elsevier, 1995.

[21] U. Seifert, "Self-consistent theory of bound vesicles," *Physical review letters*, vol. 74, no. 25, p. 5060, 1995.

[22] ——, "Configurations of fluid membranes and vesicles," *Advances in physics*, vol. 46, no. 1, pp. 13–137, 1997.

[23] U. Seifert and R. Lipowsky, "Morphology of vesicles," *Handbook of biological physics*, vol. 1, pp. 403–464, 1995.

[24] D. E. Ingber, "The architecture of life," *Scientific American*, vol. 278, no. 1, pp. 48–57, 1998.

[25] D. Boal and D. H. Boal, *Mechanics of the Cell*. Cambridge University Press, 2012.

[26] A. G. Petrov, "Flexoelectricity of model and living membranes," *Biochimica et Biophysica Acta (BBA)-Biomembranes*, vol. 1561, no. 1, pp. 1–25, 2002.

[27] ——, "Electricity and mechanics of biomembrane systems: flexoelectricity in living membranes," *Analytica chimica acta*, vol. 568, no. 1-2, pp. 70–83, 2006.

[28] V. Vitkova and A. G. Petrov, "Lipid bilayers and membranes: material properties," in *Advances in planar lipid bilayers and liposomes*. Elsevier, 2013, vol. 17, pp. 89–138.

[29] A. D. Rey, "Liquid crystal model of membrane flexoelectricity," *Physical Review E*, vol. 74, no. 1, p. 011710, 2006.

[30] L.-T. Gao, X.-Q. Feng, Y.-J. Yin, and H. Gao, "An electromechanical liquid crystal model of vesicles," *Journal of the Mechanics and Physics of Solids*, vol. 56, no. 9, pp. 2844–2862, 2008.

[31] P. Mohammadi, L. Liu, and P. Sharma, "A theory of flexoelectric membranes and effective properties of heterogeneous membranes," *Journal of Applied Mechanics*, vol. 81, no. 1, p. 011007, 2014.

[32] D. Steigmann and A. Agrawal, "Electromechanics of polarized lipid bilayers," *Mathematics and Mechanics of Complex Systems*, vol. 4, no. 1, pp. 31–54, 2016.

[33] D. S. Bruhn, M. A. Lomholt, and H. Khandelia, "Quantifying the relationship between curvature and electric potential in lipid bilayers," *The Journal of Physical Chemistry B*, vol. 120, no. 21, pp. 4812–4817, 2016.

[34] R. Phillips, J. Theriot, J. Kondev, and H. Garcia, *Physical biology of the cell*. Garland Science, 2012.

[35] U. Seifert, K. Berndl, and R. Lipowsky, "Shape transformations of vesicles: Phase diagram for spontaneous-curvature and bilayer-coupling models," *Physical Review A*, vol. 44, no. 2, p. 1182, 1991.

[36] L. Bouzar, F. Menas, and M. M. Müller, "Toroidal membrane vesicles in spherical confinement," *Physical Review E*, vol. 92, no. 3, p. 032721, 2015.

[37] H. Lodish, J. E. Darnell, A. Berk, C. A. Kaiser, M. Krieger, M. P. Scott, A. Bretscher, H. Ploegh, P. Matsudaira *et al.*, *Molecular cell biology*. Macmillan, 2008.

[38] R. Lipowsky and E. Sackmann, "Structure and dynamics of membranes—from cells to vesicles (handbook of biological physics vol 1)," 1995.

[39] M. Deserno, "Fluid lipid membranes–a primer," *See http://www. cmu. edu/biolphys/deserno/pdf/membrane_theory. pdf*, 2007.

[40] E. Gorter and F. Grendel, "On bimolecular layers of lipoids on the chromocytes of the blood," *Journal of experimental medicine*, vol. 41, no. 4, pp. 439–443, 1925.

[41] D. Vance and J. Vance, "Physical properties and functional roles of lipids in membranes," *Biochemistry of lipids, lipoproteins and membranes*, vol. 31, pp. 1–33, 1996.

[42] P. R. Cullis and M. J. Hope, "Physical properties and functional roles of lipids in membranes," in *New Comprehensive Biochemistry*. Elsevier, 1991, vol. 20, pp. 1–41.

[43] R. Lipowsky, "The conformation of membranes," *Nature*, vol. 349, no. 6309, p. 475, 1991.

[44] U. Seifert and S. A. Langer, "Viscous modes of fluid bilayer membranes," *EPL (Europhysics Letters)*, vol. 23, no. 1, p. 71, 1993.

[45] R. Bingham, S. Smye, and P. Olmsted, "Dynamics of an asymmetric bilayer lipid membrane in a viscous solvent," *EPL (Europhysics Letters)*, vol. 111, no. 1, p. 18004, 2015.

[46] P. B. Canham, "The minimum energy of bending as a possible explanation of the biconcave shape of the human red blood cell," *Journal of theoretical biology*, vol. 26, no. 1, pp. 61–81, 1970.

[47] W. Helfrich, "Elastic properties of lipid bilayers: theory and possible experiments," *Zeitschrift für Naturforschung C*, vol. 28, no. 11-12, pp. 693–703, 1973.

[48] E. A. Evans, "Bending resistance and chemically induced moments in membrane bilayers," *Biophysical journal*, vol. 14, no. 12, pp. 923–931, 1974.

[49] F. Ahmadpoor and P. Sharma, "Flexoelectricity in two-dimensional crystalline and biological membranes," *Nanoscale*, vol. 7, no. 40, pp. 16 555–16 570, 2015.

[50] J. Curie and P. Curie, "Développement par compression de l'électricité polaire dans les cristaux hémièdres à faces inclinées," *Bulletin de minéralogie*, vol. 3, no. 4, pp. 90–93, 1880.

[51] G. Gautschi, "Piezoelectric sensors," in *Piezoelectric Sensorics*. Springer, 2002, pp. 73–91.

[52] J. D. Madden, N. A. Vandesteeg, P. A. Anquetil, P. G. Madden, A. Takshi, R. Z. Pytel, S. R. Lafontaine, P. A. Wieringa, and I. W. Hunter, "Artificial muscle technology: physical principles and naval prospects," *IEEE Journal of oceanic engineering*, vol. 29, no. 3, pp. 706–728, 2004.

[53] M. Labanca, F. Azzola, R. Vinci, and L. F. Rodella, "Piezoelectric surgery: twenty years of use," *British Journal of Oral and Maxillofacial Surgery*, vol. 46, no. 4, pp. 265–269, 2008.

[54] R. B. Meyer, "Piezoelectric effects in liquid crystals," *Physical Review Letters*, vol. 22, no. 18, p. 918, 1969.

[55] J. Seelig, "31p nuclear magnetic resonance and the head group structure of phospholipids in membranes," *Biochimica et Biophysica Acta (BBA)-Reviews on Biomembranes*, vol. 515, no. 2, pp. 105–140, 1978.

[56] H. Frischleder and G. Peinel, "Quantum-chemical and statistical calculations on phospholipids," *Chemistry and Physics of Lipids*, vol. 30, no. 2-3, pp. 121–158, 1982.

[57] D. T. Warshaviak, M. J. Muellner, and M. Chachisvilis, "Effect of membrane tension on the electric field and dipole potential of lipid bilayer membrane," *Biochimica et Biophysica Acta (BBA)-Biomembranes*, vol. 1808, no. 10, pp. 2608–2617, 2011.

[58] J. Guven, "Membrane geometry with auxiliary variables and quadratic constraints," *Journal of Physics A: Mathematical and General*, vol. 37, no. 28, p. L313, 2004.

[59] D. Steigmann, E. Baesu, R. E. Rudd, J. Belak, and M. McElfresh, "On the variational theory of cell-membrane equilibria," *Interfaces and Free Boundaries*, vol. 5, no. 4, pp. 357–366, 2003.

[60] R. Goetz and W. Helfrich, "The egg carton: theory of a periodic superstructure of some lipid membranes," *Journal de Physique II*, vol. 6, no. 2, pp. 215–223, 1996.

[61] M. M. Müller, "Theoretical examinations of interface mediated interactions between colloidal particles," Ph.D. dissertation, Johannes Gutenberg Universität Mainz, 2004.

[62] D. J. Steigmann, *The Role of Mechanics in the Study of Lipid Bilayers*. Springer, 2017, vol. 577.

[63] M. M. Müller, "Theoretical studies of fluid membrane mechanics," Ph.D. dissertation, Johannes Gutenberg-Universität Mainz, 2007.

[64] J. Guven, "Laplace pressure as a surface stress in fluid vesicles," *Journal of Physics A: Mathematical and General*, vol. 39, no. 14, p. 3771, 2006.

[65] S. A. Teukolsky, B. P. Flannery, W. Press, and W. Vetterling, "Numerical recipes in c," *SMR*, vol. 693, no. 1, pp. 59–70, 1992.

[66] M. Deserno, M. M. Müller, and J. Guven, "Contact lines for fluid surface adhesion," *Physical Review E*, vol. 76, no. 1, p. 011605, 2007.

[67] J. S. Rowlinson and B. Widom, *Molecular theory of capillarity*. Courier Corporation, 2013.

[68] P.-G. De Gennes, F. Brochard-Wyart, and D. Quéré, *Capillarity and wetting phenomena: drops, bubbles, pearls, waves*. Springer Science & Business Media, 2013.

[69] A. Agrawal and D. J. Steigmann, "Boundary-value problems in the theory of lipid membranes," *Continuum Mechanics and Thermodynamics*, vol. 21, no. 1, pp. 57–82, 2009.

[70] S. Kuure, R. Vuolteenaho, and S. Vainio, "Kidney morphogenesis: cellular and molecular regulation," *Mechanisms of development*, vol. 92, no. 1, pp. 31–45, 2000.

[71] M. Zick, R. Rabl, and A. S. Reichert, "Cristae formation—linking ultrastructure and function of mitochondria," *Biochimica et Biophysica Acta (BBA)-Molecular Cell Research*, vol. 1793, no. 1, pp. 5–19, 2009.

[72] C. A. Mannella, "Structure and dynamics of the mitochondrial inner membrane cristae," *Biochimica et Biophysica Acta (BBA)-Molecular Cell Research*, vol. 1763, no. 5-6, pp. 542–548, 2006.

[73] W. T. D'ARCY *et al.*, *ON GROWTH AND FORM*. STELLAR EDITIONS, 2016.

[74] R. Thom, *Structural stability and morphogenesis*. CRC press, 2018.

[75] J. D. Jackson, "Classical electrodynamics," 1999.

[76] A. Sakashita, M. Imai, and H. Noguchi, "Morphological variation of a lipid vesicle confined in a spherical vesicle," *Physical Review E*, vol. 89, no. 4, p. 040701, 2014.

[77] C. A. Mannella, "Structure and dynamics of the mitochondrial inner membrane cristae," *Biochimica et Biophysica Acta (BBA)-Molecular Cell Research*, vol. 1763, no. 5-6, pp. 542–548, 2006.

[78] I. E. Scheffler, *Mitochondria*. John Wiley & Sons, 2011.

[79] M. R. Taylor, E. J. Simon, J. L. Dickey, K. A. Hogan, and J. B. Reece, *Campbell Biology: Concepts & Connections*. Pearson, 2017.

[80] C. A. Mannella, "Structure and dynamics of the mitochondrial inner membrane cristae," *Biochimica et Biophysica Acta (BBA)-Molecular Cell Research*, vol. 1763, no. 5-6, pp. 542–548, 2006.

[81] H. Noguchi, "Shape transitions of high-genus fluid vesicles," *EPL (Europhysics Letters)*, vol. 112, no. 5, p. 58004, 2015.

[82] R. De Pascalis, G. Napoli, and S. S. Turzi, "Growth-induced blisters in a circular tube," *Physica D: Nonlinear Phenomena*, vol. 283, pp. 1–9, 2014.

[83] J. Guven, J. A. Santiago, and P. Vázquez-Montejo, "Confining spheres within hyperspheres," *Journal of Physics A: Mathematical and Theoretical*, vol. 46, no. 13, p. 135201, 2013.

[84] F. Feng and W. S. Klug, "Finite element modeling of lipid bilayer membranes," *Journal of Computational Physics*, vol. 220, no. 1, pp. 394–408, 2006.

[85] L. Ma and W. S. Klug, "Viscous regularization and r-adaptive remeshing for finite element analysis of lipid membrane mechanics," *Journal of Computational Physics*, vol. 227, no. 11, pp. 5816–5835, 2008.

[86] U. Seifert, K. Berndl, and R. Lipowsky, "Shape transformations of vesicles: Phase diagram for spontaneous-curvature and bilayer-coupling models," *Physical review A*, vol. 44, no. 2, p. 1182, 1991.

[87] R. Dimova, K. A. Riske, S. Aranda, N. Bezlyepkina, R. L. Knorr, and R. Lipowsky, "Giant vesicles in electric fields," *Soft matter*, vol. 3, no. 7, pp. 817–827, 2007.

[88] R. L. Knorr, M. Staykova, R. S. Gracià, and R. Dimova, "Wrinkling and electroporation of giant vesicles in the gel phase," *Soft Matter*, vol. 6, no. 9, pp. 1990–1996, 2010.

[89] K. A. Riske, R. L. Knorr, and R. Dimova, "Bursting of charged multicomponent vesicles subjected to electric pulses," *Soft Matter*, vol. 5, no. 10, pp. 1983–1986, 2009.

[90] P. M. Vlahovska, "Voltage-morphology coupling in biomimetic membranes: dynamics of giant vesicles in applied electric fields," *Soft matter*, vol. 11, no. 37, pp. 7232–7236, 2015.

[91] L. C. McConnell, P. M. Vlahovska, and M. J. Miksis, "Vesicle dynamics in uniform electric fields: squaring and breathing," *Soft Matter*, vol. 11, no. 24,

pp. 4840–4846, 2015.

[92] D. R. Nelson, T. Piran, and S. Weinberg, *Statistical mechanics of membranes and surfaces*. World Scientific, 2004.

[93] M. M. Müller, "Theoretical studies of fluid membrane mechanics," Ph.D. dissertation, Johannes Gutenberg-Universität Mainz, 2007.

[94] M. Deserno, "Notes on differential geometry," 2004.

[95] D. J. Steigmann, *The Role of Mechanics in the Study of Lipid Bilayers*. Springer, 2017, vol. 577.

[96] F. Cirak, M. Ortiz, and P. Schröder, "Subdivision surfaces: a new paradigm for thin-shell finite-element analysis," *International Journal for Numerical Methods in Engineering*, vol. 47, no. 12, pp. 2039–2072, 2000.

[97] M. Labanca, F. Azzola, R. Vinci, and L. F. Rodella, "Piezoelectric surgery: twenty years of use," *British Journal of Oral and Maxillofacial Surgery*, vol. 46, no. 4, pp. 265–269, 2008.

[98] D. Andelman, "Electrostatic properties of membranes: the poisson-boltzmann theory," in *Handbook of biological physics*. Elsevier, 1995, vol. 1, pp. 603–642.

APPENDICES

Appendix A: Differential Geometry of Fluid Membranes

Differential Geometry of fluid membranes

From a geometrical point of view, fluid lipid bilayer membranes can be modeled as two-dimensional surfaces at physiological temperature due to having a large-scale length in comparison with their thickness. This section aims to summarize some of the critical aspects of the differential geometry of the membrane (two-dimensional surfaces). For more information in this context see [92–94], and [95].

Basic definitions

Parametrization of surfaces

It is possible to describe a surface membrane by mapping surface parametrization into the three-dimensional space, $\mathbb{R}^3$, as following:

$$\mathbf{X}(u^1,u^2) \rightarrow \mathbf{X}(u^1,u^2) \tag{A.1}$$

in which u^1,and u^2 are two local curvilinear coordinates. In this parametrization, the two tangent vectors of the membrane at every point define as:

$$\mathbf{e}_\alpha = \partial_\alpha \mathbf{X}\,, \quad \alpha = 1,2\,, \tag{A.2}$$

the surface Jacobian is constructed as $\sqrt{g} = |\mathbf{e}_1 \times \mathbf{e}_2|$. By making use of these vectors, one can describe the normal vector as:

$$\mathbf{n} = \frac{\mathbf{e}_1 \times \mathbf{e}_2}{\sqrt{g}}\,, \tag{A.3}$$

One should consider $\mathbf{n}$ unit normal vector, however $\mathbf{e}_a$ are not generally unit vectors. It is possible to construct any vector field on the surface by making use of these basis

vectors $\mathbf{e}_1, \mathbf{e}_2, \mathbf{n}$, in which $\mathbf{e}_\alpha \cdot \mathbf{n} = 0$, and $\mathbf{n} \cdot \mathbf{n} = 1$.

The metric tensor

One can construct the metric tensor induced on the membrane or the first fundamental form with the two tangent vectors as following:

$$g_{ab} := \mathbf{e}_a \cdot \mathbf{e}_b \,, \tag{A.4}$$

The determinant of the first fundamental form given by:

$$g := det\mathbf{g} = det(g_{ab}) = g_{11}g_{22} - g_{22}g_{11} = |\mathbf{e}_1 \times \mathbf{e}_2|^2 \,, \tag{A.5}$$

by taking advantage of g, one can calculate the infinitesimal area element as following:

$$dA = |\mathbf{e}_1 \times \mathbf{e}_2| ds^1 ds^2 = \sqrt{g} d^2 s \,. \tag{A.6}$$

Curvatures

To compute the curvatures of surfaces, one needs to fit the best circles pass through the specific point on the plane such that it cuts through the surface. The intersection result of surface and plane will be a space curve. One can calculate the best circle that fits the specific point. Therefore, the curvatures' value depends on the orientation of the intersected plane, but searching for a unique solution is the aim. To bypass this problem, one can consider two orthogonal planes as specific choices that they have extreme curvatures known as principal curvatures, one maximum, and the other minimum. For instance, principal curvatures captured by a sphere are identical and equal to $\frac{1}{R}$, in which R is the sphere's radius. A cylinder with radius r has principal curvatures of $\frac{1}{r}$ and 0.

The extrinsic curvature tensor

Surfaces with different curvature properties can have the same metric tensor g_{ab}. To be able to illustrate curvature properties, one may assume the existence of a curve on the surface where its curvature at any point is $k > 0$, with the parametrization $\mathbf{X}(u^1(s), u^2(s))$ with s as the arc length of the curve. On every point of this curve, one may define a comoving coordinate $\{\mathbf{t}, \mathbf{p}, \mathbf{b}\}$ with $\mathbf{t} = \dot{\mathbf{X}}$ as the unit tangent vector, $\mathbf{p} = \frac{\dot{\mathbf{t}}}{|\dot{\mathbf{t}}|} = \frac{\dot{\mathbf{t}}}{k}$ as the unit principal normal vector, and $\mathbf{b} = \mathbf{t} \times \mathbf{p}$ as the unit binormal vector. One may define the following equations:

$$\mathbf{p} \cdot \mathbf{n} = \cos\psi\,, \qquad \dot{\mathbf{t}} = k\mathbf{p}\,, \quad \textit{and} \quad \dot{\mathbf{t}} \cdot \mathbf{n} = k\cos\psi \tag{A.7}$$

In which ψ is the angle between the two unit vectors of $\mathbf{n}$ and $\mathbf{p}$. The normal curvature which is the relations between first and second fundamental forms calculates how membrane bends in space. One may define the normal curvature in the direction of $\mathbf{t}$ at any point on the curve as:

$$K_n := -\dot{\mathbf{t}} \cdot \mathbf{n} = -k(\mathbf{p} \cdot \mathbf{n}) = -k\cos\psi, \tag{A.8}$$

and the definition of the geodesic curvature which calculates how curve curves on a membrane given by:

$$K_g := \mathbf{t} \cdot (\mathbf{t} \times \mathbf{n}) = k\mathbf{t} \cdot (\mathbf{p} \times \mathbf{n}) = k\sin\psi \tag{A.9}$$

The extrinsic curvature tensor obtains:

$$K_{ab} := -\mathbf{n} \cdot \nabla_a \mathbf{e}_b\,. \tag{A.10}$$

It is possible to define the trace of the extrinsic curvature:

$$K := Tr(K_a^b) = -g^{ab}K_{ab} = k_1 + k_2 \ , \tag{A.11}$$

and the Gaussian curvature as:

$$K_G := det(K_a^b) = k_1 k_2 \ . \tag{A.12}$$

The Gauss and Weingarten equations

By making use of the extrinsic curvature it is possible to capture the relation between intrinsic and extrinsic geometry. The Gauss equations are:

$$\nabla_a \mathbf{e}_b = -K_{ab}\mathbf{n} \ , \tag{A.13}$$

And the Weingarten equations are:

$$\partial_a \mathbf{n} = \nabla_a \mathbf{n} = K_a^b \mathbf{e}_b \ . \tag{A.14}$$

The Gauss-Bonnet formula

The relation between the geometry of surfaces and their topology known as the Gauss-Bonnet theorem.

$$\int_{\partial M} ds K_g + \int_M dA K_G = 2\pi\chi(M) \tag{A.15}$$

Where $\chi(M)$ is the Euler characteristic of M. One may apply this theorem to the closed membranes that they have homomorphic topology to the sphere with g handles, which known as a genus of the surface. In this respect, a sphere has genus 0, and a torus has genus 1, etc. For any closed oriented membrane of genus g:

$$\int_M dA K_G = 4\pi(1-g) \tag{A.16}$$

Surface Parametrization

There exist some parametrization framework to describe the curvature of a surface embedded in three-dimensional space.

Monge parametrization

Monge parametrization, as one of the surface parametrization, is mostly applying to the horizontal plane. This parametrization describes the surface by a height function above an arbitrary reference flat surface as following:

$$h: \begin{cases} \mathbb{R}^2 \supset U \longrightarrow \mathbb{R}^3 \\ (x,y) \longrightarrow h(x,y) \end{cases} . \tag{A.17}$$

In the cartesian coordinate system, the position vector and two tangent vector obtain as:

$$\mathbf{X} = \begin{pmatrix} x \\ y \\ h(x,y) \end{pmatrix}, \quad \mathbf{e}_x = \begin{pmatrix} 1 \\ 0 \\ h_x \end{pmatrix}, \quad \textit{and} \quad \mathbf{e}_y = \begin{pmatrix} 0 \\ 1 \\ h_y \end{pmatrix}. \tag{A.18}$$

where $h_i = \partial_i h(i, j \in \{x,y\})$. In this parameterization, one may write the metric tensor as:

$$g_{ij} = \delta_{ij} + h_i h_j, \tag{A.19}$$

where δ_{ij} is the Kronecker symbol. For the two-dimensional surfaces, one can describe the nabla operator ∇, which can have the below form for the local Cartesian coordinates:

$$\nabla = \begin{pmatrix} \partial_x \\ \\ \partial_y \end{pmatrix}, \tag{A.20}$$

which leads us to redefine the following equations. The metric determinant as:

$$g = 1 + (\nabla h)^2 \tag{A.21}$$

the normal vector:

$$\mathbf{n} = \frac{(-\nabla h + z)}{\sqrt{1 + (\nabla h)^2}}. \tag{A.22}$$

the extrinsic curvature tensor:

$$K_{ij} = -\frac{h_{ij}}{\sqrt{g}} \tag{A.23}$$

its trace is:

$$K = -\nabla \cdot \left(\frac{\nabla h}{\sqrt{1 + (\nabla h)^2}} \right). \tag{A.24}$$

Angle-arc length parametrization

It is possible to parametrize the membranes by the angle $\psi(s)$ between the horizontal plane and the tangential plane, which is the function of arc length s, in the case that surfaces have translational or rotational symmetry. The surface profile does not vary along the $y-axis$ if the surface is translational symmetric. One can write the projection of the tangent and normal vectors in the Cartesian coordinate system as:

$$\rho \cdot \mathbf{l} = \mathbf{z} \cdot \mathbf{n} = \cos\psi, \qquad \textit{and} \qquad \rho \cdot \mathbf{n} = -\mathbf{z} \cdot \mathbf{l} = -\sin\psi\,. \tag{A.25}$$

In the case of having axisymmetric surfaces, it is possible to describe the principal curvatures by the meridians and parallels on the surface as:

$$K_{\perp} = -\dot{\psi}, \qquad \textit{and} \qquad K_{\parallel} = -\frac{\sin\psi}{\rho} \; . \tag{A.26}$$

where ρ and $\mathbf{l}$ are the horizontal and the tangential vector, respectively.

Appendix B: Monge Gauge

The spherical Monge gauge

Special cases

First case: The perfect sphere with $h(\theta,\varphi)=R$. This in turn implies $h_{,\theta}=h_{,\varphi}=0$ and therefore:

$$K_i^j=\begin{bmatrix}\frac{1}{R} & 0\\ 0 & \frac{1}{R}\end{bmatrix} \tag{B.1}$$

and therefore $\kappa=\frac{1}{R}$ and $\kappa_G=\frac{1}{R^2}$.

Second case: By setting $h(\theta,\varphi)=h(\varphi)$ and consequently $h_{,\theta}=0$. These result in

$$g_{ij}=\begin{bmatrix}h^2 & 0\\ 0 & h^2\sin^2\theta+h_{,\varphi}^2\end{bmatrix} \tag{B.2}$$

and

$$K_i^j=\begin{bmatrix}\frac{h^2\sin^2\theta+h_{,\varphi}^2}{h^3\sin^2\theta\Delta^{3/2}} & \frac{h_{,\varphi}h^2\sin^2\theta\cos\theta+h_{,\varphi}^3\cos\theta}{h^4\sin^3\theta\Delta^{3/2}}\\ \frac{h_{,\varphi}\cos\theta}{h^2\sin^3\theta\Delta^{3/2}} & \frac{h^2\sin^2\theta-hh_{,\varphi\varphi}+2h_{,\varphi}^2}{h^3\sin^2\theta\Delta^{3/2}}\end{bmatrix} \tag{B.3}$$

in which $\Delta=1+\frac{h_{,\varphi}^2}{h^2\sin^2\theta}$.

Following K_i^j one finds:

$$\kappa=\frac{2h^2\sin^2\theta+3h_{,\varphi}^2-hh_{,\varphi\varphi}}{2h^3\Delta^{3/2}\sin^2\theta} \tag{B.4}$$

and

$$\kappa_G = \frac{h^2 \sin^4\theta + \left(2h_{,\varphi}^2 - h h_{,\varphi\varphi}\right)\sin^2\theta - h_{,\varphi}^2 \cos^2\theta}{\left(h^2 \sin^2\theta + h_{,\varphi}^2\right)^2}. \tag{B.5}$$

Third case: By setting $h(\theta,\varphi) = h(\theta)$ with $h_{,\varphi} = 0$. The induced metric tensor becomes:

$$g_{ij} = \begin{bmatrix} h^2 + h_{,\theta}^2 & 0 \\ 0 & h^2 \sin^2\theta \end{bmatrix} \tag{B.6}$$

with the second fundamental form

$$K_i^j = \begin{bmatrix} \frac{h^2 - h h_{,\theta\theta} + 2h_{,\theta}^2}{h^3 \Delta^{3/2}} & 0 \\ 0 & \frac{\left(h^2 + h_{,\theta}^2\right)\left(h\sin\theta - h_{,\theta}\cos\theta\right)}{h^4 \sin\theta \Delta^{3/2}} \end{bmatrix}. \tag{B.7}$$

Finally we find

$$\kappa = \frac{\left(3h h_{,\theta}^2 + 2h^3 - h^2 h_{,\theta\theta}\right)\sin\theta - h_{,\theta}^3 \cos\theta - h^2 h_{,\theta}\cos\theta}{2h\left(h^2 + h_{,\theta}^2\right)^{\frac{3}{2}} \sin\theta} \tag{B.8}$$

and

$$\kappa_G = \frac{\left(h^2 - h h_{,\theta\theta} + 2h_{,\theta}^2\right)\left(h\sin\theta - h_{,\theta}\cos\theta\right)}{h\left(h^2 + h_{,\theta}^2\right)^2 \sin\theta} \tag{B.9}$$

with

$$\Delta = 1 + \frac{h_{,\theta}^2}{h^2}\,. \tag{B.10}$$

Fourth case: A spheres with a bump

In Fig. B.1 a sphere with a bump is plotted, whose equation is given by:

$$h(\theta) = R\left(1 + \varepsilon_0 \exp\left(-\alpha\theta^2\right)\right) \tag{B.11}$$

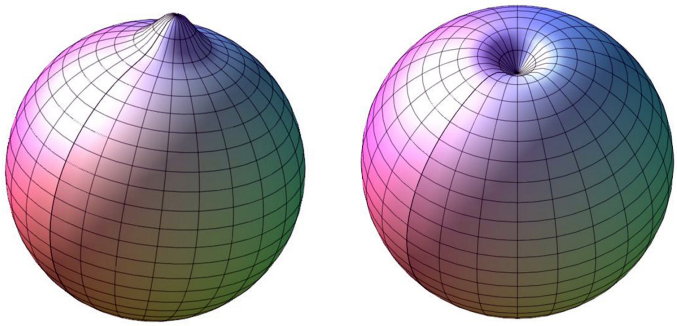

Figure B.1: A sphere with a bump on the left and a miss/reverse bump on the right. The exact value of the parameters in Eq. (B.11) are as follows: $R = 1$, $\alpha = 40$ and $\varepsilon_0 = \pm 0.2$. The positive and negative ε_0 results in the left and in the right figures, respectively.

in which R is the radius of the background sphere and ε_0 and α are constants. Depending on the value of ε_0 and α, the size of the bump changes and even results in a reversed shape with negative ε_0 (see fig. B.1 right). Using Eqs. (B.8) and (B.9) we find:

$$\kappa = \frac{\left(\lambda_1 \varepsilon_0^2 e^{-2\alpha\theta^2} + \lambda_2 \varepsilon_0 e^{-\alpha\theta^2} + (1+\Delta)\sin\theta\right)}{2R\left(1+\varepsilon_0 e^{-\alpha\theta^2}\right)^3 \Delta^{3/2}\sin\theta} \tag{B.12}$$

$$\kappa_G = \left\{ \frac{\left(1+\varepsilon_0 e^{-\alpha\theta^2}\left(-4\alpha^2\theta^2+2\alpha+2\right)+\varepsilon_0^2 e^{-2\alpha\theta^2}\left(4\alpha^2\theta^2+2\alpha+1\right)\right)}{R^2\sin\theta\left(1+\varepsilon_0 e^{-\alpha\theta^2}\right)\left(1+2\varepsilon_0 e^{-\alpha\theta^2}+\varepsilon_0^2 e^{-2\alpha\theta^2}\left(4\alpha^2\theta^2+1\right)\right)^2} \right. \tag{B.13}$$
$$\left. \left(\varepsilon_0 e^{-\alpha\theta^2}\left(2\alpha\theta\cos\theta+\sin\theta\right)+\sin\theta\right)\right\}$$

in which

$$\begin{pmatrix} \lambda_1 \\ \lambda_2 \end{pmatrix} = \begin{pmatrix} \left(2\alpha+4\alpha^2\theta^2+\Delta+1\right)\sin\theta + 2\Delta\alpha\theta\cos\theta \\ 2\Delta\alpha\theta\cos\theta + \left(2-4\alpha^2\theta^2+2\alpha+2\Delta\right)\sin\theta \end{pmatrix}$$

and

$$\Delta = 1 + \frac{4\varepsilon_0^2\alpha^2\theta^2 e^{-2\alpha\theta^2}}{\left(1+\varepsilon_0 e^{-\alpha\theta^2}\right)^2}. \tag{B.14}$$

At $\theta = 0$ one finds $\Delta = 1$ and consequently

$$\kappa = \frac{2\alpha\varepsilon_0 + \varepsilon_0 + 1}{R\left(1+\varepsilon_0\right)^2} \tag{B.15}$$

and

$$\kappa_G = \frac{\left(2\varepsilon_0\alpha + \varepsilon_0 + 1\right)^2}{R^2\left(1+\varepsilon_0\right)^4} = \kappa^2. \tag{B.16}$$

Fifth case: A sphere with a delta type inflation: It is considered

$$h = R\left(1 + \frac{\zeta}{\left(\left(\theta-\theta_0\right)^2 + \zeta^2\right)\pi}\right) \tag{B.17}$$

in which θ_0, ζ and R are constants. This model provides a delta-type inflation at $\theta = \theta_0$ on a sphere of radius R such that a smaller ζ produces more localized and sharper inflation. In Fig. B.2 we plot h for $R = 1$, $\theta_0 = \frac{\pi}{2}$ and $\zeta = 0.1$. The sharp symmetric deformation at the equator of the sphere is displayed in this figure.

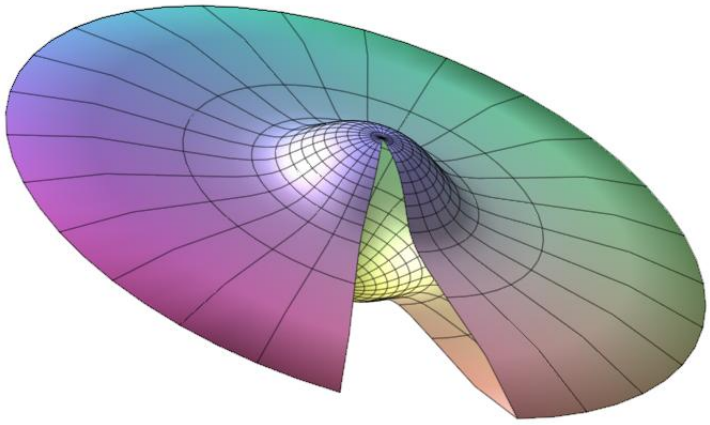

Figure B.2: A delta-dirac form of inflation at the equator of a sphere with radius $R = 1$. The other parameters in Eq. (B.17) are as follows: $\theta_0 = \frac{\pi}{2}$ and $\zeta = 0.1$. For a better visibility we imposed $\varphi \in [0, 11\pi/12]$.

Using the general equations we find the total curvature given by:

$$\kappa = \frac{-x\zeta\left(\Lambda^2\pi^2H^4+4\zeta^2x^2\right)\cot\theta+\pi H^2\Lambda\left(\Lambda^2\pi^2H^4-\pi\left(3x^2-\zeta^2\right)\zeta H\Lambda+6\zeta^2x^2\right)}{R\Lambda\left(\Lambda^2\pi^2H^4+4\zeta^2x^2\right)^{\frac{3}{2}}} \tag{B.18}$$

in which $x=\theta-\theta_0$, $H=(\theta-\theta_0)^2+\zeta^2$ and $\Lambda=1+\frac{\zeta}{\pi H}$. In addition, the Gaussian curvature is also obtained as:

$$\kappa_G = \frac{\left(-6\Lambda\zeta\pi Hx^2+2\Lambda\zeta^3\pi H+\Lambda^2\pi^2H^4+8\zeta^2x^2\right)\left(\Lambda\pi H^2-2\zeta x\cot\theta\right)\pi H^2}{R^2\Lambda\left(\Lambda^2\pi^2H^4+4\zeta^2x^2\right)} \,. \tag{B.19}$$

The limit of κ and κ_G when $\theta\to\theta_0$ are found to be:

$$\lim_{\theta\to\theta_0}\kappa = \frac{1+\zeta^2+\zeta^3}{R\zeta\left(1+\zeta\right)^2} \,, \tag{B.20}$$

$$\lim_{\theta\to\theta_0}\kappa_G = \frac{2+\zeta^2+\zeta^3}{R^2\left(1+\zeta\right)^3} \tag{B.21}$$

while their limits when $\zeta\to 0$ becomes $\frac{1}{R}$ and $\frac{1}{R^2}$, respectively, for all θ except for $\theta=\theta_0$. At $\theta=\theta_0$ we find $\lim_{\zeta\to0}\kappa=\infty$ and $\lim_{\zeta\to0}\kappa_G=\frac{2}{R^2}$. In Fig. B.3. we plot κ and κ_G in terms of θ for the specific choice of the parameters presented in Fig. B.2.

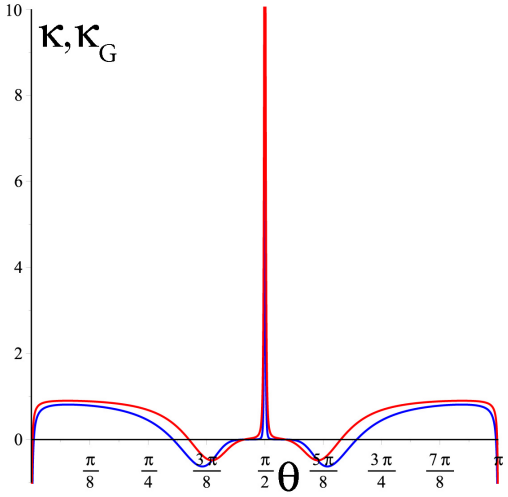

Figure B.3: κ (red/above) and κ_G(blue/below) in terms of θ for the second example i.e., Eq. (B.17). The specific values of parameters are as given in Fig. B.2.

The cylindrical Monge gauge

Special cases

First case: the perfect cylinder with $h(\varphi, z) = \rho$. This in turn implies $h_{,z} = h_{,zz} = h_{,\varphi\varphi} = h_{,z\varphi} = h_{,\varphi z} = 0$, $\Delta = 1$,

$$K_i^j = \begin{bmatrix} \frac{1}{R} & 0 \\ 0 & 0 \end{bmatrix} \tag{B.22}$$

and consiquently $\kappa = \frac{1}{2R}$ and $\kappa_G = 0$.

Second case: one can set $h(\varphi, z) = h(\varphi)$ which implies $h_{,z} = h_{,zz} = h_{,z\varphi} = h_{,\varphi z} = 0$.

The induced metric and its inverse are given by:

$$g_{ij} = \begin{bmatrix} h^2 + h_\varphi^2 & 0 \\ 0 & 1 \end{bmatrix} \tag{B.23}$$

and

$$g^{ij} = \frac{1}{h^2\Delta}\begin{bmatrix} 1 & 0 \\ 0 & h^2 + h_{\varphi}^2 \end{bmatrix} \tag{B.24}$$

which the extrinsic curvature tensor becomes:

$$K_i^j = \begin{bmatrix} \frac{-hh_{,\varphi\varphi} + h^2 + 2h_{,\varphi}^2}{h^3\Delta^{\frac{3}{2}}} & 0 \\ 0 & 0 \end{bmatrix} \tag{B.25}$$

where $\Delta = 1 + \frac{h_{,\varphi}^2}{h^2}$. Following K_i^j, one finds:

$$\kappa = \frac{-hh_{,\varphi\varphi} + h^2 + 2h_{,\varphi}^2}{2h^3\Delta^{\frac{3}{2}}} \tag{B.26}$$

and

$$\kappa_G = 0. \tag{B.27}$$

Third case: it is possible to write as $h(\varphi, z) = h(z)$ with $h_{,\varphi} = h_{,\varphi z} = h_{,z\varphi} = h_{,\varphi\varphi} = 0$.

The induced metric tensor and its inverse becomes:

$$g_{ij} = \begin{bmatrix} h^2 & 0 \\ 0 & h_{,z}^2 + 1 \end{bmatrix} \tag{B.28}$$

and

$$g^{ij} = \frac{1}{h^2\Delta}\begin{bmatrix} 1 + h_z^2 & 0 \\ 0 & h^2 \end{bmatrix} \tag{B.29}$$

with the second fundamental form given by:

$$K_i^j = \begin{bmatrix} \frac{(1+h_{,z}^2)}{h\Delta^{3/2}} & 0 \\ 0 & \frac{-h_{,zz}}{\Delta^{3/2}} \end{bmatrix}. \tag{B.30}$$

The mean and Gaussian curvature are given as:

$$\kappa = \frac{(1+h_{,z}^2 - hh_{,zz})}{2h\Delta^{\frac{3}{2}}} \tag{B.31}$$

and

$$\kappa_G = \frac{-h_{,zz}(h_{,z}^2+1)}{h\Delta^3} \tag{B.32}$$

in which

$$\Delta = 1 + h_{,z}^2. \tag{B.33}$$

Fourth case: Deformation of Cylindrical Symmetric Lipid Membrane

In the following, it is possible to consider an infinitely large cylinder of radius ρ_0 which is deformed at $z = 0$ (XY-plane) such that the function $h(z)$ is symmetric to z-axis (h(z) is an even function).

Biophysicists have been interested in the deformation of the living-cells membrane for a long time. Cylindrical symmetric bio-cells are deformed by imposing external forces; for example, one can mention the aggregation of proteins on the plasma membrane. The crucial point is that geometry is the only degree of freedom on the bilayer membrane on a large scale. To model the deformation, we can consider these kinds of cells as two-dimensional hypersurfaces embedded in three-dimensional cylindrical space $\mathbb{R}^3$. In the current work, we would like to apply the geometrical approach for finding the minimum energy of our deformed system by perturbation

methods, to predict the deformation effect on the membrane.

Let us now consider the third special case which was identified as $h(\varphi,z)=h(z)$ with $h_{,\varphi}=h_{,\varphi z}=h_{,z\varphi}=h_{,\varphi\varphi}=0$. In order to find the total energy of our deformed large cylinder, one needs to find the action of the Hamiltonian $H_{CH}=\oint_M dA(\sigma+\frac{1}{2}\kappa(K_0-K)^2+\overline{\kappa}K_G)$, by substituting K and K_G from Eq. B.31 and Eq. B.32 into H_{CH}, we get:

$$H_{CH}=\frac{1}{2}\oint\left[\sigma+\kappa\left(\left(\frac{1+h_{,z}-hh_{,zz}^2}{(2h(1+h_{,z}^2)^{3/2}}\right)-K0\right)^2-\overline{\kappa}\left(\frac{h_{,zz}}{h(1+h_{,z}^2)}\right)\right]dA \tag{B.34}$$

In which $dA=\sqrt{g}dzd\varphi$ is area element of the bilayer membrane, and g is the the determinant of $2-$dimensional induced metric tensor of the membrane, given by:

$$g=h^2(1+h_{,z}) \tag{B.35}$$

Finally, equation (B.34) turns to:

$$H_{CH}=\frac{1}{2}\int\int\left[\sigma+\kappa\left(\left(\frac{1+h_{,z}-hh_{,zz}^2}{(2h(1+h_{,z}^2)^{3/2}}\right)-K0\right)^2-\overline{\kappa}\left(\frac{h_{,zz}}{h(1+h_{,z}^2)}\right)\sqrt{h^2(1+h_{,z})}\right]dzd\varphi \tag{B.36}$$

Henceforward, applying the variational methods, we will try to find the shape equation of a gradually deformed long cylinder. considering our Lagrangian as:

$$L(h_{,zz},h_{,z},h,\theta)=\sigma+\kappa\left(\frac{1+h_{,z}-hh_{,zz}^2}{2h(1+h_{,z}^2)^{3/2}}-K0\right)^2-\overline{\kappa}\left(\frac{h_{,zz}}{h(1+h_{,z}^2)}\right)\sqrt{h^2(1+h_{,z})} \tag{B.37}$$

One can write the Euler-Lagransian equation:

$$\frac{d^2}{dz^2}(\frac{\partial L}{\partial h_{,zz}}) - \frac{d}{dz}(\frac{\partial L}{\partial h_{,z}}) + \frac{\partial L}{\partial h} = 0 \tag{B.38}$$

we will try to solve the linearized shape equation analytically, considering some assumptions. Primary, since we are investigating small deformations, we assume:

$$h(z) = \rho_0((1 + \lambda\varepsilon(z)) \tag{B.39}$$

where $\varepsilon(z)$ represents the deviation from the initial unit cylinder and $\|\varepsilon(z\| << 1$. Also, the magnitude of first, second third and fourth derivatives of $\varepsilon(z)$ concerning z are all presumed to be much smaller than a unit. In which surface tension is given by:

$$\sigma = \kappa\frac{(2K_0^2\rho_0^2 - 1)}{2\rho_0^2} \tag{B.40}$$

And,

$$\varepsilon(z) + 2\rho_0^3\frac{d^2}{dz^2}\varepsilon(z)K_0 + \rho_0^4\frac{d^4}{dz^4}\varepsilon(z) = 0 \tag{B.41}$$

where spontaneous curvature defined as $K_0 = \frac{\xi}{\rho_0}$ which can be solved exactly with the following solution:

$$\varepsilon(z) = C_1 e^{\frac{-\sqrt{-\xi-\sqrt{\xi^2-1}}}{\rho_0}z} + C_2 e^{\frac{-\sqrt{-\xi-\sqrt{\xi^2-1}}}{\rho_0}z} + C_3 e^{\frac{-\sqrt{-\xi+\sqrt{\xi^2-1}}}{\rho_0}z} + C_4 e^{\frac{-\sqrt{-\xi+\sqrt{\xi^2-1}}}{\rho_0}z} \tag{B.42}$$

We suppose that our surface is spontaneous curvature free, $\xi = 0$, one can obtain:

$$\varepsilon(z) = C_1 e^{\frac{-(\frac{1}{\sqrt{2}}-\frac{i}{\sqrt{2}})}{\rho_0}z} + C_2 e^{\frac{(\frac{1}{\sqrt{2}}-\frac{i}{\sqrt{2}})}{\rho_0}z} + C_3 e^{\frac{-(\frac{1}{\sqrt{2}}-\frac{i}{\sqrt{2}})}{\rho_0}z} + C_4 e^{\frac{-(\frac{1}{\sqrt{2}}-\frac{i}{\sqrt{2}})}{\rho_0}z} \tag{B.43}$$

Solution of this equation written as:

$$\varepsilon(z) = e^{\frac{z}{\sqrt{2}\rho_0}} \left[C_1 cos(\frac{z}{\sqrt{2}\rho_0}) + C_2 sin(\frac{z}{\sqrt{2}\rho_0}) \right] \tag{B.44}$$

as first boundary condition we demand $\frac{d^2}{dz^2 h(z)}$, and so $\frac{d^2}{dz^2}\varepsilon(z)$ to vanish at $z = 0$, and $z = \infty$. Exerting these two conditions to (B.44) equation we get $C_1 = C_2$ and $C_1 = \varepsilon_0$. Substituting the latter results into (B.44), we will have:

$$\varepsilon(z) = e^{\frac{z}{\sqrt{2}\rho_0}} \varepsilon_0 \left[cos(\frac{z}{\sqrt{2}\rho_0}) + sin(\frac{z}{\sqrt{2}\rho_0}) \right] \tag{B.45}$$

which in turn, considering equation (B.39), gives rise to:

$$h(z) = 1 + e^{-\sqrt{(z^2)}} \lambda \left(cos(\sqrt{z^2}) + sin(\sqrt{z^2}) \right) \tag{B.46}$$

To have a better understanding of the validity of the solution (B.39), we draw:

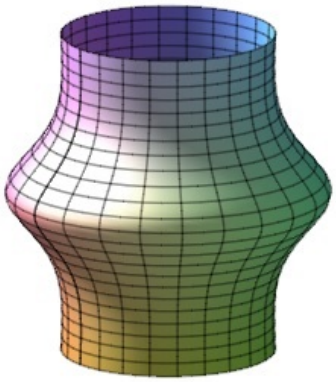

Figure B.4: A large cylinder with small deformation on the $z = 0$ $(xy - plane)$ and $\lambda = -0.3$

Appendix C: Numerical Approaches

Numerical approaches

In this appendix, we briefly present the numerical methods we have used in this manuscript. The details of both methods *without* the flexoelectric contribution can be found in the Appendices of Ref. [2]. Flexoelectricity appends additional terms to the differential equations of the system.

Finite Element Analysis

To find the equilibrium shapes of spherically confined flexoelectric fluid membrane vesicles in an external uniform electric field, we use a finite elements method based on the subdivision surface concept [84, 85, 96]. This ensures the necessary C^1 continuity of the surface vector function $X(s^1, s^2)$ of the flexoelectric membrane. The membrane is parametrized by local curvilinear coordinates (s^1, s^2) (see Fig. C.1). The covariant tangent vectors are given by $e_\alpha = \partial_\alpha X$ with $\alpha = 1, 2$. The normal vector is defined as $\mathbf{n} = \frac{e_1 \times e_2}{\sqrt{g}}$, and the surface Jacobian is constructed as $\sqrt{g} = |e_1 \times e_2|$ so that the area $A = \int_\Omega \mathrm{d}A = \int_\Omega \sqrt{g}\,\mathrm{d}s^1\mathrm{d}s^2$.

In the simulations the membrane surface is discretised by a set of triangles with $N \sim$ 3000 nodes.

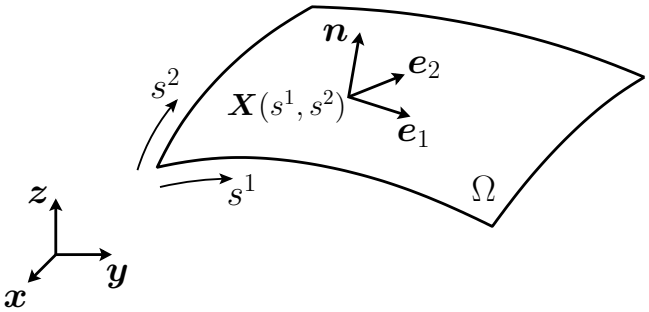

Figure C.1: Surface parametrization.

The position of the surface is then interpolated by the weighted sum:

$$X_h(s^1,s^2) = \sum_{i=1}^{N} X_i N^i(s^1,s^2)\,, \tag{C.1}$$

where X_i is the position of node i, and the N^i are the loop subdivision trial functions [96].

The energy functional

$$E^M = \int_\Omega \left\{ 2\kappa H^2 + \frac{1}{2D}\left[(\mathbf{E}_{\text{ext}}\cdot\mathbf{n})^2 - |\mathbf{E}_{\text{ext}}|^2\right]\right\}\sqrt{g}\,\mathrm{d}s^1\mathrm{d}s^2 + \int_\Omega \frac{\mu_A}{2}(\sqrt{g}-\sqrt{\bar{g}})^2\,\mathrm{d}s^1\mathrm{d}s^2 + \frac{\mu_V}{2}(V-\bar{V})^2 \tag{C.2}$$

is minimised while taking into account the container constraint and self-contacts of the membrane (see below). The constraints on surface and volume are enforced in Eq. (C.2) *via* a penalty method to improve convergence [2]. The constants μ_A and μ_V are chosen large enough to fulfill these constraints to a numerical error of about 10^{-3}. Their values range from 10^4 to 10^7 depending on the value of the electric field $\mathbf{E}_{\text{ext}}$. Note that the area constraint is local to avoid mesh distortions during the simulation.

Energy (C.2) can be discretised in terms of the nodal positions X_i. To calculate the force f_i^M that acts on each node, one considers the variation of the energy with respect to a displacement of the nodal position:

$$\delta E^M = \frac{\partial E^M}{\partial X^i}\delta X^i = -f_i^M \delta X^i\,, \tag{C.3}$$

which gives:

$$f_i^M = \int_\Omega \left[s^\alpha\cdot\partial_i e_\alpha + m^\alpha\cdot(\partial_i\mathbf{n})_{,\alpha} + fN^i\right]\sqrt{g}\,\mathrm{d}s^1\mathrm{d}s^2\,, \tag{C.4}$$

where

$$
\begin{aligned}
s^{\alpha} &= 2\kappa H g^{\alpha\beta}\mathbf{n}_{,\beta} + 2\kappa H^2 e^{\alpha} - \frac{1}{D}(\mathbf{E}_{\text{ext}}\cdot\mathbf{n})(\mathbf{E}_{\text{ext}}\cdot e^{\alpha})\mathbf{n} - \frac{1}{2D}\left[\mathbf{E}_{\text{ext}}^2 - (\mathbf{E}_{\text{ext}}\cdot\mathbf{n})^2\right] e^{\alpha} \\
&\quad + \mu_A(\sqrt{g}-\sqrt{\bar{g}})e^{\alpha} + \mu_V \frac{V-\bar{V}}{3}\left[(X\cdot\mathbf{n})e^{\alpha} - (X\cdot e^{\alpha})\mathbf{n}\right] , \qquad \text{(C.5)} \\
m^{\alpha} &= -2\kappa H e^{\alpha} , \qquad \text{and} \qquad \text{(C.6)} \\
f &= \mu_V \frac{V-\bar{V}}{3}\mathbf{n} . \qquad \text{(C.7)}
\end{aligned}
$$

are the stress and moment resultants. In addition to the terms already implemented by Klug and coworkers [84, 85], s^{α} now contains a contribution due to the flexoelectric effect. Note that its continuous version was found in Ref. [32].

The contact between the membrane and the container is modeled by a quadratic force field applied to the nodes that leave the container. The corresponding force is given by:

$$f_i^{C_1} = -k_1 d_i^2 \mathbf{n} , \qquad \text{(C.8)}$$

where $k_1 \sim 10^5$ is the stiffness constant, d_i the penetration depth, and $\mathbf{n}$ the outward-pointing normal of the container surface. An additional force field is needed to disentangle intersections of the membrane surface that occur during the course of the simulation: at first the contour line of the intersecting polygons is determined. In a second step, the gradient G_i of the contour length with respect to the position of each node i of a triangle involved in the intersection is calculated. The resulting contact force is linear in G_i:

$$f_i^{C_2} = k_2 G_i , \qquad \text{(C.9)}$$

where we set $k_2 = 10$. Adding all terms together one obtains the resulting force on each node

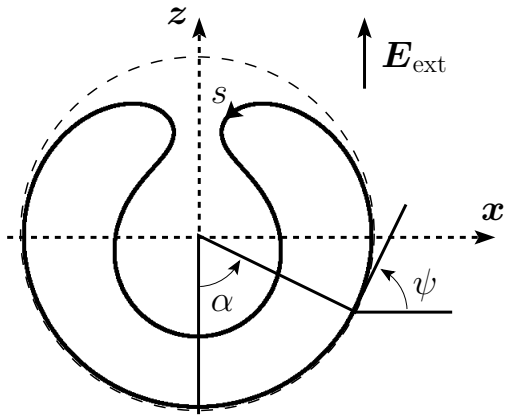

Figure C.2: Parametrization of the axisymmetric flexoelectric fluid membrane in spherical confinement. The solid black line represents the cross-section of the membrane. The dashed line indicates the spherical confinement. s is the arc length, ψ is the angle between the x axis and the tangent of the flexoelectric membrane and α represents the detachment angle of the flexoelectric membrane from the confinement. We assume that the membrane consists of two segments, a spherical segment in contact with the confinement (bottom part) and an upper free segment whose shape is determined by solving the Hamilton equations (C.19) together with the appropriate boundary conditions (C.20).

$$f_i = f_i^M + f_i^{C_1} + f_i^{C_2} \,. \tag{C.10}$$

During the simulation, we integrate these nodal forces in time according to Newton's equations of motion with a damping term until we reach equilibrium, $f_i = 0$ (for more details see Appendix B of Ref. [2]).

Hamiltonian formulation for the axisymmetric case

Angle-arc-length parameterization

In the special case of an axisymmetric configuration, one can resort to a Hamiltonian formulation of the problem. In the following we assume that the flexoelectric membrane vesicle is symmetric with respect to the **z** axis (see Fig. C.2). We make use of the angle-arc length parametrization $\psi(s)$, where ψ is the angle between the tangent vector and the x axis, whereas s denotes the arc length.

In this parametrization the area element dA is given by:

$$dA = 2\pi\rho\,\mathrm{d}s \tag{C.11}$$

and the volume element dV:

$$\mathrm{d}V = \pi\rho^2 \sin\psi\,\mathrm{d}s\,. \tag{C.12}$$

The mean curvature is obtained as:

$$H = -\frac{1}{2}\left(\dot{\psi} + \frac{\sin\psi}{\rho}\right)\,, \tag{C.13}$$

where the curvature in the meridian direction is $c_\perp = -\dot{\psi}$, and the curvature along the parallel direction is $c_\parallel = -\frac{\sin\psi}{\rho}$. The flexoelectric energy term simplifies to:

$$\frac{1}{2D}\left[(\mathbf{E}_{\mathrm{ext}}\cdot\mathbf{n})^2 - |\mathbf{E}_{\mathrm{ext}}|^2\right] = \frac{-{E_{\mathrm{ext}}}^2}{2D}\sin^2\psi\,. \tag{C.14}$$

The scaled energy functional of the free part of the membrane vesicle follows as:

$$\begin{aligned}\tilde{E} &:= \frac{E}{\pi\kappa} = \int_{\underline{s}}^{\bar{s}} \tilde{L}\,\mathrm{d}s \\ &= \int_{\underline{s}}^{\bar{s}} \left[\rho\left(\dot{\psi} + \frac{\sin\psi}{\rho}\right)^2 + 2\tilde{\sigma}\rho + \lambda_\rho(\dot{\rho} - \cos\psi) + \lambda_z(\dot{z} - \sin\psi) + \tilde{P}\rho^2\sin\psi - \rho e\sin^2\psi\right]\mathrm{d}s,\end{aligned} \tag{C.15}$$

where $\tilde{\sigma} = \frac{\sigma R^2}{\kappa}$ and $\tilde{P} = \frac{PR^3}{\kappa}$ are the scaled surface tension and pressure, respectively. The Lagrange multiplier functions λ_ρ and λ_z fix the geometrical constraints $\dot{z} = \sin\psi$ and $\dot{\rho} = \cos\psi$ along the profile. In the integral, $\underline{s}$ represents the arc length at the contact point and $\bar{s}$ corresponds to the arc length at the $\mathbf{z}$ axis where the tangent of the membrane is parallel to x. All lengths are scaled with the radius R of the confining

sphere. The dimensionless electric field parameter e is defined as:

$$e = \frac{E_{\text{ext}}^2 R^2}{D\kappa} \,. \tag{C.16}$$

The conjugate momenta of the system are:

$$p_\psi = \frac{\partial \tilde{L}}{\partial \dot{\psi}} = 2\rho \left(\dot{\psi} + \frac{\sin\psi}{\rho} \right) , \tag{C.17a}$$

$$p_\rho = \frac{\partial \tilde{L}}{\partial \dot{\rho}} = \lambda_\rho \,, \tag{C.17b}$$

$$p_z = \frac{\partial \tilde{L}}{\partial \dot{z}} = \lambda_z \,. \tag{C.17c}$$

One obtains the scaled Hamiltonian *via* the Hamiltonian formalism:

$$\begin{aligned} \tilde{H} &= \dot{\psi} p_\psi + \dot{\rho} p_\rho + \dot{z} p_z - \tilde{L} \\ &= \frac{p_\psi^2}{4\rho} - p_\psi \frac{\sin\psi}{\rho} - 2\tilde{\sigma}\rho + p_\rho \cos\psi + p_z \sin\psi - \tilde{P}\rho^2 \sin\psi + e\rho \sin^2\psi \end{aligned} \tag{C.18}$$

yielding the Hamilton equations:

$$\dot{\psi} = \frac{\partial \tilde{H}}{\partial p_\psi} = \frac{p_\psi}{2\rho} - \frac{\sin\psi}{\rho} \,, \tag{C.19a}$$

$$\dot{\rho} = \frac{\partial \tilde{H}}{\partial p_\rho} = \cos\psi \,, \tag{C.19b}$$

$$\dot{z} = \frac{\partial \tilde{H}}{\partial p_z} = \sin\psi \,, \tag{C.19c}$$

$$\dot{p}_\psi = -\frac{\partial \tilde{H}}{\partial \psi} = \left(\frac{p_\psi}{\rho} + \tilde{P}\rho^2 - p_z \right) \cos\psi + p_\rho \sin\psi - 2e\rho \sin\psi \cos\psi \,, \tag{C.19d}$$

$$\dot{p}_\rho = -\frac{\partial \tilde{H}}{\partial \rho} = \frac{p_\psi}{\rho} \left(\frac{p_\psi}{4\rho} - \frac{\sin\psi}{\rho} \right) + 2\tilde{\sigma} + 2\tilde{P}\rho \sin\psi - e\sin^2\psi \,, \tag{C.19e}$$

$$\dot{p}_z = -\frac{\partial \tilde{H}}{\partial z} = 0 \,. \tag{C.19f}$$

For $e = 0$ one obtains the classical Hamilton equations of a lipid membrane vesicle as expected [2]. The flexoelectric effect adds terms which are linear in e and simple analytical functions of the surface parametrization. The Hamilton equations can be solved with a standard shooting method [97] subject to boundary conditions which we

discuss in the following.

The Hamiltonian H does not explicitly depend on the arc length s. Since we have not fixed the total arc length $\bar{s} - \underline{s}$ for the integration, the Hamiltonian is conserved:

$$\tilde{H} = 0 \,. \tag{C.20a}$$

At the contact point ($s = \underline{s}$) the free part of the flexoelectric membrane detaches from the container and the angle ψ has to equal α since the membrane must not have kinks. At the $\mathbf{z}$ axis ($s = \bar{s}$) the free profile is horizontal, which leaves us with the following boundary conditions:

$$\psi(\underline{s}) = \alpha \,, \qquad \psi(\bar{s}) = \pi \,. \tag{C.20b}$$

A variation of the contact line as was, for example, done for the non-electric case in Refs. [66, 69], yields:

$$\psi(\underline{s}) = 1 + \sqrt{|e_\mathrm{c} - e_\mathrm{f}|}\sin\alpha \,, \tag{C.20c}$$

where e_c is the electric field parameter at the membrane in contact with the confinement and e_f is the electric field parameter of the free membrane. For a uniform external electric field, however, the second term equals zero and we are left with the classical contact curvature condition of the case without electric field.

The Hamilton equations are integrated with a fourth-order Runge-Kutta method. For a fixed $\tilde{\sigma}$ and $\tilde{P}$ and a trial angle α we search for shapes which fulfill all of the boundary conditions. When a profile is found we calculate its area and volume *a posteriori*. By scanning the parameter space $(\tilde{\sigma}, \tilde{P})$ we obtain vesicles with variable area and volume.

For more details we again refer to Ref. [1].

Appendix D: Dielectric Sphere Model Within Electrolyte in an Applied Uniform Electric Field $\mathbf{E_{ext}}$

Dielectric sphere model within electrolyte in an applied uniform electric field $\mathbf{E_{ext}}$

This section takes a step into a more realistic model of the system. One may adds an electrolyte (e.g, Na^+Cl^-) inside of our system, a dielectric sphere with inner radius **a** and outer radius **b** in the uniform electric field $\mathbf{E_a}$ which is anti-parallel to the z-axis (see Fig. 4.1). It is possible to examine the behavior of the electric field inside, between, and outside of the membranes. In the new model, the challenge is to formulate the electric field inside of confinement. For this purpose, one may capture the potential inside of the sphere by making use of the Poisson-Boltzmann equation:

$$\nabla^2\Phi = -\frac{4\pi}{\varepsilon_w}\rho(\vec{r}) \tag{D.1}$$

where $\rho(\vec{r}) = ez_+n_+ + ez_-n_-$ is the Poisson equation for the charge density, $n_\pm = n_0 e^{\frac{-ez_\pm\phi}{k_BT}}$ is the Boltzmann distribution for the number density and n_0 is the electrolyte concentration in the reservoir. The valency of the cations and anions for Na^+Cl^- is $z_\pm = \pm 1$, k_B is the Boltzmann constant, and T is the temperature [98]. The potential inside of the sphere is ϕ-independent due to the symmetry along the z-axis. Suppose there exist a small electrostatic potential: as a result, one can linearize the Poisson-Boltzmann equation as:

$$\nabla^2\phi - K_D^2\phi = 0 \tag{D.2}$$

where $K_D = \sqrt{\frac{8\pi e^2 n_0}{\varepsilon_w k_B T}}$ is the Debye-Hückel screening length. The solution of the linearized Poisson-Boltzmann equation in spherical coordinates with azimuthal symmetry is as below:

$$\phi_l(\vec{r},\theta) = \sum_{l=0}^{\infty} \Big(A_l (i)^l i_l(K_D r) + B_l k_l(K_D r) \Big) P_l(\cos\theta). \tag{D.3}$$

The second term diverges at the origin, and one can rewrite the potential as:

$$\phi_l(\vec{r},\theta) = \sum_{l=0}^{\infty} A_l (i)^l i_l(K_D r) P_l(\cos\theta), \tag{D.4}$$

where i_1 is the modified spherical Bessel function of the first kind. This problem is closely related to a dielectric sphere in an external uniform electric field, which discussed in Chapter. 4. The potential of the initial field is $\phi_0 = E_0 Z = E_0 r\cos\theta = E_0 r P_1(\theta)$ in which θ is the polar angle with respect to the z-axis and P_1 is the Legendre polynomial of first order [75]. Thus, it is possible to recollect the previous case, a uniform dielectric sphere where the potential contains terms only in P_1, and one may expect the same here. So, the electric potential inside of the sphere reads as:

$$\phi_1(\vec{r},\theta) = A_1 (i)^1 i_1(K_D r) P_1(\cos\theta) \tag{D.5}$$

in which the spherical Bessel function is:

$$i_1(K_D r) = \frac{K_D r\cosh(K_D r) - \sinh(K_D r)}{(K_D r)^2}. \tag{D.6}$$

It is possible to keep the potentials of the second and third regions from the previous model without electrolyte. Therefore, the potentials of all regions are:

$$\phi_1(\vec{r},\theta) = -A' i_1(K_D r)\cos(\theta) \qquad 0 < r < a; \;\; \varepsilon_w \tag{D.7a}$$

$$\phi_2(\vec{r},\theta) = E_0 r\cos(\theta) + B\frac{r}{a}\cos(\theta) + C\frac{b^2}{r^2}\cos(\theta) \;\; a < r < b; \;\; \varepsilon_M \tag{D.7b}$$

$$\phi_3(\vec{r},\theta) = E_0 r\cos(\theta) + D\frac{b^2}{r^2}\cos(\theta) \qquad r > b; \;\; \varepsilon_w \tag{D.7c}$$

where $A' = \frac{A}{i}$, and ε_w is water dielectric constant, and ε_M is the dielectric constant of

the membrane. For the sake of simplicity, one can scale the potentials in all regions again:

$$\widetilde{\Phi}_1(\vec{r},\theta) = -\widetilde{A}' i_1(\widetilde{K}_D\widetilde{r})\cos\theta \qquad 0<\widetilde{r}<1 \tag{D.8a}$$

$$\widetilde{\Phi}_2(\vec{r},\theta) = \left(1+\widetilde{B}\right)\widetilde{r}\cos\theta+\widetilde{C}(\frac{\widetilde{b}}{\widetilde{r}})^2\cos\theta \qquad 1<\widetilde{r}<\widetilde{b} \tag{D.8b}$$

$$\widetilde{\Phi}_3(\vec{r},\theta) = \left(\widetilde{r}+\widetilde{D}(\frac{\widetilde{b}}{\widetilde{r}})^2\right)\cos\theta \qquad \widetilde{r}>\widetilde{b} \tag{D.8c}$$

Considered as a boundary-value problem, the perturbation of the field $\mathbf{E}_{\text{ext}}$ must be finite at $r=0$ and $r=\infty$, and the potential is continuous at $r=a$ and $r=b$ [75]. Therefore, the scaled boundary conditions are:

$$\widetilde{\Phi}_1(1,\theta) = \widetilde{\Phi}_2(1,\theta), \tag{D.9a}$$

$$\widetilde{\Phi}_3(\widetilde{b},\theta) = \widetilde{\Phi}_2(\widetilde{b},\theta). \tag{D.9b}$$

and boundary conditions of the scaled normal components of the electric displacement field, $\mathbf{D}$, are:

$$\frac{\partial\widetilde{\Phi}_1(1)}{\partial\widetilde{r}} = \widetilde{\varepsilon}\frac{\partial\widetilde{\Phi}_2(1)}{\partial\widetilde{r}}, \tag{D.10a}$$

$$\widetilde{\varepsilon}\frac{\partial\widetilde{\Phi}_2(\widetilde{b})}{\partial\widetilde{r}} = \frac{\partial\widetilde{\Phi}_3(\widetilde{b})}{\partial\widetilde{r}}. \tag{D.10b}$$

With operating the scaled boundary conditions into the four linear equations, it is possible to obtain four unknown parameters:

$$\widetilde{A} = \frac{-\widetilde{k_D}(1+\widetilde{B}+\widetilde{C}\widetilde{b}^2)}{\widetilde{k_D}\cosh(\widetilde{k_D})-\sinh(\widetilde{k_D})}, \tag{D.11a}$$

$$\widetilde{B} = \frac{2\widetilde{\varepsilon}\widetilde{C}-\widetilde{\varepsilon}\widetilde{b}-2\widetilde{D}+\widetilde{b}}{\widetilde{\varepsilon}\widetilde{b}}, \tag{D.11b}$$

$$\widetilde{C} = \frac{\widetilde{A}\widetilde{k}_D^2\sinh(\widetilde{k}_D)+\widetilde{\varepsilon}\widetilde{B}\widetilde{k}_D^2+\widetilde{\varepsilon}\widetilde{k_D}^2-2\widetilde{A}\widetilde{k}_D\cosh(\widetilde{k}_D)+2\widetilde{A}\sinh(\widetilde{k}_D)}{2\widetilde{\varepsilon}\widetilde{k_D}^2\widetilde{b}^2}, \tag{D.11c}$$

$$\widetilde{D} = \widetilde{B}\widetilde{b}+\widetilde{C}. \tag{D.11d}$$

Therefore, one can write down the general expression for the scaled electric field at

any point in the space as:

$$\widetilde{E}_1(\vec{r},\theta) = \widetilde{A}\left(\frac{\sinh(\widetilde{k}_D\widetilde{r})}{\widetilde{r}} + 2\frac{\sinh(\widetilde{k}_D\widetilde{r}) - \widetilde{k}_D\widetilde{r}\cosh(\widetilde{k}_D\widetilde{r})}{\widetilde{k}_D^2\widetilde{r}^3}\right)\cos\theta\hat{r} \quad \text{(D.12a)}$$

$$+ \widetilde{A}\left(\frac{\sinh(\widetilde{K}_D\widetilde{r}) - \widetilde{K}_D\widetilde{r}\cosh(\widetilde{K}_D\widetilde{r})}{\widetilde{r}^3\widetilde{K}_D^2}\right)\sin\theta\hat{\theta}, \quad \text{(D.12b)}$$

$$\widetilde{E}_2(\vec{r},\theta) = -\left(1+\widetilde{B}-2\widetilde{C}\frac{\widetilde{b}^2}{\widetilde{r}^3}\right)\cos\theta\hat{r} + \left(1+\widetilde{B}+\widetilde{C}\frac{\widetilde{b}^3}{\widetilde{r}^2}\right)\sin\theta\hat{\theta}, \quad \text{(D.12c)}$$

$$\widetilde{E}_3(\vec{r},\theta) = \left(-1+2\widetilde{D}\frac{\widetilde{b}^2}{\widetilde{r}^3}\right)\cos\theta\hat{r} + \left(1+\widetilde{D}\frac{\widetilde{b}^2}{\widetilde{r}^3}\right)\sin\theta\hat{\theta}. \quad \text{(D.12d)}$$

After simplification, one may calculate:

$$\widetilde{E}_1(\vec{r},\theta) = \widetilde{A}\left(i_0(\widetilde{K}_D\widetilde{r})\cos\theta\hat{r} + \frac{i_1(\widetilde{K}_D\widetilde{r})}{\widetilde{r}}(-2\cos\theta\hat{r}+\sin\theta\hat{\theta})\right), \quad \text{(D.13a)}$$

$$\widetilde{E}_2(\vec{r},\theta) = (1+\widetilde{B})\left(-\cos\theta\hat{r}+\sin\theta\hat{\theta}\right) + \widetilde{C}\frac{\widetilde{b}^2}{r^3}\left(2\cos\theta\hat{r}+\sin\theta\hat{\theta}\right), \quad \text{(D.13b)}$$

$$\widetilde{E}_3(\vec{r},\theta) = \left(-\cos\theta\hat{r}+\sin\theta\hat{\theta}\right) + \widetilde{D}\frac{\widetilde{b}^2}{r^3}\left(2\cos\theta\hat{r}+\sin\theta\hat{\theta}\right). \quad \text{(D.13c)}$$

by making use of ascending series for modified spherical Bessel functions of the first kind as below:

$$i_n(x) = \sqrt{\frac{\pi}{2x}}I_{n+\frac{1}{2}} = \frac{x^n}{(2n+1)!}1 + \frac{\frac{x^2}{2}}{1!(2n+3)+\frac{x^4}{4}}2!(2n+3)(2n+5) \quad \text{(D.14)}$$

$$i_0(\widetilde{K}_D\widetilde{r}) = 1 + \frac{(\widetilde{K}_D\widetilde{r})^2}{6} + \frac{(\widetilde{K}_D\widetilde{r})^4}{120} + ... \quad \text{(D.15)}$$

$$i_1(\widetilde{K}_D\widetilde{r}) = \frac{(\widetilde{K}_D\widetilde{r})}{6} + \frac{(\widetilde{K}_D\widetilde{r})^3}{60} + ... \quad \text{(D.16)}$$

it is possible to simplify the electric field inside of the membrane:

$$\widetilde{E}_1(\vec{r},\theta) = \widetilde{A}\left((1+\frac{(\widetilde{K}_D\widetilde{r})^2}{6}+...)\cos\theta\hat{r} + \frac{(\frac{(\widetilde{K}_D\widetilde{r})}{6}+...)}{\widetilde{r}}(-2\cos\theta\hat{r}+\sin\theta\hat{\theta})\right) \quad \text{(D.17)}$$

One may simplify further for a pair of experimental examples, by assign the parameter values of the following figure:

Parameters	Giant vesicle	Mitochondria
a	$5\mu m$	$0.5\mu m$
$\widetilde{b}$	$1+10^{-3}$	$1+10^{-2}$
$\widetilde{K_D}$	5	0.5
$\widetilde{\varepsilon}$	$\frac{1}{20}$	$\frac{1}{20}$

Figure D.1: Scaled parameters.

Giant unilamelar vesicles (GUVs)

For giant unilamellar vesicles, the numerical value of the scaled coefficients are $\widetilde{A} = -0.04$, $\widetilde{B} = 12.57$, $\widetilde{C} = -13.08$, and $\widetilde{D} = -0.49$. Therefore, substituting the scaled coefficients into the Eqs. (D.13) and Eqs. (D.17) one may write the scaled electric field at any point in the space as:

$$\widetilde{E}_1(\vec{r},\theta) = -0.04\left(\frac{\sinh(5\widetilde{r})}{\widetilde{r}}\cos\theta\hat{r} + \frac{(5\widetilde{r}\cosh(5\widetilde{r}) - \sinh(5\widetilde{r}))}{25\widetilde{r}^3}(-2\cos\theta\hat{r} + \sin\theta\hat{\theta})\right), \tag{D.18a}$$

$$\widetilde{E}_2(\vec{r},\theta) = -13.57\hat{z} - \frac{13.11}{\widetilde{r}^3}\left(2\cos\theta\hat{r} + \sin\theta\hat{\theta}\right), \tag{D.18b}$$

$$\widetilde{E}_3(\vec{r},\theta) = -\hat{z} - \frac{0.49}{\widetilde{r}^3}\left(2\cos\theta\hat{r} + \sin\theta\hat{\theta}\right). \tag{D.18c}$$

After simplification, one may obtain:

$$\widetilde{E}_1(\vec{r},\theta) = -0.04\left(i_0(5\widetilde{r})\cos\theta\hat{r} + \frac{i_1(5\widetilde{r})}{\widetilde{r}}(-2\cos\theta\hat{r} + \sin\theta\hat{\theta})\right), \tag{D.19a}$$

$$\widetilde{E}_2(\vec{r},\theta) = -13.57\hat{z} - \frac{13.11}{\widetilde{r}^3}\left(2\cos\theta\hat{r} + \sin\theta\hat{\theta}\right), \tag{D.19b}$$

$$\widetilde{E}_3(\vec{r},\theta) = -\hat{z} - \frac{0.49}{\widetilde{r}^3}\left(2\cos\theta\hat{r} + \sin\theta\hat{\theta}\right). \tag{D.19c}$$

Mitochondrion

For a mitochondrion, it is possible to calculate the numerical value of the scaled

coefficients as: $\widetilde{A} = -5.13$, $\widetilde{B} = 5.72$, $\widetilde{C} = -5.73$, and $\widetilde{D} = 0.049$. Thus, one can write the scaled electric fields in all regions as:

$$\widetilde{E}_1(\vec{r},\theta) = -5.13\left(\frac{\sinh(0.5\widetilde{r})}{\widetilde{r}}\cos\theta\hat{r} + \frac{0.5\widetilde{r}\cosh(0.5\widetilde{r}) - \sinh(0.5\widetilde{r})}{0.25\widetilde{r}^3}(-2\cos\theta\hat{r} + \sin\theta\hat{\theta})\right), \tag{D.20a}$$

$$\widetilde{E}_2(\vec{r},\theta) = -6.72\hat{z} - \frac{5.79}{\widetilde{r}^3}\left(2\cos\theta\hat{r} + \sin\theta\hat{\theta}\right), \tag{D.20b}$$

$$\widetilde{E}_3(\vec{r},\theta) = -\hat{z} + \frac{0.05}{\widetilde{r}^3}\left(2\cos\theta\hat{r} + \sin\theta\hat{\theta}\right). \tag{D.20c}$$

After simplification, one can get:

$$\widetilde{E}_1(\vec{r},\theta) = -5.13\left(i_0(0.5\widetilde{r})\cos\theta\hat{r} + \frac{i_1(0.5\widetilde{r})}{\widetilde{r}}(-2\cos\theta\hat{r} + \sin\theta\hat{\theta})\right), \tag{D.21a}$$

$$\widetilde{E}_2(\vec{r},\theta) = -6.72\hat{z} - \frac{5.79}{\widetilde{r}^3}\left(2\cos\theta\hat{r} + \sin\theta\hat{\theta}\right), \tag{D.21b}$$

$$\widetilde{E}_3(\vec{r},\theta) = -\hat{z} + \frac{0.05}{\widetilde{r}^3}\left(2\cos\theta\hat{r} + \sin\theta\hat{\theta}\right). \tag{D.21c}$$